Extraction of Hot QCD Matter Transport Coefficients Utilizing Microscopic Transport Theory

by

Nasser Soliman Demir

Department of Physics
Duke University

Date: _____

Approved:

_____
Steffen A. Bass, Supervisor

_____
Berndt Mueller

_____
Richard G. Palmer

_____
John E. Thomas

_____
Werner Tornow

Dissertation submitted in partial fulfillment of the requirements for the degree of
Doctor of Philosophy in the Department of Physics
in the Graduate School of Duke University
2010

Abstract

(Physics)

Extraction of Hot QCD Matter Transport Coefficients Utilizing Microscopic Transport Theory

by

Nasser Soliman Demir

Department of Physics
Duke University

Date: _____

Approved:

_____
Steffen A. Bass, Supervisor

_____
Berndt Mueller

_____
Richard G. Palmer

_____
John E. Thomas

_____
Werner Tornow

An abstract of a dissertation submitted in partial fulfillment of the requirements for the degree of Doctor of Philosophy in the Department of Physics in the Graduate School of Duke University
2010

Abstract

Ultrarelativistic heavy-ion collisions at the Relativistic Heavy-Ion Collider (RHIC) are thought to have produced a state of matter called the Quark-Gluon-Plasma (QGP). The QGP forms when nuclear matter governed by Quantum Chromodynamics (QCD) reaches a temperature and baryochemical potential necessary to achieve the transition of hadrons (bound states of quarks and gluons) to *deconfined* quarks and gluons. Such conditions have been achieved at RHIC, and the resulting QGP created exhibits properties of a near perfect fluid. In particular, strong evidence shows that the QGP exhibits a very small shear viscosity to entropy density ratio η/s, near the lower bound predicted for that quantity by Anti-deSitter space/Conformal Field Theory (AdS/CFT) methods of $\eta/s = \frac{\hbar}{4\pi k_B}$, where $\hbar$ is Planck's constant and k_B is Boltzmann's constant. As the produced matter expands and cools, it evolves through a phase described by a hadron gas with rapidly increasing η/s.

This thesis presents robust calculations of η/s for hadronic and partonic media as a function of temperature using the Green-Kubo formalism. An analysis is performed for the behavior of η/s to mimic situations of the hadronic media at RHIC evolving out of chemical equilibrium, and systematic uncertainties are assessed for our method. In addition, preliminary results are presented for the bulk viscosity to entropy density ratio ζ/s, whose behavior is not well-known in a relativistic heavy ion collisions. The diffusion coefficient for baryon number is investigated, and an algorithm is presented to improve upon the previous work of investigation of heavy quark diffusion in a

thermal QGP.

By combining the results of my investigations for η/s from our microscopic transport models with what is currently known from the experimental results on elliptic flow from RHIC, I find that the trajectory of η/s in a heavy ion collision has a rich structure, especially near the deconfinement transition temperature T_c. I have helped quantify the viscous hadronic effects to enable investigators to constrain the value of η/s for the QGP created at RHIC.

To Soliman M. Demir, who shall always be remembered in our lives.

Contents

List of Tables

List of Figures

List of Abbreviations and Symbols

Symbols and Conventions

Natural units are used , where $\hbar = k_B = c = 1$ unless explicitly stated. Repeated indices are summed over. Indices given by Latin letters run from 1-3 unless otherwise specified.

Abbreviations

QCD Quantum Chromodynamics (see chapter 1).

QGP Quark Gluon Plasma (see chapter 1).

RHIC (Relativistic Heavy Ion Collider) (see chapter 1)

KSS Kovtun, Son, Starinets (see chapter 1).

AdS/CFT Anti-deSitter Space/Conformal Field Theory (see chapter 2).

AMY Arnold, Moore, and Yaffe (see chapter 2).

UrQMD Ultrarelativistic Quantum Molecular Dynamics Model (see chapters 4).

PCM Parton Cascade Model (see chapter 4).

HG Hadron Resonance Gas (see chapter 4).

Acknowledgements

There certainly is not enough space in a few pages to mention all the people who have been instrumental in helping me complete my doctoral program and dissertation. There are undoubtedly many individuals not mentioned here who also deserve credit for helping me directly or indirectly in the completion of this dissertation. Nevertheless, I shall list all who immediately come to mind.

I shall begin by thanking my doctoral supervisor, Steffen Bass. I remember his warm demeanor when I visited Duke University during the Prospective Graduate Student Visit, and his presentation to my first year graduate research seminar that got me interested in his subject. Coming from an undergraduate research background in experimental condensed matter physics, I found his presentation was accessible enough that it piqued my interest. What makes Steffen unique is that he finds just the right balance between pushing a student to his limits, and being patient with the student's learning curve. His understanding when my father, Soliman Demir, passed away suddenly on January 4, 2009 helped me navigate through the most difficult time in my life. He also gave me the proper push when I needed it to complete my dissertation.

I must also thank my PhD advisory committee for asking thought provoking questions during my Preliminary Examination and Dissertation Defense. In particular, I would like to thank Berndt Müller for working with Steffen to make sure that I was well prepared for my first conferences as a graduate student. After several years of

attending conferences, I can conclude with certainty that the mentoring of students in the Duke QCD Theory group is exceptional. Credit also goes to Abhijit Majumdar, Guangyou Qin, Hannah Petersen, Hung Ming Tsai, Chris Coleman-Smith, Dilun Yang , and Shanshan Cao for all their comments and questions during group meetings.

I also would like to thank my fellow graduate students at Duke who have provided friendship and support. In particular, I thank Arya Roy for all his help in learning about technical theoretical issues during my first and second years at Duke, and for helping me survive my first years in graduate school. In addition, he has been and continues to be a good source for advice. I could not have been more fortunate to share an office for a total of four years at Duke with Bryon Neufeld. He was there both as a colleague and as a very good friend. He asked me to be a groomsman at his wedding, and was a great listener when things got especially difficult in my life. His grasping of difficult concepts in quantum field theory is quite impressive, and his work ethic the most admirable. I would also like to thank James Esterline, Willie Ong and Charles Cao, who asked excellent questions during my practice defense and provided very useful feedback. Credit also goes to my "Duke Mom", Donna Ruger, for helping me with all the volumes of paperwork I've had to deal with over the years and how she has helped keep operations at Duke Physics run smoothly.

There are those outside the Duke Physics community who I would like to thank. In particular, my discussions with Derek Teaney, Jorge Casalderrey-Solana, Giorgio Torrieri, Ulrich Heinz, Pasi Huovinen, Jorge Noronha, Huichao Song, Scott Pratt, and Sourendu Gupta have been very enriching.

I must emphasize that I could not have made it through the toughest times of my graduate school years without the love and support of my caring family. Unfortunately my father, Soliman, could not be here to witness the moment of completion of my dissertation. He was the best kind of father, one who pushed me and was frank

with me when he needed to be, yet was the most loving, generous father one could ask for. My mother, Shafikah, has been the rock that provided me support all my life, and words cannot describe how much her love has provided me with the energy to succeed in life through both pleasant and unpleasant times. My wonderful brother Husam, is the best brother one could ask for, no one who has ever met him has not liked him. Last, but not least, I thank God, the Most Gracious, Most Merciful, for if one were to enumerate all the blessings He has bestowed upon our family, the list would never end.

1

Introduction

In the first few microseconds following the Big Bang, the very hot and dense Universe was thought to be in a state of matter known as the *Quark Gluon Plasma* (QGP). The QGP is rather different from the normal matter we observe everyday; molecules, atoms, nuclei, matter composed of protons and neutrons are examples of particles in which quarks and gluons are bound. It is said that quarks and gluons are *confined* in Nature; we do not observe them individually as free particles, but only in composite objects which are composed of quarks and gluons bound together tightly. For example, while we observe the proton (a particle consisting of two up quarks and one down quark), we do not observe those three quarks individually in Nature. However, it is thought that at sufficiently hot and dense conditions, one can "liberate" quarks and gluons from the confined state. The state in which quarks and gluons are not confined, but quasi-free or *deconfined*, is known as the QGP. Why is the QGP useful to study? It will not only give us insight into how the medium of the Early Universe behaved, but will help us understand how nuclear matter behaves under extreme conditions. Scientists at many high energy accelerators, including the Relativistic Heavy Ion Collider (RHIC) at Brookhaven National Laboratory on

Long Island, New York attempt to recreate the QGP by colliding heavy nuclei (such as Copper, Lead, and Gold) at speeds very close to the speed of light. The hope is that colliding sufficiently heavy particles at very fast speeds will compress and heat the matter to the degree necessary to produce the QGP. However, one of the biggest challenges involved in analyzing the QGP is that the state is transient; it is so short lived (lifetime is on the order of $\sim 10^{-23}$ s), that the quarks and gluons recombine to from bound states (known as *hadrons*), before any measurement can take place. The particle detectors in such experiments measure properties of the final-state hadrons rather than the free quarks themselves [62]. As a result, there is a great deal of detective work in phenomenology and theoretical modeling involved in identifying possible signatures for the existence of a QGP, and investigating such properties.

One of the top science stories of 2005 was the discovery of a "near perfect fluid" at RHIC [62, 48]. It was previously expected that if a QGP were to be created at RHIC energies, the resulting matter would be a gas. However, a great deal of experimental evidence exists suggesting that the state created ted at RHIC is not only not a gas, but a nearly ideal fluid [3, 12, 8, 2]. The resistance to flow in a fluid is characterized by a quantity known as the shear viscosity (η). Traditionally, an ideal fluid has been defined as having $\eta = 0$. However, semiclassical arguments show such a fluid is unphysical [23], and there has been a paradigm shift in defining an "ideal fluid." The related quantity proposed for this definition is the viscosity to entropy ratio η/s, where s is the *entropy density*. Calculations utilizing one of the big recent revolutions in string theory, the anti-deSitter Space/Conformal Field Theory (AdS/CFT) conjecture, suggest that a possible value for the "most perfect fluid" $\eta/s \geq \hbar/4\pi k_B$, where hbar is Planck's constant divided by 2π, and k_B is Boltzmann's constant [47]. Thus, understanding the QGP created at RHIC will also help us better understand the nature of near perfect fluidity.

My research is specifically concerned with extraction of transport coefficients of

the hadronic and QGP phases of a relativistic heavy ion reaction. Transport coefficients are physical quantities which characterize the nature of medium interactions. The "transport" refers to the transfer of physical properties through the medium. In particular, the transport coefficients relevant to my research are the shear viscosity coefficient and the diffusion coefficient. The shear viscosity coefficient is relevant for momentum transfer in the medium, and the diffusion coefficient is relevant for transfer of particle concentration in the medium. The media created in these relativistic heavy ion collisions involves a large number of different particle species, and traditional theoretical methods in nuclear and high energy physics give at best very crude approximations for describing the media created in such collisions. However, with the multiple advances in computational power and modeling, sophisticated models have been successfully developed (known as microscopic transport models)and tested which provide fairly accurate descriptions of the deconfined and hadronic media created in relativistic heavy ion collisions. My research exploits such microscopic transport models, and involves calculating the shear viscosity, viscosity to entropy ratio, bulk viscosity and the diffusion coefficients for a system which resembles an equilibriated QGP or a hadron gas. We have performed a careful calculation of η/s, D_B, and are currently improving ζ/s calculation for self-consistency. With these tasks executed, one could obtain a much better constraint on the values for the transport coefficients of the elusive state of matter sought after at RHIC and the LHC. Knowledge of the transport coefficients of hot and dense nuclear matter is not very well known, and must be improved if one is to gain a better understanding not only of the medium interactions in the Early Universe, but also of systems which are thought to be "near-ideal" in Nature.

1.1 The QGP:Deconfinement and Chiral Symmetry Restoration

QCD is the field theory of strong interactions, and a very interesting phenomenon worth investigating is the effect of chiral symmetry breaking in QCD. In the Early Universe, it was believed the degrees of freedom corresponding to the strong, electromagnetic, weak, and gravitational forces were unified to one. All the fundamental particles and gauge bosons were in thermal equilibrium. However, the system cooled and it is believed $\sim 10^{-35}$ seconds after the Big Bang, the strong interaction decoupled from the electroweak interaction. The phenomenon known as the *electroweak phase transition* took place $\sim 10^{-11}$ seconds after the Big Bang; the electromagnetic interaction decoupled from the weak interaction. As the system cooled further, $\sim 10^{-6}$ seconds after the Big Bang is when the quarks formed hadronic bound states of quarks: baryons (qqq bound states) and mesons($q\bar{q}$ bound states) [72]. This last step is known as the *deconfinement transition*.

When one speaks about the QCD transition, there are two distinct types of transitions being discussed. One is the deconfinement transition, which involves the transition from hadronic degrees of freedom to quasifree quarks and gluons. The other transition is chiral symmetry restoration, which involves the light quarks acquiring zero effective mass. The relevant order parameter in discussing the deconfinement transition is the expectation value of the Polyakov loop [53].

The Polyakov Loop is related to the free energy of a static quark F through

$$\langle L \rangle \sim \exp^{-\frac{F}{T}} . \tag{1.1}$$

Since the free energy is related to the energy required to place a free test quark in a thermal medium of gluons, in the confined phase, F would be infinite, leading to $\langle L \rangle = 0$ in the confined phase, and acquires a nonzero value in the deconfined phase. Although equilibrium statistical mechanics can be used with lattice QCD techniques to calculate static properties of a medium such as energy density, pressure, etc as a

function of temperature, it does not help us to ascertain values of dynamic properties such as transport coefficients.

1.2 Structure of Thesis

This dissertation shall discuss what is known about the shear viscosity and bulk viscosity coefficients at RHIC in Chapter 2, a summary of known methods to calculate transport coefficients in Chapter 3, a detailed description of microscopic transport models in Chapter 4, and calculation of transport coefficients from microscopic transport models in Chapter 5, and description of a Langevin algorithm to investigate heavy quark diffusion in Chapter 6. The material in the dissertation is summarized in Chapter 7.

2

The Viscosity of QCD Matter at RHIC

One of the top science stories of 2005 was the discovery of a "near-perfect fluid" at RHIC [3, 12, 8, 2]. It was thought that the energies accessible at RHIC would yield high enough temperatures that the resulting QGP created would have the properties of a perturbative QGP, so that a weakly interacting gas of quarks and gluons behaves like an ideal gas rather than an ideal fluid. Whenever one speaks of ideal fluid behavior, it is necessary to quantify the viscosity of the discussed fluid. Traditionally an ideal fluid has been described as having "zero viscosity", and setting viscosity terms to zero in order to facilitate hydrodynamic calculations is justified in approximating ideal fluid behavior, but we shall see there is a quantitative difference between "ideal fluid" and a "most perfect fluid." While "ideal fluid" traditionally means setting $\eta = 0$ in the relevant calculations, "most perfect fluid" implies fluids with low (but non-zero) values of η/s. We shall begin with a review of the experimental observable used to characterize the quality and character of the fluid, namely elliptic flow.

2.1 Discovery of Ideal Fluid Behavior at RHIC

2.1.1 Elliptic Flow

One of the strongest features of the QGP discovered at RHIC is the large value of a quantity called elliptic flow, observed for various particle species. The best way this can be illustrated is in a noncentral heavy ion collision, as depicted in Figure 2.1. In a given noncentral collision, the overlap of the two colliding nuclei creates an almond-like shape region comprising the participant matter of the reaction. This participant matter is what is heated and compressed which then forms the QGP. As a consequence of the sudden shaving off of the spectator matter, there is a much larger pressure gradient along the x-z plane (reaction plane) than perpendicular to the reaction plane (y direction). As a result, a preferential collective flow of matter in the reaction plane versus out of the reaction plane develops. One way to quantify this asymmetry of particle emission is to examine the azimuthal distribution of emitted hadrons and expand in a Fourier series

$$\frac{dN}{d\phi} \sim \frac{1}{2\pi}\left(1 + 2v_2 cos(2\phi) + ...\right) \tag{2.1}$$

where v_2 is the elliptic flow coefficient, and ϕ is the azimuthal angle with respect to the reaction plane [3]. If the medium were highly viscous, then dissipative effects would reduce the collective buildup of elliptic flow, so a large elliptic flow is expected for systems which are "ideal fluid like". What is more remarkable is that calculations using ideal relativistic hydrodynamics have reproduced the v_2 data from RHIC rather well, as shown in Figure 2.2 [2].

2.1.2 Ultracold Fermionic Systems

Elliptic flow has been observed in ultracold fermionic systems, such as Lithium atoms in a magneto-optical trap, subject to an applied magnetic field tuned to near the

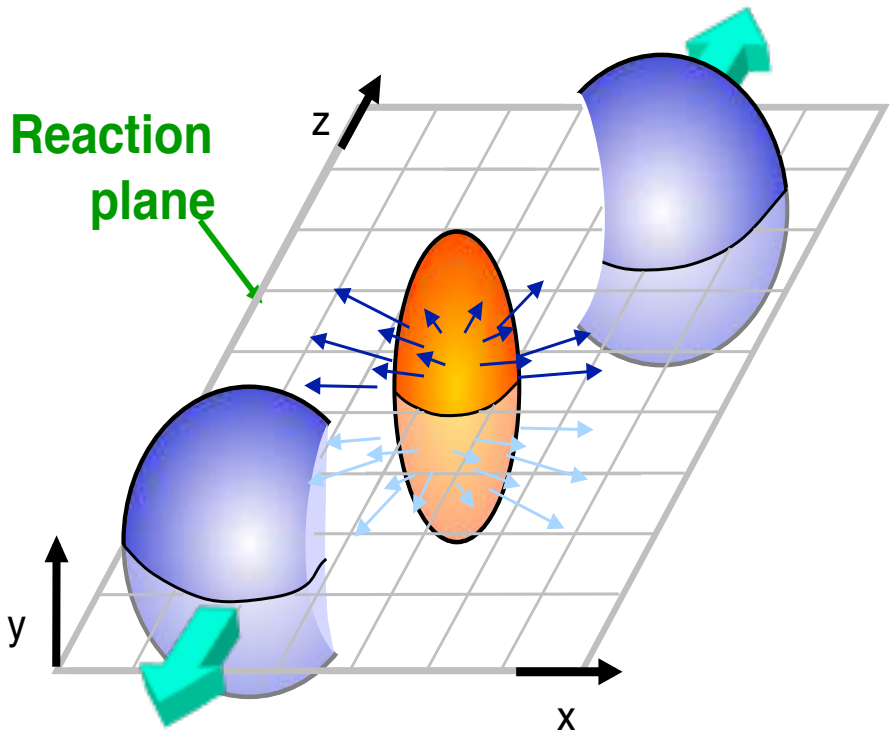

FIGURE 2.1: Reaction plane in an event of a heavy ion collision. The almond shaped overlap region is where the QGP is formed.

Feshbach resonance. The strength of the interactions between the Lithium atoms is controlled by the applied magnetic field, and near the Feshbach resonance, the strongly interacting regime of the system can be studied. An optical trap is designed such that the Lithium atoms trapped in it form an initial almond shape as in Figure 2.3. After the atoms are released from the optical trap, elliptic flow develops, as in Figure 2.4. With elliptic flow evident in heavy ion reactions as well as ultracold, strongly interacting Lithium atoms we are led to identify elliptic flow as a general feature of strongly interacting systems. Strongly interacting systems are systems that have very large interaction cross sections and hence are expected to exhibit features such as low η/s and significant elliptic flow [69, 44, 85]. Ultracold fermionic atoms, neutron stars, and the quark gluon plasma are all manifestations of strongly interacting matter. In fact, η/s values as low as ≈ 0.3 been measured for strongly

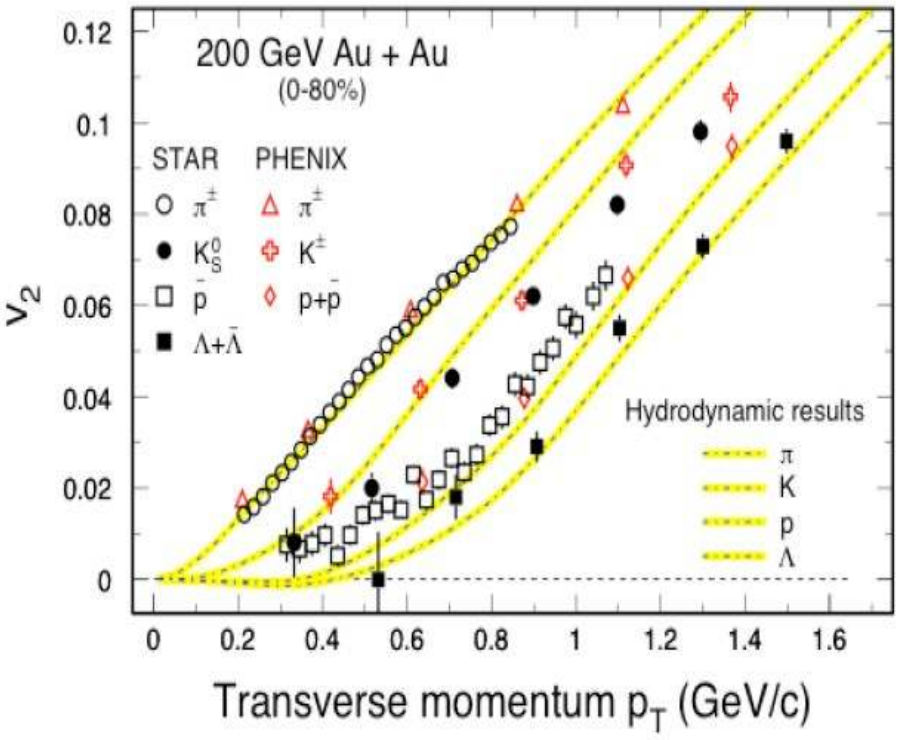

FIGURE 2.2: [v_2 as function of p_T from pure ideal hydro with Glauber initial condition, compared with STAR and PHENIX data [2].

interacting ultracold Lithium atoms as illustrated in Figure 2.5 [85].

2.1.3 Solving ideal relativistic fluid dynamics

The formulation of ideal relativistic fluid dynamics is to write the conservation laws for energy-momentum and conserved charges.

$$\partial_\mu T^{\mu\nu} = 0, \tag{2.2}$$

where $\nu = 0, 1, 2, 3$.

$$\partial_\mu j_i^\mu = 0, \tag{2.3}$$

where $i = 1, 2, ..., M$.

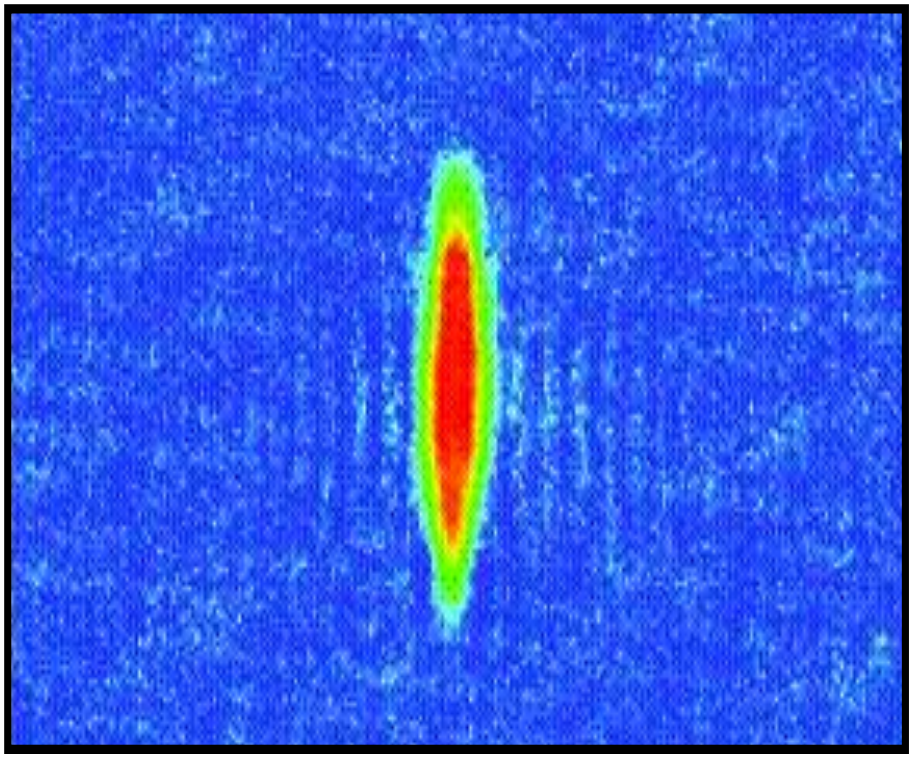

FIGURE 2.3: Profile of lithium atoms in a magnetooptical trap [69].

Equation 2.2 expresses the conservation of energy and momentum, while equation 2.3 expresses conservation of M different sorts of charges, labeled by j_i. $T_{\mu\nu}$ is the energy momentum tensor, whose components are given by

$$T^{\mu\nu} = \int \frac{d^3p}{p^0} p^\mu p^\nu f(x,p). \tag{2.4}$$

p^i is a component of a particles 4-momentum, and $f(x,p)$ is the particle and momentum distribution function of the system. Hence, the energy momentum tensor for a system in a fluid cell with position x at rest is given by

$$T^{\mu\nu}(x) = diag(\epsilon(x), p(x), p(x), p(x)), \tag{2.5}$$

where $\epsilon(x)$ is the cell's energy density and $p(x)$ is its pressure. If the fluid cell moves with a 4-velocity u, then we would need to construct the Lorentz boost matrix Λ,

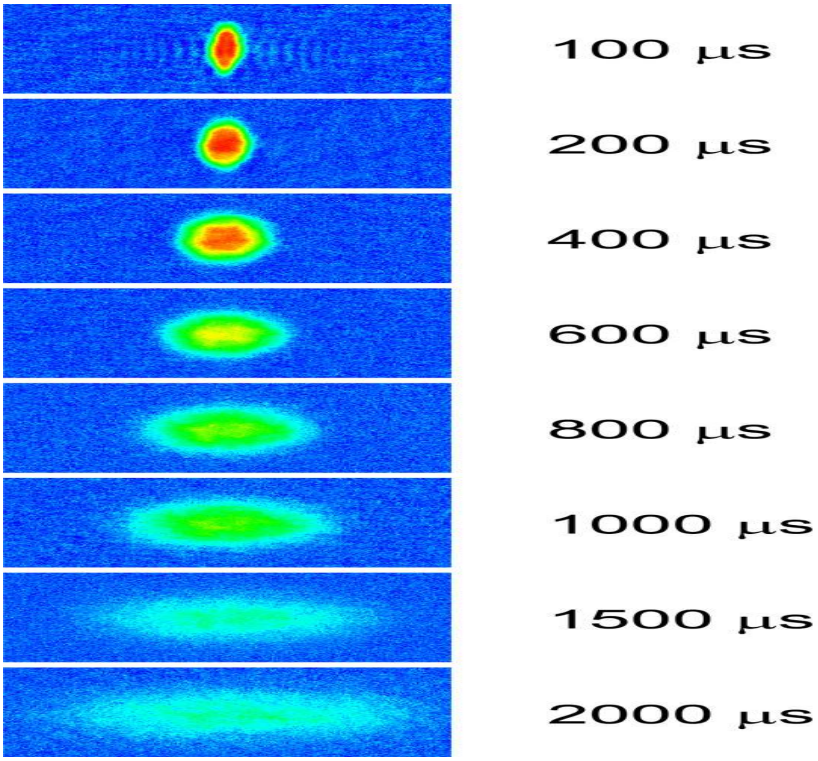

FIGURE 2.4: Time profile of lithium atoms released from a trap. with an applied magnetic field tuned to near the Feshbach resonance [69].

and boost through $T^{\mu\nu} = \Lambda^T T^{\mu\nu} \Lambda$. The equations for ideal hydrodynamics involve $4 + M$ independent differential equations. Whereas equation 2.3 involves the charges of the M independent equations (and hence M independent variables), equation 2.2 involves the energy-momentum tensor, which contains the flow velocity, pressure, and energy density. Since the flow velocity has 3 components, equation 2.2 contains a total of 5 independent variables. Hence, the $4+M$ differential equations governing the evolution of the system described by ideal hydrodynamics contain a total of $5+M$ independent variables. This requires us to input an additional equation to be able to close the system of differential equations. This additional necessary input equation is the *equation of state* $p = p(\epsilon)$, which relates the pressure of the system to its energy density. In principle, the equation of state that is needed to close the system does not necessarily have the form $p = p(\epsilon)$, but must relate the thermodynamic quantities of

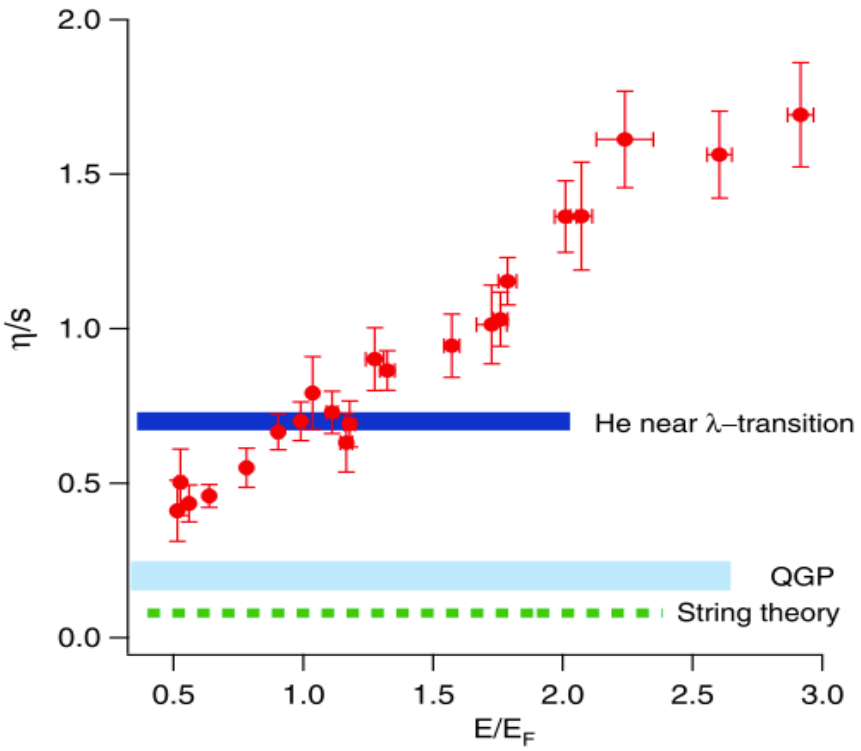

FIGURE 2.5: η/s as a function of energy, taken from [85]. The "string theory" dashed line refers to the KSS bound of $\eta/s = \hbar/(4\pi k_B)$, and the "QGP" band is 2-3 times the KSS bound.

the system.

Hence, investigators performing ideal relativistic hydrodynamics calculations must specify an equation of state in their calculations, and also specify an initial condition for the distribution of matter. In practice, two types of initial conditions are often used for ideal hydrodynamics calculations, the Glauber and Color Glass Condensate (CGC) initial conditions. The Glauber initial condition specifies that the initial distribution of energy and particle density is given by a superposition of two contributions, one proportional to the number of wounded nucleons, and one proportional to number of binary collisions. Another widely used initial condition, the CGC initial condition specifies that the initial gluon distribution is given by the CGC model[43, 54, 55]. Once the initial condition and EoS are specified, the system of

ideal hydrodynamics equation in 2.2 and 2.3 is closed and the time evolution of the fluid cells can be calculated. As the system reaches $T < T_c$ the v_2 of the hadrons in the simulation can be deduced from azimuthal particle distributions. The v_2 data presented in Figure 2.2 was reproduced with ideal hydrodynamics calculations using an equation of state (EoS) which assumed a strong first-order phase transition (i.e. a long-lived mixed phase), and a Glauber initial condition.

As noted, practitioners of both viscous and ideal relativistic hydrodynamics calculations need to chose an initial condition and EoS in their simulations. Recent investigations by lattice QCD indicate that the QCD transition is not likely a first-order phase transition but a crossover [19]. If one uses the currently favored CGC initial conditions with a Lattice-inspired EoS, ideal hydrodynamics would yield v_2 values that are too large relative to the RHIC data [51]. If viscous effects were included, the elliptic flow would be reduced. This implies that although signatures of ideal fluid like behavior were found in the RHIC data, more work needs to be performed to quantify the small, but finite, viscosity in the QGP phase, and to quantify the hadronic viscous effects.

2.1.4 Hybrid Ideal and Microscopic Transport Approaches

Since ideal hydrodynamics calculations assumes zero viscosity for both the deconfined and hadronic phases of a heavy ion reaction, and using currently favored GCG initial conditions and a more realistic EoS for ideal hydrodynamics yield v_2 values that are too large, alternative approach(es) need to be suggested which include viscous effects. One such approach suggested was to use a hybrid approach that uses ideal hydrodynamics to model the deconfined phase until T_c, then use a microscopic transport approach to model the system for $T < T_c$ [13, 66].

The advantages of the hybrid approach are that, in addition to incorporating viscous effects of the hadronic phase, there exists a self-consistent calculation of

freezeout, and the separation of chemical and kinetic freezeout is treated. Chemical and kinetic freezeout are discussed in the next subsection.

For such a model, one needs a proper prescription for treating the transition from the hydrodynamic regime to the microscopic transport regime, which is done via the Cooper Frye prescription. In the Cooper Frye prescription, a hypersurface of cells at the transition temperature gets translated into an ensemble of particles. A microscopic transport model such as UrQMD(discussed in detail in Chapter 4) then is used to propagate the particles in the hadronic phase. Freezeout occurs when the particles are "frozen out", or stop interacting.

The hybrid ideal hydro plus micro approach reproduces the v_2 data as shown in Figures 2.6 and 2.7, providing us with an additional indication that the viscous effects in the QGP phase have to be small.

2.1.5 Partial Chemical Equilibrium (PCE) Approach

When discussing freezeout, it is necessary to further distinguish between thermal freezeout and chemical freezeout. Thermal freezeout occurs when the momentum distributions of the particles cease to change as a function of time in a heavy ion reaction. Chemical freezeout occurs when the particle yields of the hadrons no longer change as a function of time in a heavy ion reaction. This separation in timescales between the thermal and chemical freezeout was discovered using two different types of analysis. The chemical freezeout temperature was extracted by performing a Statistical Model fit to the measured hadronic yields, whereas the thermal freezeout temperature is extracted by performing a Boltzmann fit to the momentum distributions of the particles. The temperatures corresponding to chemical and thermal freezeout are $T_{chem} \approx 160$ MeV and $T_{kin} \approx 130$ MeV, respectively. Practitioners of the PCE approach, such as Hirano, Rapp, and Heinz,[38, 46] use ideal hydrodynamics until the temperature reaches T_{chem}, then introduce species-dependent fugacity

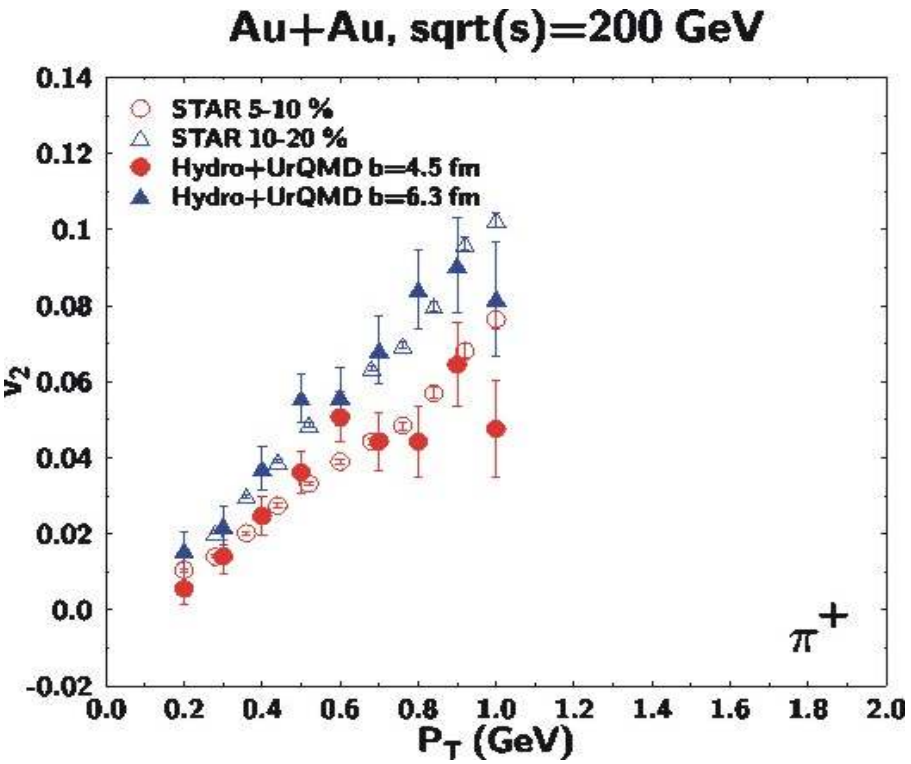

FIGURE 2.6: v_2 from a hybrid calculation as a function of transverse momentum p_T. The STAR data at different centralities are also shown for extracted π^+ v_2. The initial condition used in the hybrid hydrodynamics calculations is a CGC rather than Glauber initial condition [13].

effects to fix the particle yields from T_{chem} until T_{kin}. The yields N_i are given by

$$N_i = \frac{g_i V}{(2\pi)^3} \int_0^\infty d^3p \lambda_i \exp\left\{-\frac{\sqrt{p^2+m_i^2}}{T}\right\}, \tag{2.6}$$

where λ_i are the fugacities for the particle species i, g_i is the isospin multiplicity factor, V is the system volume, and T is the temperature. The condition for fixing the fugacities is obtained from the following constraint

$$\frac{n_i(T,\lambda_i)}{s(T,\lambda_i)} = \frac{n_i(T,\lambda_i=1)}{s(T,\lambda_i=1)}, \tag{2.7}$$

where n_i are the particle densities of species i and s is the total entropy density of the system. The constraint in equation 2.7 assumes that the hadrons follow an

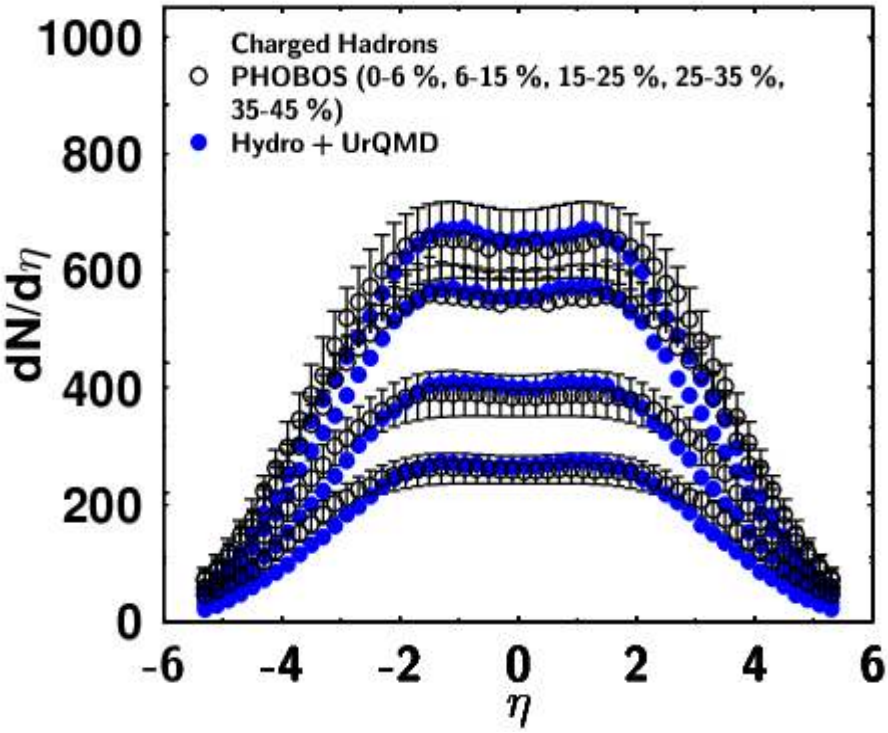

FIGURE 2.7: Pseudorapidity distribution for charged hadrons, taken from [13]. Both the hybrid hydrodynamics plots and data points are shown. The hybrid calculation uses aCGC initial condition, as opposed a Glauber condition.

adiabatic path for $T < T_c$. Note that as the system cools below $T = T_c$, the particle yields acquire nonunit fugacities ($\lambda_i > 1$), which means that the system, though maintaining kinetic equilibrium, evolves out of chemical equilibrium in the hadronic phase. This is an important effect, as we shall later show that introducing non-unit fugacities strongly affects η/s in the hadronic phase [25, 27].

2.2 "Ideal Fluid" versus "Most Perfect Fluid"

The definition of viscosity follows from the definition of expanding the energy-momentum tensor T_{ij} about its value in local equilibrium in terms of gradients of velocities. Specifically,

$$T^{\mu\nu} = T^{\mu\nu,\text{ideal}} + \Pi^{\mu\nu} \tag{2.8}$$

where $\Pi^{\mu\nu}$ is the shear viscous tensor, and $T^{\mu\nu}$ is the ideal fluid energy momentum tensor.

$$T^{\mu\nu,\text{ideal}} = (\epsilon + p)\, u^\mu u^\mu + p g^{\mu\nu}, \tag{2.9}$$

where ϵ is the energy density, p is the pressure, and u^μ is the flow four velocity. Solving the relativistic second order hydrodynamic equations of motion is nontrivial, and much discussion has taken place as to which of the higher order terms are important. For example, Luzum and Romatschke [51] use the following equation for the evolution of the shear viscous tensor:

$$\begin{aligned} \Pi^{\mu\nu} &= \eta\nabla^{<\mu}u^{\nu>} - \tau_\Pi\left[\Delta^\mu_\alpha\Delta^\nu_\beta D\Pi^{\alpha\beta} + \frac{4}{3}\Pi^{\mu\nu}\left(\nabla_\alpha u^\alpha\right)\right] \\ &+\frac{\kappa}{2}\left[R^{\mu\nu} + 2u_\alpha R^{\alpha<\mu\nu>\beta}u_\beta\right] \\ &-\frac{\lambda_1}{2\eta^2}\Pi^{<\mu}_\lambda\Pi^{\nu>\lambda} + \frac{\lambda_2}{2\eta}\Pi^{<\mu}_\lambda\omega^{\nu>\lambda} - \frac{\lambda_3}{2}\omega^{<\mu}_\lambda\omega^{\nu>\lambda}, \end{aligned} \tag{2.10}$$

where η is the shear viscosity, τ_Π is the Israel Stewart relaxation time, κ, λ_{1-3} are the second order Israel Stewart transport coefficients. $\omega_{\mu\nu} = -\nabla_{[\mu}u_{\nu]}$ is the fluid vorticity, and $R^{\alpha\mu\nu\beta}$ and $R^{\mu\nu}$ are the Riemann and Ricci tensors, respectively. Note that bulk viscosity terms are neglected. However, Song and Heinz[81, 82] attempted to investigate the influence of bulk viscosity in Israel Stewart viscous hydrodynamics by solving the following equations of motion [40, 41]:

$$d_\mu T^{\mu\nu} = 0 \tag{2.11}$$

$$T^{\mu\nu} = eu^\mu u^\nu - (p+\Pi)\Delta^{\mu\nu} + \pi^{\mu\nu}, \tag{2.12}$$

$$\Delta^{\mu\alpha}\Delta^{\nu\beta}D\pi_{\alpha\beta} = -\frac{1}{\tau_\pi}(\pi^{\mu\nu} - 2\eta\sigma^{\mu\nu}) \tag{2.13}$$

$$-\frac{1}{2}\pi^{\mu\nu}\frac{\eta T}{\tau_\pi}d_\lambda\left(\frac{\tau_\pi}{\eta T}u^\lambda\right), \tag{2.14}$$

$$D\Pi = -\frac{1}{\tau_\Pi}(\Pi + \zeta\theta) - \frac{1}{2}\Pi\frac{\zeta T}{\tau_\Pi} d_\lambda \left(\frac{\tau_\Pi}{\zeta T} u^\lambda\right), \tag{2.15}$$

Here, $T^{\mu\nu}$ is the energy momentum tensor, $\pi^{\mu\nu}$ is the shear pressure tensor, and Π is the bulk pressure. d_μ denotes the covariant derivative components (see [36, 60] for details) in the curvilear coordinates (τ, x, y, η_s) where $\tau = \sqrt{t^2 - z^2}$ is the longitudinal proper time and $\eta_s = \frac{1}{2}\ln\frac{t+z}{t-z}$ is the space-time rapidity. The shear and bulk viscosities are η and ζ and their associated relaxation times τ_π and τ_Π, respectively. Approximating ideal fluid behavior traditionally means approximating $\Pi^{\mu\nu} = 0$, but we shall present two arguments how a real physical system cannot have a zero viscosity, and why the viscosity cannot be arbitrarily small.

2.2.1 Semiclassical Arguments

A standard result from kinetic theory is the relationship between the shear viscosity η and the mean free path λ_f of a representative particle in the medium [75].

$$\eta \approx \frac{1}{3} n \bar{p} \lambda_f, \tag{2.16}$$

where n is the number density of the medium and $\bar{p}$ is the mean momentum per particle in the medium. The mean free path can be expressed in terms of the scattering cross section σ of the medium

$$\lambda_f = \frac{1}{n\sigma} \tag{2.17}$$

implying

$$\eta \approx \frac{\bar{p}}{3\sigma} \tag{2.18}$$

the unitarity bound from quantum mechanics implies a maximum on the cross section, which yields a minimum for the shear viscosity. Specifically, Gyulassy and

Danielewicz [23] suggested that the smallest mean free path making sense in a quasi-particle description of a system is the DeBroglie wavelength, implying $\lambda_f \sim \frac{1}{p}$. It is interesting to investigate what the corresponding dimensionless quantity (in mass dimensions) would be for such a system, as often dimensionless quantities give one a more quantitative sense of the comparison of key energy or length scales in the system. Note that η and s, the entropy density, have the same dimensions if $\hbar = c = k_B = 1$. For an ideal gas of massless particles, $s \sim 4n$ (the coefficient is 3.6 for Bosons and 4.2 for Fermions), implying that the minimum viscosity to entropy density ratio for such a system would be

$$\eta/s \approx \frac{1}{12}. \tag{2.19}$$

2.2.2 The KSS Bound via AdS/CFT Correspondence

Calculating transport coefficients in QCD using effective kinetic theory in the perturbative limit is a well-established technique. However, perturbation theory only works when the QCD coupling is small. The well-known Arnold, Moore, and Yaffe (AMY) formalism derives the shear viscosity coefficient by solving the linearized Boltzmann equation with temperature dependent scattering amplitudes derived from finite temperature QCD perturbation theory. The AMY result for η/s for a system of 3 light quarks and gluons is [7]

$$\frac{\eta_C}{s} \approx \frac{5}{g^4 log(1/g)}. \tag{2.20}$$

For quantities of interest at RHIC, the coupling is not small (especially near $T \approx T_c$) and hence nonperturbative techniques must be used. An important discovery in the field of string theory was the anti-deSitter Space/Conformal Field Theory (AdS/CFT) correspondence[52]. The idea is that for every CFT there exists a gravity dual on a 5 dimensional AdS space. Although QCD is not a CFT, $\mathcal{N} = 4$ Supersymmetry Yang Mills (SUSY) theory is a CFT, which means that in addition

to not having a running coupling, no spontaneous symmetry breaking or deconfinement is exhibited. $\mathcal{N}$ is the number of supersymmetric generators. Below $T = T_c$, QCD exhibits confinement and spontaneous breaking of chiral symmetry. However, above $T = T_c$, the quarks become deconfined, and chiral symmetry is restored, so although the coupling still runs, QCD and $\mathcal{N} = 4$ SUSY become more similar. One should take great caution in making too close a comparison between the two even in the limit $T \approx T_c^+$. What has been useful is that calculations of transport coefficients which are very difficult in QCD can be performed relatively easily in $\mathcal{N} = 4$ SUSY via the AdS/CFT correspondence.

The mapping of physical quantities using the AdS/CFT correspondence is that the temperature of the dual field theory is the Hawking temperature of the black hole in the corresponding AdS_5 theory, and the entropy of the dual field theory is the entropy of the black brane in the corresponding AdS_5 theory. According to Bekenstein [15], the largest entropy one could reach in the infinite volume limit is that the entropy is proportional to the area of the event horizon in the black hole of the theory, given by

$$S = \frac{A}{4G}, \tag{2.21}$$

where G is Newton's constant. For black branes A contains a trivial infinite factor V equal to the spatial volume along directions parallel to the horizon. Hence the entropy density s is equal to $a/4G$, where $a \equiv A/V$. In a rotationally invariant field theory, the formula for the shear viscosity of a system is given by Kubo's formula, which is to be discussed in Chapter 3

$$\eta = lim_{\omega \to 0} \frac{1}{2\omega} \int dt dx e^{i\omega t} \langle [T_{xy}(t,x), T_{xy}(0,0)] \rangle, \tag{2.22}$$

where T_{xy} is the xy component of the energy-momentum tensor. The physical interpretation of the viscosity in this AdS/CFT corresponding calculation is that the

right hand side of the Kubo formula for the shear viscosity can be related to the absorption cross section of gravitons. According to the formalism of Klebanov [45], the absorption cross section of a graviton of frequency ω, polarized in the xy direction propagating in a direction transverse to the brane is given by

$$\sigma_{abs}(\omega) = \frac{8\pi G}{\omega} \int dt dx e^{i\omega t} \langle [T_{xy}(t,x), T_{xy}(0,0)] \rangle. \tag{2.23}$$

This implies

$$\eta = \frac{\sigma_{abs}(0)}{16\pi G}. \tag{2.24}$$

The absorption cross section is constrained by a theorem stating that in the low-frequency limit $\omega \to 0$, the cross section is equal to the area of the horizon, $\sigma_{abs} = a$. This implies the minimum shear viscosity to entropy density ratio is

$$\frac{\eta}{s} = \frac{1}{4\pi}, \tag{2.25}$$

the famous Kovtun-Son-Starinets (KSS) bound [47]. It is important to note that while "ideal fluid" like behavior has been discovered at RHIC, it is not the shear viscosity of the discovered matter which is expected to be small, but rather η/s which is expected to be very small. Supporting evidence for ideal fluid like behavior are now to be given.

2.2.3 Relativistic Viscous Hydrodynamics

Writing the full spatial and temporal components of the momentum tensor, one would write

$$T^{\mu\nu} = \epsilon u^\mu u^\nu - p\Delta^{\mu\nu} + \Pi^{\mu\nu}, \tag{2.26}$$

where $\Delta^{\mu nu} = g^{\mu\nu} - u^\mu u^\nu$, ϵ is the energy density, and $\Pi^{\mu\nu}$ is the viscous shear tensor, and u is the flow velocity. Whereas Navier-Stokes hydrodynamics goes to

only first derivatives in the flow velocity in its expression for $\Pi^{\mu\nu}$, Israel-Stewart Hydrodynamics goes to higher order, as seen in equations 2.8 and 2.10.

Often, the second order transport coefficients defined in equation 2.10 are set to zero to facilitate the calculation, and a crucial parameter is the so-called Israel Stewart relaxation time (τ_Π as defined in equation 2.10). Bulk viscosity terms are neglected in some calculations.

The relativistic hydrodynamics calculations by Luzum and Romatschke [51] reproduce the PHOBOS v_2 data with values of η/s ranging from 0.08-0.16 or 0.16-0.24 depending upon whether one uses an extreme version of a Glauber or a CGC initial condition (Figures 2.9 and 2.8, respectively.) The parameters for the CGC and Glauber initial conditions were tuned to the most extreme allowable to investigate what range of η/s would be allowed. Bulk viscosity was neglected in the calculations in the CGC and Glauber initial conditions by Luzum and Romatschke [51]. The same lattice-based EoS is used for both calculations. However, such calculations assume a fixed value of η/s throughout the whole evolution. We shall see later that there is a strong temperature dependence of η/s in a heavy ion collision [21, 27].

2.3 Theoretical Understanding of η/s Behavior

2.3.1 Lattice Calculations

Calculating η/s on the lattice using the Kubo formulae is a challenge due to the difficulties associated with working with a Euclidean as opposed to Minkowski metric. First calculations of η/s, as well as ζ/s using lattice techniques have been performed by Meyer [56, 57]. However, in order to make progress on extracting robust quantitative predictions of transport coefficients from lattice calculations, the calculations must be performed on spatial volumes greater than 10^3 time the number of lattice sites used in current calculations [68].

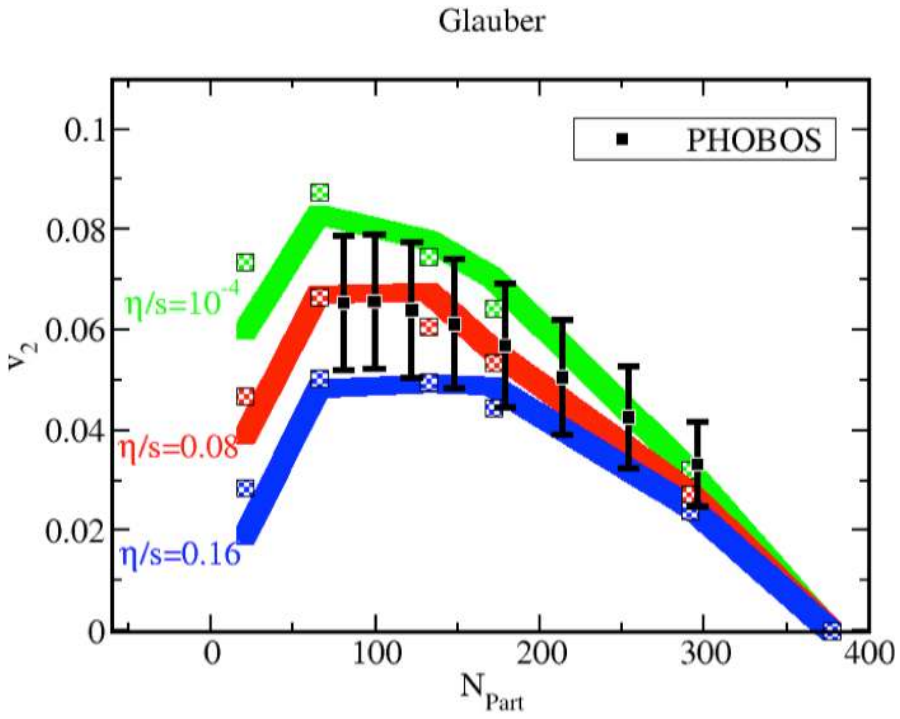

FIGURE 2.8: v_2 as a function of p_T for an extreme implemention of a CGC initial condition for a viscous hydro calculation, taken from [51]. The PHOBOS data are also shown. This was used to indirectly obtain a range of allowable values for η/s.

2.3.2 Parton Recombination

Ideal and viscous hydrodynamics analysis of the large v_2 values observed at RHIC show that matter with very low η/s was created at RHIC. The recombination model provided strong evidence that was of a partonic origin. In fact, it was named the "smoking gun" for the production of a QGP at RHIC [30].

The recombination model is a very simple picture in which the previously deconfined partons recombine into hadrons at T_c [30, 31]. It also predicts that the elliptic flow of hadrons likewise should scale with the elliptic flow of constituent quarks, such that

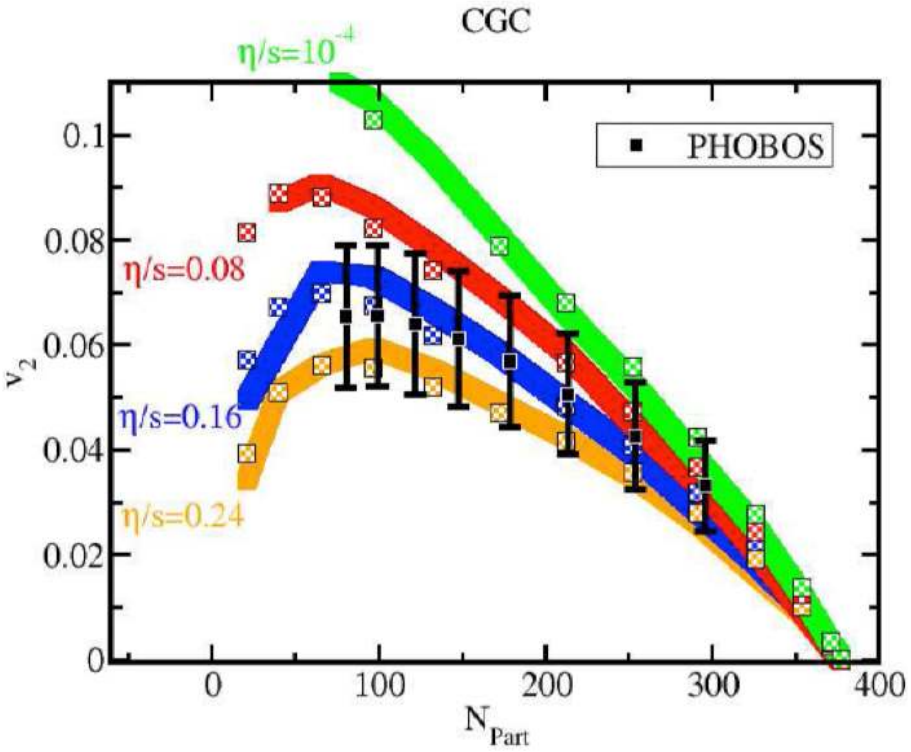

FIGURE 2.9: v_2 as a function of p_T for the Glauber initial condition for a viscous hydro calculation, taken from [51]. The PHOBOS data are also shown. This was used to indirectly obtain a range of allowable values for η/s.

$$v_{2,M}(p_T) = \frac{2v_2(\frac{p_T}{2})}{1 + 2v_2^2(\frac{p_T}{2})} \tag{2.27}$$

and

$$v_{2,B}(p_T) = \frac{3v_2(\frac{p_T}{3}) + 3v_2^3(\frac{p_T}{3})}{1 + 6v_2^2(\frac{p_T}{2})} \tag{2.28}$$

Note that since typically values for v_2 of interest are on the order of $\approx$ 10 %, neglecting the cubic and quadratic terms in equations 2.27 and 2.28 yield

$$v_{2,M}(p_T)/2 \approx v_2\left(\frac{p_T}{2}\right) \tag{2.29}$$

$$v_{2,B}(p_T)/3 \approx v_2\left(\frac{p_T}{3}\right) \tag{2.30}$$

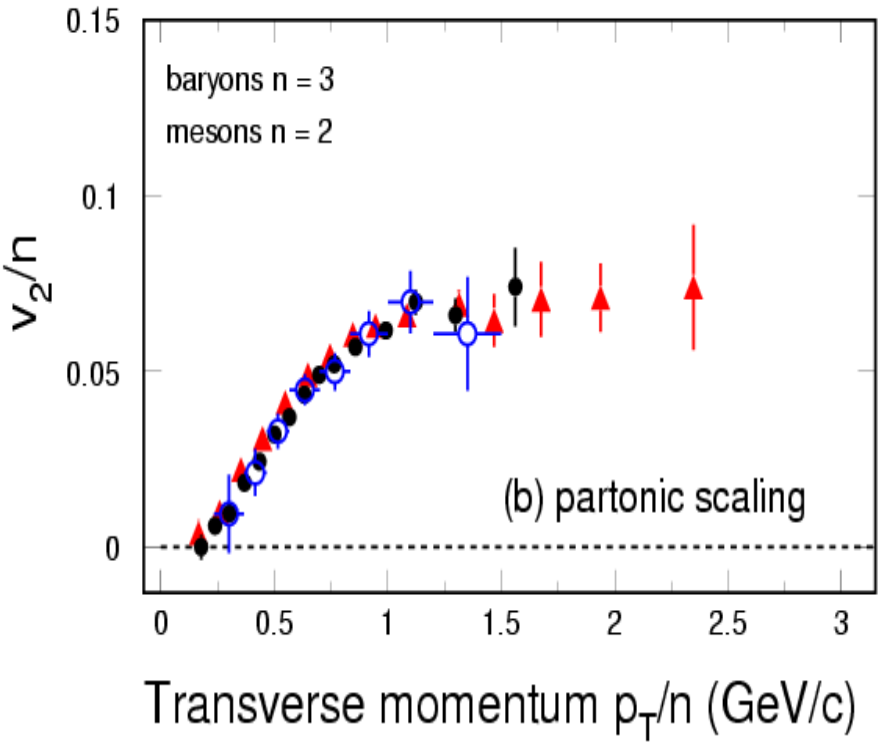

FIGURE 2.10: v_2 scaled by constituent quark number vs p_T scaled by constituent quark number. Taken from [31].

Since the momentum of the hadron should be equal to the sum of the momenta of the constituent quarks, scaling behavior would be observed if v_2 and transverse momenta p_T were simultaneously scaled by the number of constituent quarks. The scaling behavior shown in Figure 2.10 is a sign that the elliptic flow was most likely of partonic rather than hadronic origin. The observation of recombination scaling laws in v_2 data also suggest that the QGP matter at T_c consists of flowing constituent quarks, namely that the QGP at T_c was quasiparticulate in nature.

2.4 Structure of η/s above and below T_c

Now that is has been established that the QGP has a low value of η/s, one asks the question what do traditional QCD techniques yield for η/s? The most sophisticated

calculations for η/s in perturbative QCD from Arnold, Moore, and Yaffe yield

$$\frac{\eta}{s} \approx \frac{5.12}{g^4 log(2.42/g)}, \tag{2.31}$$

which, taken with a temperature dependent coupling, yields values of $\eta/s \approx 1-3$ for appropriate values in the perturbative limit [6]. Such values are much larger than what viscous hydrodynamics calculations constrain η/s to be in the deconfined phase. Since perturbative QCD predicts a large value of η/s in the weak coupling limit, one has to ask the question how does hadronic η/s behave? The result for η/s of a pure pion gas of chiral (massless) pions is

$$\eta/s = \frac{15}{16\pi}\left(\frac{f_\pi}{T}\right)^4. \tag{2.32}$$

η/s for chiral pions, and 3 flavor pQCD is illustrated in Figure 2.11 [73]. Note that the behavior of η/s is unknown near T_c, but a potentially rich structure is observed in other substances such as water and helium, with a possible minimum in η/s existing near T_c. This feature could be a more universal feature of classes of phase transitions, as one observes a similar structure in Figures 2.12 and 2.13 for water and helium, respectively [21]. If one examines Figure 2.11, one sees that for $T \gg T_c$, η/s is expected to be large, whereas the behavior becomes unknown (but suspected to be very small) near $T \approx (1-2)T_c$. η/s then is expected to become much larger in the hadronic phase, although the behavior is unknown again near $T \approx T_c^-$. In order to constrain η/s of the QGP, one must work to unmask the highly dissipative effects in the hadronic phase from the QGP phase. This provides the motivation for a my calculations of η/s and ζ/s in UrQMD, to be discussed in Chapter 5.

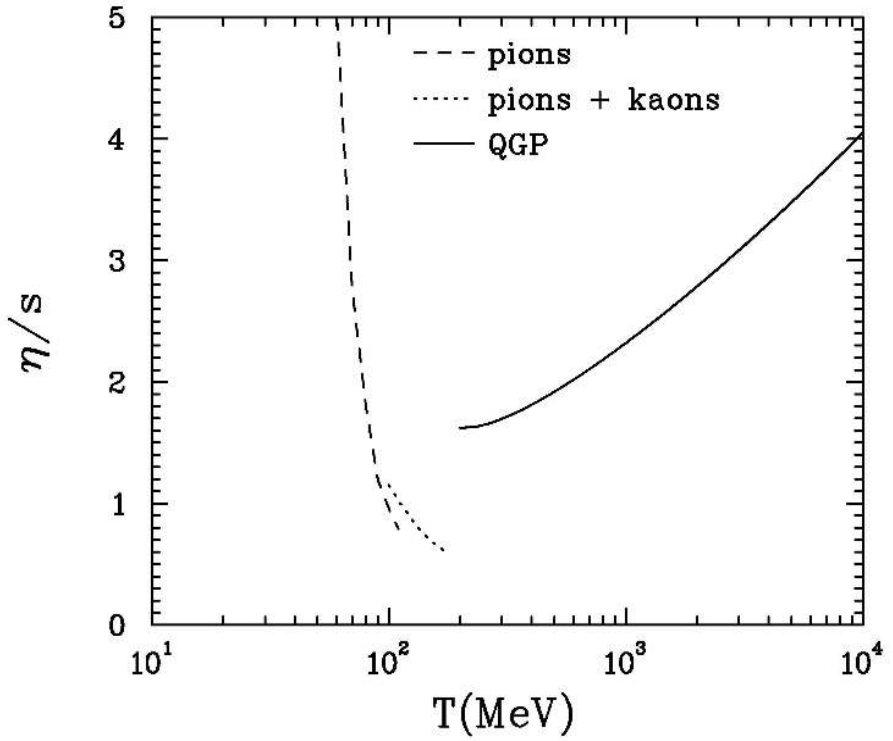

FIGURE 2.11: η/s versus temperature for chiral pions and pQCD, taken from [21].

2.5 Strongly Interacting QGP and an Alternative Explanation for low η/s

The signatures that the quark gluon plasma is a system exhibiting low η/s and large elliptic flow are plentiful and consistent with lattice calculations confirming large values of QCD coupling near T_c, and as a result a consensus has emerged in the RHIC community that the QGP is strongly interacting. However, an alternative explanation for low η/s is offered if one thinks about an anomalous viscosity. Before discussing the idea of the anomalous viscosity, we should note that there are some inconsistencies in the strongly interacting QGP (sQGP) picture.

Microscopic transport theory shows that assuming a quasiparticle description of quark and gluonic degrees of freedom would require unphysically large cross sections in order to be consistent with v_2 data. In Figure 2.14, a plot of v_2 as a function of

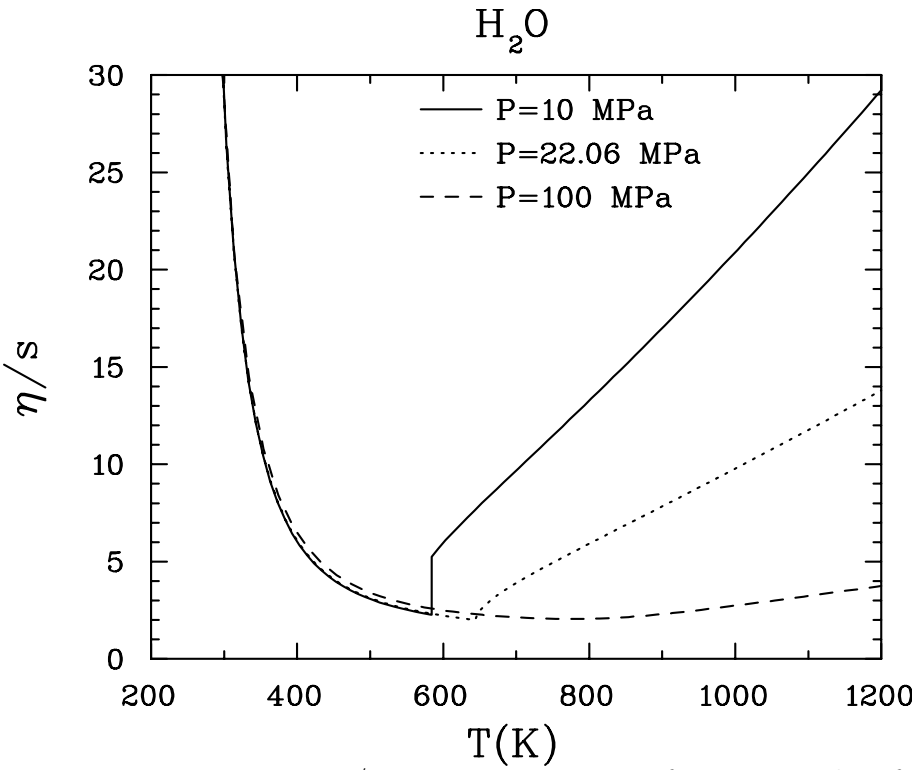

FIGURE 2.12: η/s versus temperature for water, taken from [21].

transverse momentum for various values of cross sections for elastic gluon-gluon collisions obtained from a microscopic transport model is illustrated. In order to agree with the STAR v_2 data, a value of $\sigma_{el} \approx 45$ mb needs to be used [58]. Perturbative QCD cross sections for the interactions among quarks and gluons are on the order of $\sigma \sim 1-3$ mb. Since unphysically large cross sections need to be used for a purely partonic transport model to match elliptic flow data, a quasiparticle description for the QGP seems inadequate, even though parton recombination suggests quarks as the proper degrees of freedom near T_c. Even for values of the mean free path close near the deBroglie wavelength, dissipative effects are too large to reproduce the desired v_2. This then must lead us to an alternative explanation for a system exhibiting low η/s, but devoid of a quasiparticle description for the QGP. We consider the idea of turbulent color fields generating a so-called "anomalous" viscosity. Anomalous viscosity is defined as any contribution to the shear viscosity originating from a source

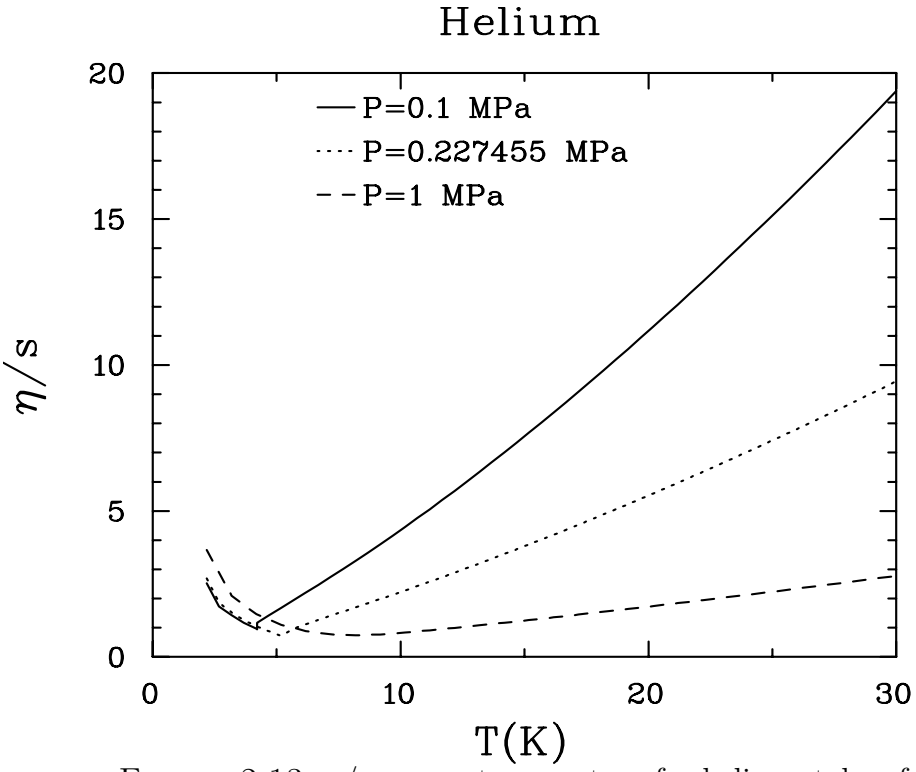

FIGURE 2.13: η/s versus temperature for helium, taken from [21].

that is not from transport cross sections. A necessary condition for the application of hydrodynamics to be applied to a medium is that the medium in question be thermal. Although the precise mechanism for the thermalization of the QGP has not been understood, the idea of plasma turbulence as a possible mechanism has been studied. A source for generating the plasma turbulence for the QGP is known as the Weibel instability [74]. It can be shown that an anomalous viscosity can result if two streams of opposing colliding color charges collide with a seed magnetic field present. Then the current induced due to the focusing and growing concentration of positive and negative charges induces a net current which creates a magnetic field constructively adding with the seed magnetic field. These fields then exponentially grow in time [76]. This can be calculated with non-Abelian Vlasov equations describing the interaction of high-p_T particles with soft color field modes that form the

basis for the "hard loop" effective theory. The coupled equations are

$$\frac{dp^\mu}{d\tau} = gQ^a F^{a\mu\nu} u_\nu \tag{2.33}$$

$$\frac{dQ^a}{d\tau} = g f_{abc} A^{b\nu} u_\nu Q^c \tag{2.34}$$

$$D_\mu F^{\mu\nu} = gJ^\nu, \tag{2.35}$$

where g is the QCD coupling, τ is the proper time, Q^a are the color charges ($a = 1, ..., N_c^2 - 1$), and $A^{b\nu}$ are the color gauges, and f_{abc} is the structure constant for the gauge, and

$$J^\nu = \sum_i \int d\tau Q_i(\tau) u_i^\nu \delta(x - x_i(\tau)) \tag{2.36}$$

are the currents for the moving point color charges. If one solves these coupled equations in a situation involving a medium with an anisotropic momentum distribution, unstable modes exist that grow exponentially. A derivation from [11, 10, 9], using linear response theory, yields the relationship between an anomalous viscosity η_A and the initial momentum anisotropy $\bar{\Delta}$ to be

$$\eta_A = -\frac{1}{15T} \int \frac{d^3p}{(2\pi)^3} \frac{\vec{p}^4}{E_p^2} \bar{\Delta}(p) \frac{\partial f_0}{\partial E_p}. \tag{2.37}$$

$\bar{\Delta}$ is defined through

$$f_1(p, r) = -\frac{\bar{\Delta}(p)}{E_p T^2} p_i p_j (\nabla u)_{ij}, \tag{2.38}$$

where f_1 is an introduced perturbation to the local distribution function, and

$$(\nabla u)_{ij} \equiv (\nabla_i u_j + \nabla_j u_i - \frac{2}{3}\delta_{ij} \nabla \cdot \vec{u}) \tag{2.39}$$

is the part of the flow gradient relevant to the shear viscosity coefficient. f_1 is related to the distribution function f and local equilibrium distribution function f_0 through

$$f(p, r) = f_0(p) \left[1 + f_1(p, r) \left(1 \pm f_0(p)\right)\right], \tag{2.40}$$

where the $+/-$ refers to Bose/Fermi systems respectively. For massless particles, $\bar{\Delta} = 5\eta/s$. If one assumes a boost invariant longitudinal expansion of the form

$$u_z = z/t, \tag{2.41}$$

then

$$f_1(p) = -\frac{\bar{\Delta}}{3E_p T^2 \tau}\left(3p_z^2 - p^2\right), \tag{2.42}$$

where $\tau = \sqrt{t^2 - z^2}$ is the proper time in local comoving coordinates. In order to investigate the response of a the plasma to such a perturbation to the distribution function, one should start by writing the Vlasov-Boltzmann equation, which is a transport equation for the phase space distribution of color charges Q^a in a color-magnetic field $\vec{B}^a$

$$\left[\frac{\partial}{\partial t} + \vec{v}\cdot\nabla_r + \vec{F}\cdot\nabla_p\right] f(r,p,t) = \mathcal{C}[f], \tag{2.43}$$

where

$$\vec{F} = gQ^a\left(\vec{E}^a + \vec{v}\times\vec{B}^a\right), \tag{2.44}$$

is the color Lorentz force, and $\mathcal{C}[f]$ is the collision term. To isolate the dissipative effects of the color field, one averages the particle trajectories over an ensemble of color-magnetic fields. Assuming $\langle B^a\rangle = 0$ and factorizing higher than second moments of the field distribution, one can show the ensemble averaged phase space distribution $\bar{f}$ satisfies the following equation

$$\left[\frac{\partial}{\partial t} + \vec{v}\cdot\nabla_r - \nabla_{i,p}D_{ij}(p,t)\nabla_{j,p}\right]\tilde{f} = \mathcal{C}[\tilde{f}], \tag{2.45}$$

with the effective diffusion tensor

$$D_{ij} = \int_{-\infty}^{t} dt' \langle F_i(\bar{r}(t'),t')F_j(\bar{r}(t),t)\rangle. \tag{2.46}$$

Recall that the energy momentum tensor T_{ij} gives the momentum density components of the system, and is defined through

$$T_{ij} = \int d^3p \frac{p_i p_j}{(2\pi)^3 E_p} f(p,r), \tag{2.47}$$

Inserting the expansion of f from 2.40 and 2.38into 2.47 yields

$$T_{ij} = T^{(0)}_{ij} + \delta T_{ij} = P\delta_{ij} + \epsilon u_i u_j - 2\eta \left(\nabla u\right)_{ij} - \zeta \delta_{ij} \nabla \cdot u \tag{2.48}$$

and hence

$$\begin{aligned} \delta T_{ij} &= \int d^3p \frac{p_i p_j}{(2\pi)^3 E_p} f_1(p) f_0(p) \left(1 \pm f_0(p)\right) && (2.49) \\ &= \frac{1}{T} \left(\nabla\right)_{mn} \int \frac{d^3p}{(2\pi)^3 E_p^2} p_i p_j \bar{\Delta}(p) p_m p_n \frac{\partial f_0}{\partial E_p} \\ &= -\eta \left(\nabla u\right)_{mn} \left[\delta_{im}\delta_{jn} + \delta_{in}\delta_{jm} + \delta_{ij}\delta_{mn}\right] && (2.50) \end{aligned}$$

yields

$$\eta = -\frac{1}{15T} \int \frac{d^3p}{(2\pi)^3} \frac{p^4}{E_p^2} \bar{\Delta}(p) \frac{\partial f_0}{\partial E_p}, \tag{2.51}$$

recapturing equation 2.37. If one assumes a decoherence time between magnetic fields at different times to be τ_{mag}, defined through

$$\int_{-\infty}^{t} dt' \langle B_i^a(t') B_j^b(t) \rangle \equiv \langle B_i^a B_j^a \rangle \tau_{mag} \tag{2.52}$$

then the authors of [11, 10, 9] find the anisotropy to be

$$\bar{\Delta}(p) = \frac{(N_c^2 - 1) E_p^2 T}{3 C_2 g^2 \langle B^2 \rangle \tau_{mag}}. \tag{2.53}$$

This then yields a relationship between the anomalous viscosity and field strength

$$\frac{\eta_A}{s} \propto \frac{T^6}{g^2 \langle B^2 \rangle \tau_{mag}} \tag{2.54}$$

where τ_{mag} is the decoherence time of the magnetic fields. The magnetic field strength is dependent upon ζ (NOT the bulk viscosity coefficient), which characterizes the anisotropy in a dimensionless fashion [76]. An ansatz is used for this dependence.

$$g^2\langle B^2\rangle \sim g^4 T^4 \zeta^n, \tag{2.55}$$

so that for a massless, dimensionless gas,

$$\zeta = 10\frac{\eta}{s}\frac{\nabla u}{T} \tag{2.56}$$

$$\frac{\eta_A}{s} = c_0\left(\frac{T}{g^2\nabla u}\right)^{3/5}, \tag{2.57}$$

where c_0 depends upon the constituents of the matter in question. The result for (collisional) shear viscosity derived in the weak coupling limit from QCD from AMY yields

$$\frac{\eta_C}{s} \approx \frac{5}{g^4 log(1/g)}. \tag{2.58}$$

For reasonable values for $g \approx 0.2 - 0.3$, $\eta_A/s < \eta_C/s$. Note that since $\eta \sim \frac{\bar{p}}{\sigma}$, and cross sections are additive,

$$1/\eta = 1/\eta_A + 1/\eta_C. \tag{2.59}$$

This suggests that the viscosity of the system is determined by the subsystem with the smaller viscosity. This smaller viscosity may be a field-induced anomalous viscosity, thus eliminating the necessity of using unphysically large binary scattering cross sections.

The uncertainty in values for η/s for Hot QCD matter in the strongly coupled region (or possibly weakly coupled region with small anomalous viscosity) highlight the need to perform a separate robust calculation of η/s in the hadronic phase.

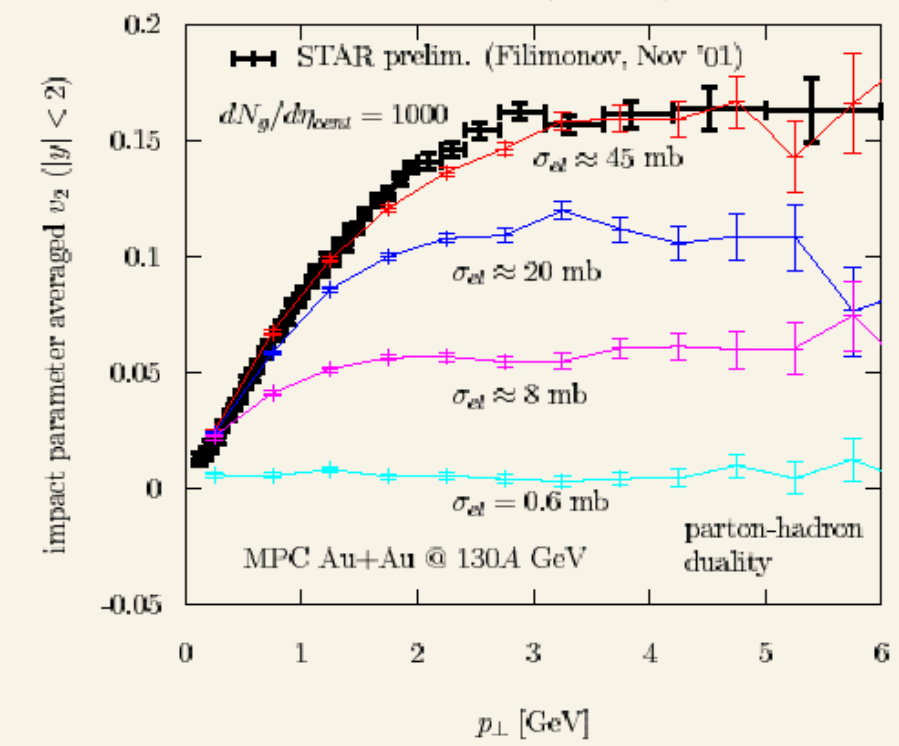

FIGURE 2.14: v_2 versus p_T from Molnar for a partonic microscopic transport model. Very large cross sections need to be used to reproduce v_2 elliptic flow data if one assumes simple binary scattering in a QGP [58].

3

Methods of Calculating Transport Coefficients

This chapter summarizes several of the standard approaches to calculate transport coefficients. Namely the approaches reviewed shall include the relaxation time approximation within the Boltzmann equation framework and the Green-Kubo formalism.

First, it is necessary to define transport coefficients. They are coefficients describing perturbations to the energy-momentum tensor in a system near local thermal equilibrium. They characterize expansion coefficients of the energy momentum tensor from its value in local thermal equilibrium. For example, to first order in velocity gradients:

$$T_{ij} = T_{ij,\text{local}} - \eta \left(\frac{\partial u_i}{\partial r_j} + \frac{\partial u_j}{\partial r_i} - \frac{2}{3}\delta_{ij}\vec{\nabla} \cdot \vec{u} \right) - \zeta \delta_{ij} \left(\vec{\nabla} \cdot \vec{u} \right), \tag{3.1}$$

where η is the shear viscosity, and ζ is the bulk viscosity. We shall discuss three standard methods to calculate transport coefficients in this chapter, and all of the following approaches have one feature in common. They assume that the system is sufficiently near equilibrium.

3.1 The Boltzmann Equation and Relaxation Times

The Boltzmann equation is a transport equation describing the full time evolution of the one-particle phase space distribution function f, which is a function describing the distribution of the particles' position and momenta assuming no ignoring interparticle correlations. The right hand side is an object known as the collision integral, which relates precollision distribution functions to postcollision distribution functions; inherent in the derivation is the assumption that particles only interact through scattering. In particular, the Boltzmann equation is derived from the following assumptions [50]:

- Particles in the medium only interact via scattering.
- The typical mean free paths of particles are long compared to the range of interaction.
- f is homogeneous over the range of interaction.
- Molecular chaos exists. Namely, that a two particle distribution function for a pair of particles can be factorized into the product of two one particle distribution functions, which assumes no interparticle correlation.

$$\left(\frac{\partial}{\partial t} + \frac{\vec{p}}{E} \cdot \vec{\nabla}\right) f = fZ^{+} - fZ^{-} \tag{3.2}$$

$fZ^{+/-}$ are the gain/loss terms, respectively. One should note that the Boltzmann equation (3.2) pertains to situations where one is not necessarily in or even near equilibrium. However, for the purposes of calculating transport coefficients, a technique has been developed known as the relaxation time approximation where one solves a linearized Boltzmann equation and expresses the shear and bulk viscosities

(as well as some other transport coefficients) in terms of a relaxation time. The term "relaxation time" by no means has a unique definition. We shall see that in fact that are several types of relaxation processes characterized by timescales and one has to be precise in defining the "relaxation time." For the purposes of the relaxation time approximation, the relaxation time is defined as a timescale characterizing the rate of change of the phase space distribution function. The relaxation time approximation is valid only for a system that is sufficiently close to thermal equilibrium.

Let us consider a specific example with a 2 body collision $12 \rightarrow 34$. We explicitly write the loss and gain terms in the Boltzmann equation for species 1:

$$f_1 Z_1^- = \frac{f_1}{2E_1} \sum_{2,3,4} \frac{g_2}{1+\delta_{12}} \int d\omega_2 d\omega_3 d\omega_4 \, (2\pi)^4 \, \delta^4 \left(k_1 + k_2 - k_3 - k_4\right) \mid T_{12\rightarrow 34} \mid^2 \, f_2 \tilde{f}_3 \tilde{f}_4 \tag{3.3}$$

$$\tilde{f}_1 Z_1^+ = \frac{\tilde{f}_1}{2E_1} \sum_{2,3,4} \frac{g_2}{1+\delta_{12}} \int d\omega_2 d\omega_3 d\omega_4 \, (2\pi)^4 \, \delta^4 \left(k_1 + k_2 - k_3 - k_4\right) \mid T_{34\rightarrow 12} \mid^2 \, \tilde{f}_2 f_3 f_4 \tag{3.4}$$

where $d\omega_i = d^3k_i / \left[(2\pi)^3 2E_i\right]$ is the Lorentz invariant phase space element of particle i, $\mid T_{12} \mid^2$ is the scattering probability, and f_i are phase space densities for species i, and $\tilde{f}_i$ are $1 \pm f_i$ for Bose/Fermi species, respectively. δ_{12} is unity for identical particles, 0 for distinguishable particles. For a system sufficiently near equilibrium, the phase space distribution for species 1 in the case above can be written as $f_1 = f_1^0 + \delta f_1$, where f^0 is the (local) equilibrium phase space distribution. The Boltzmann equation then linearized in the relaxation time approximation reads

$$\left(\frac{\partial}{\partial t} + \frac{\vec{p}}{E} \cdot \vec{\nabla}\right) f \approx \tilde{f}_1 Z^{+,0} - f_1 Z^{-,0} \equiv \frac{-\delta f_1}{\tau_1^r(k_1)}, \tag{3.5}$$

where τ_1^r, the distribution function relaxation time, is in principal momentum dependent. Hence the approximation occurs in the linearization, where the local equilibrium values of f are used to evaluate the gain and loss terms $Z^{+,-}$ [73]. For multiple scattering channels,

$$[\tau_1^r(k_1)]^{-1} = \sum_2 [\tau_{12}^r(k_1)]^{-1} . \tag{3.6}$$

Since the energy momentum tensor is constructed from the phase space distribution functions through

$$T_{ij}(x) = \int d^3p \frac{p^i p^j}{p^0} f(x,p), \tag{3.7}$$

one can derive expressions for the shear and bulk viscosities in the relaxation time approximation. The formulae for the shear and bulk viscosities using a momentum dependent relaxation time are

$$\eta = \frac{1}{15T} \sum_a \int \frac{d^3p}{(2\pi)^3} \frac{\tau_a p_a^4}{E_a^2} f_a^{eq}(E_a/T), \tag{3.8}$$

$$\zeta = \frac{1}{9T} \sum_a \int \frac{d^3p}{(2\pi)^3} \frac{\tau_a (E_a)}{E_a^2} \left[\left(1 - 3c_s^2\right) E_a^2 - m_a^2 \right]^2 f_a^{eq}(E_a/T), \tag{3.9}$$

where c_s^2 is the speed of sound squared [33]. For a perfectly conformal system, such as an ideal gas of massless particles, the bulk viscosity would vanish because $c_s^2 = 1/3$ for such a system.

3.1.1 Weinberg's Scaling Relation

Weinberg has derived similar results for a fluid consisting of a medium with a very short mean free path and mean free times, with radiation quanta (such as photons,

neutrinos, or gravitons for instance) with a finite mean free time τ. The results are

$$\zeta = 4bT^4\tau\left(\frac{1}{3} - c_s^2\right)^2 \tag{3.10}$$

$$\eta = \frac{4}{15}bT^4\tau, \tag{3.11}$$

where $b = \frac{8(7)}{15}\pi^5$ for bosonic(fermionic) radiative quanta [87]. The bulk viscosity vanishes for $c_s^2 = 1/3$ as desired, and note that in equation 3.9, in the limit of massless particles, equation 3.10 is recovered, with the distribution relaxation time happening to coincide with the radiative quanta mean free time in Weinberg's derivation. Hence, the Weinberg scaling viscosity law becomes

$$\zeta = 15\left(\frac{1}{3} - c_s^2\right)^2 \eta. \tag{3.12}$$

This scaling law might be accurate for a hadronic system of purely chiral pions, but is not expected to hold for a system of massive pions. The next formalism to be discussed involves calculating linear transport coefficients from correlation functions of fluctuations of dissipative fluxes near equilibrium.

3.2 Linear Response Theory: The Kubo/Green-Kubo Formalisms

The presentation of the Kubo formalism here is motivated by the discussion in Zubarev [90]. There exists a systematic method to extract linear transport coefficients by calculating correlation functions of fluctuations of fluxes perturbing a system that is near equilibrium. We begin by defining the statistical operator (also known as the distribution function) for both equilibrium and nonequilibrium systems. The statistical operator, ρ_ℓ, for an equilibrium system is given by

$$\rho_\ell = Q_\ell^{-1}\exp\left\{-\int dx\beta(x)\left[H^{'}(x) - \sum_i \mu_i(x)n_i^{'}(x)\right]\right\}, \tag{3.13}$$

where

$$Q_\ell = \mathrm{Tr}\exp\left\{-\int \mathrm{dx}\beta(\mathrm{x})\left[\mathrm{H}^{'}(\mathrm{x}) - \sum_{\mathrm{i}} \mu_{\mathrm{i}}\mathrm{n}_{\mathrm{i}}^{'}(\mathrm{x})\right]\right\} \tag{3.14}$$

is the partition function, $H(x)$ is the Hamiltonian density of the system, μ_i are the chemical potentials of constituent particle species, and $n_i^{'}(x)$ are the constituent particle densities.

The statistical operator of a nonequilibrium system, is defined as follows

$$\begin{aligned} \rho &= Q^{-1}\exp\left\{-\sum_m \int [F_m(x,t)P_m(x)\right. \qquad (3.15)\\ &\quad -\int_{-\infty}^{0} e^{\epsilon t_1}\left(j_m(x,t_1)\cdot\nabla F_m(x,t+t_1)\right.\\ &\quad \left.\left.+P_m(x,t_1)\frac{\partial F_m(x,t+t_1)}{\partial t}\right)dt_1\right]dx\Bigg\} \qquad (3.16)\end{aligned}$$

where $F_0(x,t) = \beta(x,t)$, $P_0(x) = H(x)$, $F_1(x,t) = -\beta(x,t)v(x,t)$, $F_{i+1,}(x,t) = -\beta(x,t)\left(\mu_i(x,t) - (\sqrt{\vec{p^2}_i + m_i^2} - m_i)\right)$, $P_1 = p(x)$ is the pressure, $P_{i+1}(x) = n_i(x)$ are number densities, $j_0(x) = j_H(x)$, $j_1(x) = T(x)$, and $j_{i+1}(x) = j_i(x)$ the number currents. β is the inverse temperature and T is the relevant momentum flux for shear or bulk viscosity. It is possible to generalize equation 3.15 to speak of general thermodynamic fluxes. This is useful because the Kubo formalism is generalized to transport coefficients for any relevant transport quantity.

We can rewrite equation 3.15 so that the statistical operator for a nonequilibrium system with thermodynamic force perturbations X_m and corresponding operators of thermal, viscous, and diffusional fluxes j^m is then

$$\rho = Q^{-1}exp\left\{-\sum_m \int\left(F_m(x,t)P_m(x) - \int_{-\infty}^{0} e^{\epsilon t_1} j^m(x,t_1)\cdot X_m(x,t+t_1)dt_1\right)dx\right\}. \tag{3.17}$$

For example, j^m may represent the viscous fluxes and X_m the velocity gradient, since transport coefficients are defined as coefficients of the terms perturbing the energy momentum tensor from local equilibrium. Viscous fluxes involve momentum transport and viscosities are coefficients of terms involving gradients in flow velocity, thermal fluxes involve heat transport and are coefficients involving gradients in temperature, and diffusional fluxes involve particle density transport and involve gradients in number concentration.

It is possible to rewrite ρ so that we may eventually expand in a series,

$$\rho = Q^{-1} e^{-A-B}, \tag{3.18}$$

where

$$A = \sum_m \int F_m(x,t) P_m(x) dx \tag{3.19}$$

and

$$B = -\sum_m \int \int_{-\infty}^{0} e^{\epsilon t_1} j^m(x,t_1) \cdot X_m(x, t+t_1) dx dt_1. \tag{3.20}$$

Introducing the operator $K(\tau)$, defined by

$$e^{-(A+B)\tau} = K(\tau)\, e^{-A\tau} \tag{3.21}$$

then implies that

$$K(\tau) = 1 - \int_0^{\tau} K(\tau_1)\, e^{-A\tau} B e^{A\tau_1} d\tau_1 \tag{3.22}$$

subject to the initial condition K(0)=1.

Iterating this equation, we then expand to linear order in B

$$e^{-(A+B)} = e^{-A} - \int_0^1 e^{-A\tau} B e^{A\tau} e^{-A} d\tau, \tag{3.23}$$

This then leads to

$$\rho = \frac{-A - \int_0^1 e^{-A\tau} B e^{A\tau} e^{-A} d\tau}{\mathrm{Tr}\left(\mathrm{e}^{-\mathrm{A}}\right) - \int_0^1 \mathrm{Tr}\left(\mathrm{e}^{-\mathrm{A}\tau}\mathrm{B}\mathrm{e}^{\mathrm{A}\tau}\mathrm{e}^{-\mathrm{A}}\right) \mathrm{d}\tau} \tag{3.24}$$

$$\rho \approx \left(1 - \int_0^1 \left(e^{-A\tau} B e^{A\tau} - \langle e^{-A\tau} B e^{A\tau} \rangle_\ell\right) d\tau\right) \rho_\ell, \tag{3.25}$$

where $\rho_\ell = \frac{e^{-A}}{\mathrm{Tr}e^{-\mathrm{A}}}$, and $\langle ... \rangle_\ell = Tr\left(\rho_\ell ...\right)$ denotes the averaging with the local-equilibrium distribution.

By means of the above, we obtain the following relationship between fluxes and thermodynamic relations:

$$\langle j^m(x) \rangle = \langle j^m(x) \rangle_\ell + \sum_n \int \int_{-\infty}^t e^{\epsilon(t-t')} \left(j^m(x), j^n(x', t'-t)\right) \cdot X_n(x', t') dt' dx', \tag{3.26}$$

where

$$\left(j^m(x), j^n(x', t)\right) \equiv \beta^{-1} \int_0^\beta \left\langle j^m(x) \left(j^n(x', t, i\tau) - \langle j^n(x', t) \right\rangle_\ell \right) \rangle_\ell d\tau \tag{3.27}$$

are the quantum time correlation functions of $j^n(x', t') = e^{-\beta^{-1}A\tau} j^n(x', t) e^{\beta^{-1}A\tau}$. The linear relations above between the fluxes and thermodynamic forces are retarded and nonlocal.

Suppose the thermodynamic forces depend periodically on the time, with frequency ω, $X_n(x', t') = X_n(x') cos\omega t'$. Then

$$\langle j^m(x) \rangle = \langle j^m(x) \rangle_\ell + \sum_n Re e^{i\omega t} \int \int_{-\infty}^t e^{\epsilon\left(t'-t\right)} \left(j^m(x), j^n(x', t'-t)\right) \cdot X_n(x') e^{i\omega(t'-t)} dt' dx' \tag{3.28}$$

The Fourier components of the quantum correlation functions are the transport coefficients in the above equations. Taking retardation into account leads to dispersion of the kinetic coefficients. Neglecting retardation in 3.28, we can take the thermodynamic forces at time $t^{'} = t$ outside the integral over time. Hence we are inherently assuming that the thermodynamic period/response times are much greater than the correlation decay times. Applying this assumption then allows us to obtain linear relations between ther thermodynamic forces and fluxes without retardation, but nonlocal in character:

$$\langle j^m(x)\rangle = \langle j^m(x)\rangle_\ell + \sum_n \int L_{mn}(x, x^{'}) \cdot X_n(x^{'}, t) dx^{'}, \tag{3.29}$$

where

$$L_{mn}(x, x^{'}) = \int_{-\infty}^{0} e^{\epsilon t} \left(j^m(x), j^n(x^{'}, t) \right) dt \tag{3.30}$$

are the transport coefficients.

If one makes a further assumption of locality, implying that thermodynamic forces vary very little over the correlation length of $L_{mn}(x, x^{'})$, then we can write

$$\langle j^m(x)\rangle = \langle j^m(x)\rangle_\ell + \sum_n L_{mn}(x) \cdot X_n(x), \tag{3.31}$$

where $L_{mn}(x) = \int L_{mn}(x, x^{'}) dx$.

Hence for the viscous and diffusional fluxes, respectively, we obtain

$$\langle T^{'}\rangle = \langle T^{'}\rangle_\ell + \sum_n \int L_{1n}(x, x^{'}) \cdot X_n(x^{'}, t) dx^{'} \tag{3.32}$$

and

$$\langle j_i^{'} \rangle = \langle j_i^{'} \rangle_\ell + \sum_n \int L_{in}(x, x^{'}) \cdot X_n(x^{'}, t) dx^{'} \tag{3.33}$$

since viscosity and diffusion refer to momentum and number density transport, respectively. The fluxes represent perturbations to local equilibrium of a system and the transport coefficients L_{in} and thermodynamic forces X_n representing the small perturbations. In order to obtain the explicit expressions for the shear and bulk viscosities, it is helpful to look at entropy production in nonequlibrium processes. One shall define the entropy of the nonequlibrium state as the entropy of the corresponding local equlibrium state given by the density operator

$$\rho_\ell = Q_\ell^{-1} \exp - \sum_m \int F_m(x, t) P_m(x) dx, \tag{3.34}$$

and from the statistical definition of entropy, $S = -\langle \rho \rangle_\ell$, implying

$$S = \phi + \sum_m \int F_m(x, t) \langle P_m(x) \rangle dx, \tag{3.35}$$

where $\phi = log Q_\ell$.

It is then possible to show

$$\frac{\partial S(x)}{\partial t} = -\nabla \cdot j_S(x) + \sigma(x) \tag{3.36}$$

where

$$j_S(x) = \sum_m F_m(x, t) \langle j_m(x) \rangle + \beta(x) v(x, t) p(x) \tag{3.37}$$

is the entropy flux density, and

$$\sigma(x) = \sum_m \left(\langle j_m(x)\rangle - \langle j_m(x)\rangle_\ell\right) \cdot \nabla F_m(x,t) \tag{3.38}$$

is the local entropy production.

Writing the local entropy production in terms of the thermodynamic forces X_m:

$$\sigma(x) = \sum_m \left(\langle j_m(x)\rangle - \langle j_m(x)\rangle_\ell\right) \cdot \nabla F_m = \sum_m \left(\langle j^m(x)\rangle - \langle j^m(x)\rangle_\ell\right) \cdot X_m(x). \tag{3.39}$$

We introduce some definitions as follows by decomposing the viscous stress tensor $\pi = T(x) - \langle T(x)\rangle_\ell$. As a result, one can write linear transport coefficient relations separately for vector, tensor, and scalar processes:

$$\langle j_Q\rangle = -L_{00} \cdot \frac{\nabla T}{T^2} - \sum_{i=1}^{l} L_{0i} \cdot \nabla\left(\frac{\mu_i}{T}\right), \tag{3.40}$$

$$\langle \mathring{\pi}\rangle = -\frac{L_{11}^{(1)}}{T} \cdot \left(\mathring{\nabla} v\right) \tag{3.41}$$

$$\langle \Pi\rangle = \frac{1}{3}\sum_{\alpha=1}^{3}\langle \pi_{\alpha\alpha}\rangle = -\frac{L_{11}^{(2)}}{T}\nabla \cdot v, \tag{3.42}$$

where the circle denotes tracelessness.

This implies

$$L_{11}^{(1)} = \int\int_{-\infty}^{0} e^{\epsilon t}\left(\mathring{T}(x), \mathring{T}(x^{'}, t)\right) dx^{'} dt \tag{3.43}$$

and

$$L_{11}^{(2)} = \int\int_{\infty}^{0} e^{\epsilon t}\left(p(x), p(x^{'}, t) - \left(\frac{\partial p}{\partial u_n}\right) H(x^{'}, t) - \sum_i \left(\frac{\partial p}{\partial n_{i\,u}}\right) n_i(x^{'}, t)\right) dx^{'} dt \tag{3.44}$$

If we are considering an isotropic medium, then the relations can be simplified and correlation functions constructed from vectors or tensors have the form of scalars multiplied by unit tensors:

$$L_{00}^{\mu\nu} = L_0 \delta_{\mu\nu} \tag{3.45}$$

$$L_{0i}^{\mu\nu} = L_{i0}^{\mu\nu} = L_i \delta_{\mu\nu} \tag{3.46}$$

$$L_{11}^{(1)\mu\nu\mu_i\nu_i} = \frac{L_1^{(1)}}{2}\left(\delta_{\mu\mu_i}\delta_{\nu\nu_i} + \delta_{\mu\nu_i}\delta_{\nu\mu_i} - \frac{2}{3}\delta_{\mu\nu}\delta_{\mu_i\nu_i}\right) \tag{3.47}$$

Comparing this with our earlier definitions of shear and bulk viscosities η and ζ, we find

$$\begin{aligned} \eta &= \frac{L_1^{(1)}}{2T} = \frac{1}{10T}\int\int_{-\infty}^{0} e^{\epsilon t}\left(\mathring{T}(x), \mathring{T}(x^{'}, t)\right) dx^{'} dt \qquad (3.48) \\ &= \frac{1}{T}\int\int_{-\infty}^{0} e^{\epsilon t}\left(T_{xy}(x), T_{xy}(x^{'}, t)\right) dx^{'} dt \\ &= \frac{1}{T}\int\int_{-\infty}^{0} e^{\epsilon t}\langle T_{xy}(x), T_{xy}(x^{'}, t)\rangle dx^{'} dt \qquad (3.49) \end{aligned}$$

since $\langle T_{xy}(x)\rangle_\ell = 0$.

The formula for bulk viscosity is then

$$\zeta = \frac{L_{11}^{(2)}}{T} = \int\int_{-\infty}^{0} e^{\epsilon t}\left(p(x), p(x^{'}, t) - \left(\frac{\partial p}{\partial u}_n\right) H(x^{'}, t) - \sum_i \left(\frac{\partial p}{\partial n_i}_u\right) n_i(x^{'}, t)\right) dx^{'} dt \tag{3.50}$$

If one neglects the term involving particle number fluctuations, then

$$\zeta = \frac{1}{T}\int\int_0^\infty e^{\epsilon t}\langle\tilde{P}(0,0)\tilde{P}(x,t)\rangle dxdt, \tag{3.51}$$

where $\tilde{P} = \frac{1}{3}\left(T_{xx}+T_{yy}+T_{zz}\right) - P_{eq} + c_s^2\left(T_{00}-\epsilon_{eq}\right)$ is the pressure current.

Similarly, one obtains for the self-diffusion coefficient

$$D = \frac{1}{3}\langle e^{\epsilon t}\vec{v}(0)\cdot\vec{v}(t)\rangle \tag{3.52}$$

The limit $\epsilon \to 0$ is implied in equations 3.48-3.52, hence yielding the Kubo formula for shear, bulk viscosity, and diffusion to be, respectively,

$$\eta = \frac{1}{T}\int d^3r\int_0^\infty dt\langle\pi^{xy}(\vec{0},0)\pi^{xy}(\vec{r},t)\rangle, \tag{3.53}$$

$$\zeta = \frac{1}{T}\int d^3r\int_0^\infty dt\langle\tilde{P}(\vec{0},0)\tilde{P}(\vec{r},t)\rangle, \tag{3.54}$$

where

$$\tilde{P} \equiv \frac{1}{3}\left(T_{xx}+T_{yy}+T_{zz}\right) - P_{eq} + c_s^2\left(T_{00}-\epsilon_{eq}\right) \tag{3.55}$$

is the pressure current. and

$$D = \frac{1}{3}\int_0^\infty dt\langle\vec{v}(0)\cdot\vec{v}(t)\rangle \tag{3.56}$$

Calculations will be presented in Chapter 5 using the relaxation time approximation in a certain limit and the Kubo formalism.

4

Microscopic Transport Models: Simulating Equilibriated Infinite Matter

This chapter describes the microscopic transport models used to simulate the hadronic and partonic media in our systems. These are the Ultrarelativistic Quantum Molecular Dynamics (UrQMD) model and the Parton Cascade Model (PCM), respectively. Both of these covariant transport models are based upon the Boltzmann equation

$$\left(\frac{\partial}{\partial t} + \frac{\vec{p}}{E} \cdot \nabla_r\right) f = fZ^+ - fZ^-, \tag{4.1}$$

where f is the one-particle phase-space distribution function for a given species, and fZ^+ and fZ^- are the gain and loss terms, respectively, as defined in Chapter 3. Interactions in our calculations are based only upon scattering, and we neglect any interparticle potential. The criterion for a collision to occur is based upon the geometric interpretation of the cross section:

$$d_{\text{trans}} \leq \sqrt{\frac{\sigma_{tot}}{\pi}}, \tag{4.2}$$

where d_{trans} is the Lorentz-invariant transverse distance at closest approach between two particles:

$$d_{\text{trans}} = \sqrt{\left(\frac{(q_n - q_m)^\nu (p_m + p_n)_\nu}{(p_n + p_m)^2} (p_n + p_m)^\mu - (q_n - q_m)^\mu \right)^2}, \tag{4.3}$$

using 4 vectors for positions q_ν, momenta p_ν.

4.1 The Ultrarelativistic Quantum Molecular Dynamics (UrQMD) Model

Our hadronic medium is simulated using Ultrarelativistic Quantum Molecular Dynamics (UrQMD), which is composed of purely hadronic degrees of freedom, and does not contain information about any possible crossover or phase transition into partonic degrees of freedom. Interactions in our calculations are based only upon scattering, and we neglect any interparticle potential. UrQMD is described in great detail in [14]. The model includes 55 baryon and baryon resonance species and 32 meson and meson resonance species, (and their antiparticles). The most massive state is a baryonic resonance with mass of 2.250 GeV. These included UrQMD include strange particles, but no particles containing heavy quarks (c or b quarks). The particle species of UrQMD are listed in Tables 4.1 and 4.2.

4.2 Treatment of Interactions

The cross sections in UrQMD are dependent on the total center of mass energy of the system, $\sqrt{s}$, and the particle types in the interaction. Optional features include enabling Pauli blocking due to Fermi statistics, although in practice this really has no significant effect at temperatures relevant for the hadronic gas ($T \sim 100 - 170$ MeV).

Table 4.1: Baryons and baryon-resonances included into the UrQMD model. Through baryon-antibaryon symmetry the respective antibaryon states are included as well.

nucleon	delta	lambda	sigma	xi	omega
N_{938}	Δ_{1232}	Λ_{1116}	Σ_{1192}	Ξ_{1315}	Ω_{1672}
N_{1440}	Δ_{1600}	Λ_{1405}	Σ_{1385}	Ξ_{1530}	
N_{1520}	Δ_{1620}	Λ_{1520}	Σ_{1660}	Ξ_{1690}	
N_{1535}	Δ_{1700}	Λ_{1600}	Σ_{1670}	Ξ_{1820}	
N_{1650}	Δ_{1900}	Λ_{1670}	Σ_{1750}	Ξ_{1950}	
N_{1675}	Δ_{1905}	Λ_{1690}	Σ_{1775}	Ξ_{2030}	
N_{1680}	Δ_{1910}	Λ_{1800}	Σ_{1915}		
N_{1700}	Δ_{1920}	Λ_{1810}	Σ_{1940}		
N_{1710}	Δ_{1930}	Λ_{1820}	Σ_{2030}		
N_{1720}	Δ_{1950}	Λ_{1830}			
N_{1900}		Λ_{1890}			
N_{1990}		Λ_{2100}			
N_{2080}		Λ_{2110}			
N_{2190}					
N_{2200}					
N_{2250}					

Table 4.2: Mesons and meson-resonances, sorted with respect to spin and parity, included into the UrQMD model.

0^{-+}	1^{--}	0^{++}	1^{++}	1^{+-}	2^{++}	$(1^{--})^{*}$	$(1^{--})^{**}$
π	ρ	a_0	a_1	b_1	a_2	ρ_{1450}	ρ_{1700}
K	K^*	K_0^*	K_1^*	K_1	K_2^*	K_{1410}^*	K_{1680}^*
η	ω	f_0	f_1	h_1	f_2	ω_{1420}	ω_{1662}
η'	ϕ	f_0^*	f_1'	h_1'	f_2'	ϕ_{1680}	ϕ_{1900}

We can summarize the types of interactions we investigate in UrQMD into the following general classes:

- Constant elastic cross sections.
- Meson-baryon or meson-meson interactions.
- Nucleon-nucleon interactions.

- Nucleon-antinucleon annihilations.

- Additive quark model.

The matrix amplitudes for each of the aforementioned classes will be described. First, one should speak of the general structure of the interactions. The interactions are described using the following equations found in standard kinematics and particle data book references [71].

If one is to consider an interaction for a process 1,2→ 3,4, then the cross section for such an interaction is given by

$$\sigma_{1,2\to 3,4} \sim (2S_3+1)(2S_4+1)\frac{\langle p_{3,4}\rangle}{\langle p_{1,2}\rangle}\frac{1}{s}|M(m_3,m_4)|^2, \tag{4.4}$$

where $S_{3,4}$ are the intrinsic spins of particles 3,4, $|M(m_3,m_4)|^2$ is the modulus of the scattering amplitude squared of such an interaction, $\sqrt{s}$ the total center of mass energy, and the relations for the momenta are given by

$$\langle p_{3,4}(\sqrt{s})\rangle = p_{\mathrm{CMS}}(\sqrt{s}) = \frac{1}{2\sqrt{s}}\sqrt{(s-(m_3+m_4)^2)\,(s-(m_3-m_4)^2)}, \tag{4.5}$$

with $m_{3,4}$ the masses of particles 3,4 and a similar expression holding for 1,2. In case the particles 3,4 are resonances, then one integrates over their respective mass distributions

$$\langle p_{3,4}(\sqrt{s})\rangle = \int\int p_{CMS}(\sqrt{s},m_3,m_4)A_3(m_3)A_4(m_4)dm_3dm_4 \tag{4.6}$$

with the distribution taking a Breit-Wigner form with a possibly mass-dependent decay width $\Gamma(m)$.

$$A_r(m) = \frac{1}{N}\frac{\Gamma(m)}{(m_r-m)^2+\Gamma(m)^2/4} \tag{4.7}$$

with normalization

$$N = \int_{-\infty}^{\infty} \frac{\Gamma(m)}{(m_r - m)^2 + \Gamma(m)^2/4} dm. \tag{4.8}$$

The full decay widths are obtained by summing over the partial decay widths [14].

$$\Gamma_{tot}(M) = \sum_{br=i,j}^{N_{br}} \Gamma_{i,j}(M) \tag{4.9}$$

$$\Gamma_{i,j}(M) \; = \; \Gamma_R^{i,j} \frac{M_R}{M} \left(\frac{\langle p_{i,j}(M) \rangle}{\langle p_{i,j}(M_R) \rangle} \right)^{2l+1} \frac{1.2}{1 + 0.2 \left(\frac{\langle p_{i,j}(M) \rangle}{\langle p_{i,j}(M_R) \rangle} \right)^{2l}} \quad , \tag{4.10}$$

here M_R denotes the pole mass of the resonance, $\Gamma_R^{i,j}$ its partial decay width into the channel i and j at the pole and l the decay angular momentum of the exit channel. All pole masses and partial decay widths at the pole are taken from the Review of Particle Properties [71]. $\Gamma_{i,j}(M)$ is constructed in such a way that $\Gamma_{i,j}(M_R) = \Gamma_R^{i,j}$ is fulfilled at the pole. In many cases only crude estimates for $\Gamma_R^{i,j}$ are given in [71] – the partial decay widths must then be fixed by studying exclusive particle production in elementary proton-proton and pion-proton reactions. The values of decay widths at pole mass $M = M_R$ are given in Tables 4.3 -4.8.

Constant elastic cross sections

If all inelastic collisions are disabled in UrQMD, there is a constant cross-section for elastic meson-meson interactions. In particular, that channel is for the process

$$\pi + \pi \rightarrow \pi + \pi(elastic). \tag{4.11}$$

The default value used in UrQMD was 5 mb, but for some studies we have also adjusted the fixed cross section to 10 mb or 50 mb. In principle it can also be adjusted to the cross section for the additive quark model (AQM), as in equation 4.19.

Meson-baryon and meson-meson interactions

The total resonant meson-baryon cross section for non-strange particles is given by

$$\sigma_{tot}^{MB}(\sqrt{s}) = \sum_{R=\Delta,N^*} \langle j_B, m_B, j_M, m_M \| J_R, M_R \rangle \frac{2S_R+1}{(2S_B+1)(2S_M+1)} \times \frac{\pi}{p_{CMS}^2} \frac{\Gamma_{R\to MB}\Gamma_{tot}}{(M_R-\sqrt{s})^2 + \frac{\Gamma_{tot}^2}{4}} \tag{4.12}$$

with the total and partial $\sqrt{s}$-dependent decay widths Γ_{tot} and $\Gamma_{R\to MB}$ (see equations (4.9) and (4.10)) [14]. Therefore, the total pion-nucleon cross section depends on all pole masses, widths and branching ratios of all N^* and Δ^* resonances listed in table 4.3.

Nucleon-nucleon interactions

The form for the scattering amplitude depends on the specific reaction channels considered. For $NN \to N\Delta_{1232}$, this is

$$|M(\sqrt{s}, m_3, m_4)|^2 = A \frac{m_\Delta^2 \Gamma_\Delta^2}{(s-m_\Delta^2)^2 + m_\Delta^2 \Gamma_\Delta^2}, \tag{4.13}$$

where $A = 40000$, $\Gamma_\Delta = 0.115$ GeV, $m_\Delta = 1.232$ GeV [14]. For $NN \to NN^*, NN \to N\Delta^*, NN \to \Delta_{1232}N^*$, and $NN \to \Delta_{1232}\Delta^*$,

$$|M(\sqrt{s}, m_3, m_4)|^2 = A \frac{1}{(m_3-m_4)^2(m_3+m_4)^2}, \tag{4.14}$$

where $A = 6.3$ for $NN \to NN^*$, $A = 12$ for $NN \to N\Delta^*$, and $A = 3.5$ for $NN \to \Delta_{1232}N^*$, and the same parameters as in equation 4.13. For $NN \to \Delta\Delta$

$$|M(\sqrt{s}, m_3, m_4)|^2 = A \tag{4.15}$$

with $A = 2.8$ [14].

Nucleon-antinucleon annihilations

To simulate nucleon-antinucleon annihilation, we have programmed two processes in such a manner that respects detailed balance. In this context, the principle of detailed balance is related to the invariance of the relevant matrix element under time-reversal. It is expressed in the form,

$$\sigma_{f\to i} = \frac{\vec{p}_i^2}{\vec{p}_f^2}\frac{g_i}{g_f}\sigma_{i\to f} \quad , \tag{4.16}$$

with g denoting the spin-isospin degeneracy factors. The above form restricts us to considering $1 \leftrightarrow 2$ and $2 \leftrightarrow 2$ processes. On average, the final state of a $N\bar{N}$ annihilation contains 5 pions. Hence, in order to implement baryon-antibaryon annihilation in such a way that respects detailed balance, one should avoid multi-particle exit states, as they cannot be handled with our collision algorithm. As such we consider the following two processes:

$$\rho\phi(1020) \leftrightarrow \mathrm{N\bar{N}} \tag{4.17}$$

and

$$\rho\omega(1420) \leftrightarrow \mathrm{N\bar{N}}. \tag{4.18}$$

Our strategy involves channeling a $N\bar{N}$ annihilation into a two resonance state corresponding to the quantum numbers representative of a five-pion state. Likewise, in order to respect detailed balance, we must mimic $N\bar{N}$ production by using a two-resonance state as the scattering channel. The logic is as follows: the ρ meson decays predominantly into 2 pions, and both the $\phi(1020)$ and $\omega(1420)$ decay into a ρ meson and a pion. Hence an effective two body resonance interaction is equivalent to creating a five pion state in such a way that detailed balance is maintained in UrQMD.

Additive quark model

The additive quark model cross sections are given (in mb) by

$$\sigma_{tot} = 40 \left(\frac{2}{3}\right)^{n_M} (1 - 0.4x_1^s)(1 - 0.4x_2^s) \tag{4.19}$$

where n_M is the number of colliding mesons, and x_i^s is the ratio of strange quarks to non-strange quarks in the ith hadron. The elastic contribution by each is then

$$\sigma_{el} = 0.039 \cdot \sigma_{tot}^{2/3}[14]. \tag{4.20}$$

4.3 The Parton Cascade Model (PCM)

The Parton Cascade Model (PCM) [35, 34] is a microscopic transport model which is used to simulate the time evolution of a system of quarks and gluons utilizing the Boltzmann equation. We define a box with periodic boundary conditions (to simulate infinite matter) and sample thermal quark and gluon distribution functions to generate an ensemble of particles at a given temperature and zero chemical potential.

$$\sum_i \mathcal{C}_i[F] \equiv fZ^+ - fZ^- \tag{4.21}$$

The PCM collision term $\mathcal{C}_i$ is a nonlinear functional of the phase-space distribution function (the summation index refers to the included processes). Although the collision term, in principle, includes factors encoding the Bose-Einstein or Fermi-Dirac statistics of the partons, we neglect those effects here.

The collision integrals have the form:

$$\mathcal{C}_i[F] = \frac{(2\pi)^4}{2S_iE_i} \cdot \int \prod_j \mathrm{d}\Gamma_j \, |\mathcal{M}|^2 \, \delta^4(P_{\text{in}} - P_{\text{out}}) \, D(F_k(x, \vec{p})) \tag{4.22}$$

Table 4.3: Masses, widths and branching ratios for non-strange baryon-resonances in UrQMD. Masses are given in GeV and the widths in MeV. All parameters are within the range given by the Review of Particle Properties [71] and have been tuned to exclusive particle production channels.

resonance	**mass**	**width**	$N\gamma$	$N\pi$	$N\eta$	$N\omega$	$N\varrho$	$N\pi\pi$	$\Delta_{1232}\pi$	$N^*_{1440}\pi$	ΛK
N^*_{1440}	1.440	200		0.70				0.05	0.25		
N^*_{1520}	1.520	125		0.60				0.15	0.25		
N^*_{1535}	1.535	150	0.001	0.55	0.35			0.05		0.05	
N^*_{1650}	1.650	150		0.65	0.05			0.05	0.10	0.05	0.10
N^*_{1675}	1.675	140		0.45					0.55		
N^*_{1680}	1.680	120		0.65				0.20	0.15		
N^*_{1700}	1.700	100		0.10	0.05		0.05	0.45	0.35		
N^*_{1710}	1.710	110		0.15	0.20		0.05	0.20	0.20	0.10	0.10
N^*_{1720}	1.720	150		0.15			0.25	0.45	0.10		0.05
N^*_{1900}	1.870	500		0.35		0.55	0.05		0.05		
N^*_{1990}	1.990	550		0.05			0.15	0.25	0.30	0.15	0.10
N^*_{2080}	2.040	250		0.60	0.05		0.25	0.05	0.05		
N^*_{2190}	2.190	550		0.35			0.30	0.15	0.15	0.05	
N^*_{2220}	2.220	550		0.35			0.25	0.20	0.20		
N^*_{2250}	2.250	470		0.30			0.25	0.20	0.20	0.05	
Δ_{1232}	1.232	115.	0.01	1.00							
Δ^*_{1600}	1.700	200		0.15					0.55	0.30	
Δ^*_{1620}	1.675	180		0.25					0.60	0.15	
Δ^*_{1700}	1.750	300		0.20			0.10		0.55	0.15	
Δ^*_{1900}	1.850	240		0.30			0.15		0.30	0.25	
Δ^*_{1905}	1.880	280		0.20			0.60		0.10	0.10	
Δ^*_{1910}	1.900	250		0.35			0.40		0.15	0.10	
Δ^*_{1920}	1.920	150		0.15			0.30		0.30	0.25	
Δ^*_{1930}	1.930	250		0.20			0.25		0.25	0.30	
Δ^*_{1950}	1.950	250	0.01	0.45			0.15		0.20	0.20	

with

$$D(F_k(x,\vec{p})) \;=\; \prod_{\text{out}} F_k(x,\vec{p}) \;-\; \prod_{\text{in}} F_k(x,\vec{p}) \tag{4.23}$$

and

$$\prod_j \mathrm{d}\Gamma_j = \prod_{\substack{j\neq i \\ \text{in,out}}} \frac{\mathrm{d}^3 p_j}{(2\pi)^3\,(2p_j^0)} \quad . \tag{4.24}$$

S_i is a statistical factor defined as $S_i = \prod_{j\neq i} K_a^{\text{in}}!\,K_a^{\text{out}}!$ with $K_a^{\text{in,out}}$ identical partons of species a in the initial or final state of the process, excluding the ith parton.

The matrix elements $|\mathcal{M}|^2$ account for the following processes in Figure 4.1.

Table 4.4: Masses, widths and branching ratios for single-strange baryon-resonances in UrQMD. Masses are given in GeV and the widths in MeV. All parameters are within the range given by the Review of Particle Properties [71] and have been tuned to exclusive particle production channels and to the total kaon-nucleon cross section.

resonance	**mass**	**width**	$N\bar{K}$	$N\bar{K}^*_{892}$	$\Sigma\pi$	$\Sigma^*\pi$	$\Lambda\gamma$	$\Lambda\eta$	$\Lambda\omega$	$\Lambda\pi$	$\Sigma\eta$	$\Lambda^*\pi$	$\Delta\bar{K}$
Λ^*_{1405}	1.407	50			1.00								
Λ^*_{1520}	1.520	16	0.45		0.43	0.11	0.01						
Λ^*_{1600}	1.600	150	0.35		0.65								
Λ^*_{1670}	1.670	35	0.20		0.50			0.30					
Λ^*_{1690}	1.690	60	0.25		0.45	0.30							
Λ^*_{1800}	1.800	300	0.40	0.20	0.20	0.20							
Λ^*_{1810}	1.810	150	0.35	0.45	0.15	0.05							
Λ^*_{1820}	1.820	80	0.73		0.16	0.11							
Λ^*_{1830}	1.830	95	0.10		0.70	0.20							
Λ^*_{1890}	1.890	100	0.37	0.21	0.11	0.31							
Λ^*_{2100}	2.100	200	0.35	0.20	0.05	0.30		0.02	0.08				
Λ^*_{2110}	2.110	200	0.25	0.45	0.30								
Σ^*_{1385}	1.384	36			0.12					0.88			
Σ^*_{1660}	1.660	100	0.30		0.35					0.35			
Σ^*_{1670}	1.670	60	0.15		0.70					0.15			
Σ^*_{1750}	1.750	90	0.40		0.05						0.55		
Σ^*_{1775}	1.775	120	0.40		0.04	0.10				0.23		0.23	
Σ^*_{1915}	1.915	120	0.15		0.40	0.05				0.40			
Σ^*_{1940}	1.940	220	0.10	0.15	0.15	0.15				0.15		0.15	0.15
Σ^*_{2030}	2.030	180	0.20	0.04	0.10	0.10				0.20		0.18	0.18

Table 4.5: Masses, widths and branching ratios for double-strange baryon-resonances in UrQMD. Masses are given in GeV and the widths in MeV. All parameters are within the range given by the Review of Particle Properties [71] and have been tuned to exclusive particle production channels.

resonance	**mass**	**width**	$\Xi\pi$	$\Xi\gamma$	$\Lambda\bar{K}$	$\Sigma\bar{K}$
Ξ^*_{1530}	1.532	9	0.98	0.02		
Ξ^*_{1690}	1.700	50	0.10		0.70	0.20
Ξ^*_{1820}	1.823	24	0.15		0.70	0.15
Ξ^*_{1950}	1.950	60	0.25		0.50	0.25
Ξ^*_{2030}	2.025	20	0.10		0.20	0.70

Table 4.6: Masses, widths and branching ratios for meson-resonances in UrQMD, part I. Masses are given in GeV and the widths in MeV. All parameters are within the range given by the Review of Particle Properties [71]. Additional branching ratios can be found in table 4.7 and 4.8.

meson	**mass**	**width**	$\gamma\pi$	$\gamma\rho$	$\gamma\omega$	$\gamma\eta$	γK	$\pi\pi$	$\pi\rho$	3π	$\pi\eta$	4π	$K\bar{K}^*$	$\bar{K}K^*$
ω	0.782	8	0.09					0.02		0.89				
ρ	0.769	151						1.00						
$f_0(980)$	0.980	100						0.70						
η'	0.958	0.2		0.30	0.05									
K^*	0.893	50												
ϕ	1.019	4				0.01			0.13	0.02				
K_0^*	1.429	287												
a_0	0.984	100									0.90			
$f_0(1370)$	1.370	200						0.10				0.70		
$K_1(1270)$	1.273	90												
a_1	1.230	400	0.10						0.90					
f_1	1.282	24		0.07								0.20		
$f_1(1510)$	1.512	350											0.50	0.50
$K_2(1430)$	1.430	100												
$a_2(1320)$	1.318	107							0.70		0.14			
$f_2(1270)$	1.275	185						0.50				0.30		
$f_2'(1525)$	1.525	76						0.01						
$K_1(1400)$	1.400	174												
$b_1(1235)$	1.235	142												
$h_1(1170)$	1.170	360							0.90	0.10				
$h_1'(1380)$	1.380	80											0.50	0.50
$K^*(1410)$	1.410	227												
$\rho(1465)$	1.465	310						0.50				0.50		
$\omega(1419)$	1.419	174							1.00					
$\phi(1680)$	1.680	150											0.40	0.40
$K^*(1680)$	1.680	323												
$\rho(1700)$	1.700	235						0.10				0.20		
$\omega(1662)$	1.662	280							0.50					
$\phi(1900)$	1.900	400											0.40	0.40

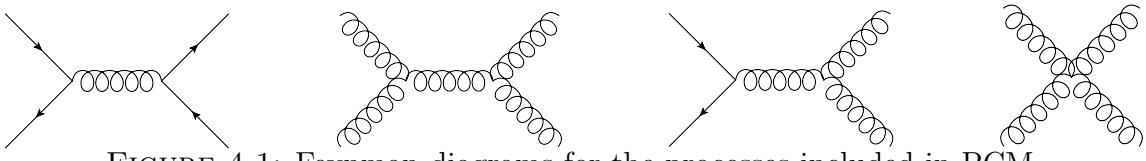

FIGURE 4.1: Feynman diagrams for the processes included in PCM.

Table 4.7: Masses, widths and branching ratios for meson-resonances in UrQMD,part II. Masses are given in GeV and the widths in MeV. All parameters are within the range given by the Review of Particle Properties [71].

meson	**mass**	**width**	$\eta\pi\pi$	$\eta\rho$	$\rho\pi\pi$	$\omega\pi\pi$	$\eta\eta$	$K\bar{K}$	$K\bar{K}\pi$	$K\pi$	$K^*\pi$	$K\rho$	$K\omega$
ω	0.782	8											
ρ	0.769	151											
$f_0(980)$	0.980	100						0.30					
η'	0.958	0	0.65										
K^*	0.893	50								1.00			
ϕ	1.019	4						0.84					
K_0^*	1.429	287								1.00			
a_0	0.984	100						0.10					
$f_0(1370)$	1.370	200						0.20					
$K_1(1270)$	1.273	90									0.47	0.42	0.11
a_1	1.230	400											
f_1	1.282	24	0.54		0.10				0.09				
$f_1(1510)$	1.512	350											
$K_2(1430$	1.430	100								0.50	0.25	0.09	0.03
$a_2(1320)$	1.318	107				0.11		0.05					
$f_2(1270$	1.275	185						0.20					
$f_2'(1525)$	1.525	76					0.10	0.89					
$K_1(1400)$	1.400	174									0.96	0.03	0.01
$b_1(1235)$	1.235	142		0.10									
$h_1(1170)$	1.170	360											
$h_1'(1380)$	1.380	80											
$K^*(1410)$	1.410	227								0.30	0.65	0.05	
$\rho(1465)$	1.465	310											
$\omega(1419)$	1.419	174											
$\phi(1680)$	1.680	150						0.10	0.10				
$K^*(1680)$	1.680	323								0.40	0.30	0.30	
$\rho(1700)$	1.700	235			0.70								
$\omega(1662)$	1.662	280				0.50							
$\phi(1900)$	1.900	400						0.10	0.10				

The corresponding scattering cross sections are expressed in terms of spin- and colour-averaged amplitudes $|\mathcal{M}|^2$:

$$\left(\frac{\mathrm{d}\hat{\sigma}}{\mathrm{d}Q^2}\right)_{ab\to cd} = \frac{1}{16\pi\hat{s}^2}\left\langle|\mathcal{M}|^2\right\rangle \tag{4.25}$$

For the transport calculation we also need the total cross section as a function of

Table 4.8: Masses, widths and branching ratios for meson-resonances in UrQMD,part III. Masses are given in GeV and the widths in MeV. All parameters are within the range given by the Review of Particle Properties [71].

meson	**mass**	**width**	$K^*\pi\pi$	$\omega\pi$
ω	0.782	8		
ρ	0.769	151		
$f_0(980)$	0.980	100		
η'	0.958	0		
K^*	0.893	50		
ϕ	1.019	4		
K_0^*	1.429	287		
a_0	0.984	100		
$f_0(1370)$	1.370	200		
$K_1(1270)$	1.273	90		
a_1	1.230	400		
f_1	1.282	24		
$f_1(1510)$	1.512	350		
$K_2(1430$	1.430	100	0.13	
$a_2(1320)$	1.318	107		
$f_2(1270$	1.275	185		
$f_2'(1525)$	1.525	76		
$K_1(1400)$	1.400	174		
$b_1(1235)$	1.235	142		0.90
$h_1(1170)$	1.170	360		
$h_1'(1380)$	1.380	80		
$K^*(1410)$	1.410	227		
$\rho(1465)$	1.465	310		
$\omega(1419)$	1.419	174		
$\phi(1680)$	1.680	150		
$K^*(1680)$	1.680	323		
$\rho(1700)$	1.700	235		
$\omega(1662)$	1.662	280		
$\phi(1900)$	1.900	400		

Mandelstam $\hat{s}$ which can be obtained from (4.25):

$$\hat{\sigma}_{ab}(\hat{s}) = \sum_{c,d} \int_{(p_T^{\min})^2}^{\hat{s}} \left(\frac{\mathrm{d}\hat{\sigma}}{\mathrm{d}Q^2}\right)_{ab\to cd} \mathrm{d}Q^2 \quad . \tag{4.26}$$

The amplitudes for the above processes have been calculated in refs. [22, 20] for massless quarks. Note that in equation 4.26 a low momentum cutoff is introduced, since the relevant cross sections diverge at low momentum. This low momentum

divergence is known as an infrared (IR) divergence, which is regularized using a temperature dependent Debye mass m_D, which is an effect to account for effects of color field screening. We shall use two different expressions for m_D – the first one is a Debye-mass for particles obeying Boltzmann statistics which has been used in [88, 28, 29, 89, 86] and which we utilize to allow our results to be compared to these calculations:

$$m_D(T) = \sqrt{\frac{24}{\pi}\alpha_s T^2} \quad , \tag{4.27}$$

and the second one is the standard Debye mass used in pQCD calculations for systems of quarks and gluons:

$$m_D(T) = gT\sqrt{(2N_c + N_f)/6} \tag{4.28}$$

The first m_D parametrization we shall refer to as Boltzmann-m_D whereas the second parametrization we shall refer to as regular m_D. In both cases the coupling constant is defined as

$$\alpha_s = \frac{g^2}{4\pi} \tag{4.29}$$

and can either be chosen as a constant parameter, or to have the following temperature dependence:

$$\frac{1}{g^2} = \frac{9}{8\pi^2}\ln\left(\frac{T}{\Lambda_T}\right) + \frac{4}{9\pi^2}\ln\left(2\ln\left(\frac{T}{\Lambda_T}\right)\right) \tag{4.30}$$

with $\Lambda_T = 30$ MeV.

4.4 Simulating a Hot QCD Gas in Equilibrium

Now that the UrQMD and PCM models have been described, I proceed to discuss our techniques for ensuring the simulated gas remains in equilibrium and maintains equilibrium.

4.4.1 Hadronic Gas in Equilibrium

To force our system into equilibrium, we confine our hadronic medium to a cubic box with periodic boundary conditions in real space. The initial particle species are initialized such that the system does not exhibit any collective center of mass motion:

$$\sum_{i=1}^{N_{part}} \vec{p_i} = 0. \tag{4.31}$$

This technique was also used in [16, 63, 64]. The input parameters of our system are as follows: volume of the box, and initial particle species.

Initialization Schemes

There are two options for initializing our calculations in UrQMD to model a thermally and chemically equilibriated hadron gas. One involves the stream-on-stream initialization, where the particles are randomly distributed in momentum space with momenta ranging from 0 to the Fermi momentum:

$$p_F = (3\pi^2 n)^{1/3}, \tag{4.32}$$

and the overall energy-density of the system is being fixed. One can also employ the thermal initialization, where particles are initialized according to a Boltzmann distribution at a given effective chemical potential μ_i and temperature T for species i:

$$N_i = V \int \frac{d^3p}{(2\pi)^3} \exp\left(-\frac{\sqrt{p^2 + m_i^2} - \mu_i}{T}\right). \tag{4.33}$$

In order to verify our system for thermal and chemical equilibrium for using the stream-on-stream initialization and for robustness of the thermal initialization, we check for chemical and thermal equilibriation in the system, as shown below.

4.4.2 Chemical Equilibriation

The time evolution of the primary stable particle species in our system for the case of $\rho_B = \rho_0$ and $\epsilon = 0.3$ GeV/fm^3 is illustrated in Figure 4.2. Note that the chemical equilibriation time for the strange particle species is much longer than for non-strange hadrons due to suppression of strange processes. We hence denote the chemical equilibriation time as the timestep when the primary particle species saturate as a function of Monte Carlo time. In order to verify that proper chemical equilibrium has been reached, we check our ratios against an independent calculation using a statistical model for a hadron resonance gas(HG).

The particular statistical model for the HG we use is known as SHARE (Statistical Hadronization with Resonances), which is described in detail in [84, 83]. The particle and decay tables of SHARE have been modified to match those of our version of UrQMD to maintain consistency of the treated degrees of freedom. We extract particle ratios from both the UrQMD simulations and from the "UrQMD-tuned" grand canonical ensemble HG statistical model. In such a model, the number density of the gas is given by

$$n(T, \mu_B) = \sum_k g_k \int \frac{d^3p}{(2\pi)^3} \frac{1}{exp\left[\frac{\sqrt{p^2+m^2}-\mu_B}{T}\right] \pm 1}, \tag{4.34}$$

where T is the temperature and μ_B is the baryochemical potential, and the particle species are indexed by k. The upper sign refers to fermions and the lower sign refers to bosons.

4.4.3 Thermal and Kinetic Equilibriation

Once we have determined that chemical equilibriation has been established for a particular case, we then examine the momenta distributions at that particular timestep to check for kinetic equilibriation. A system which has attained thermal equilibrium

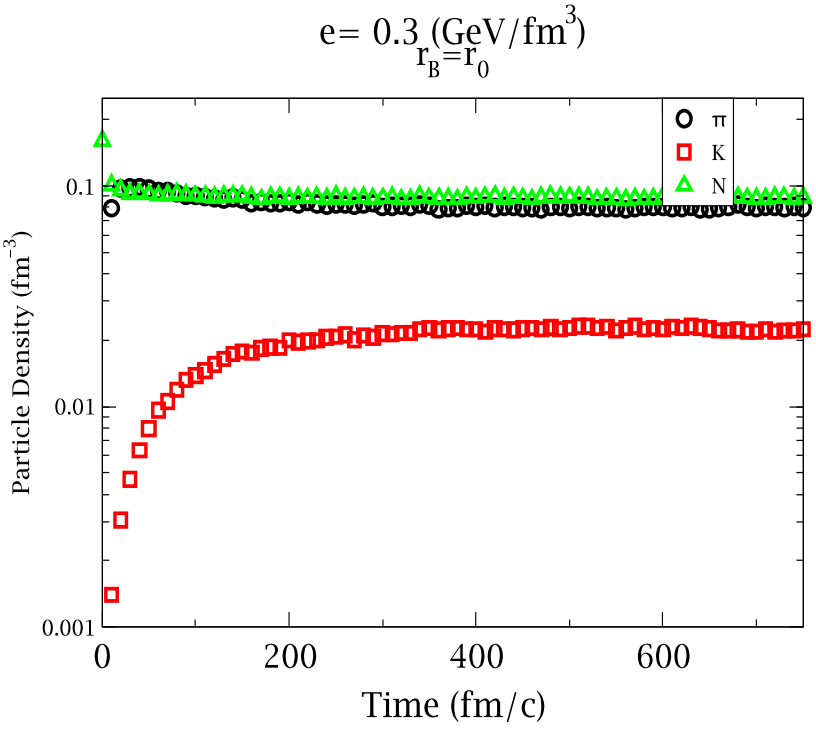

FIGURE 4.2: Particle density versus time for the primary particle species in our system for the case $\epsilon = 0.3$ GeV/fm^3, at ground state nuclear density [26]. Note the longer equilibriation time for the kaons, which contain strange quarks, relative to that for the pions or nucleons.

should have its momenta distributions following a Boltzmann distribution:

$$\frac{d^3N_i}{d^3p} \propto exp\left(-\frac{E_i}{T}\right) \tag{4.35}$$

for a given species N_i. We know that for a system realizing kinetic equilibrium, the momenta distributions should be isotropic, enabling us to write $d^3p = 4\pi p^2 dp$, where p is the three-momentum magnitude. Using the relativistic dispersion relation $E_i = \sqrt{p_i^2 + m_i^2}$ enables us to use the alternate observable $\frac{1}{pE}\frac{dN_i}{dE}$. Figure 4.3 shows the momenta distribution in the x, y, and z directions evaluated at chemical equilibriation time for the case $\rho_B = \rho_0$ and $\epsilon = 0.5$ GeV/fm^3.

The temperatures extracted from individual reduced χ^2 fits to the particle species of Boltzmann distributions agree within a certain window of 5-10 MeV. There are

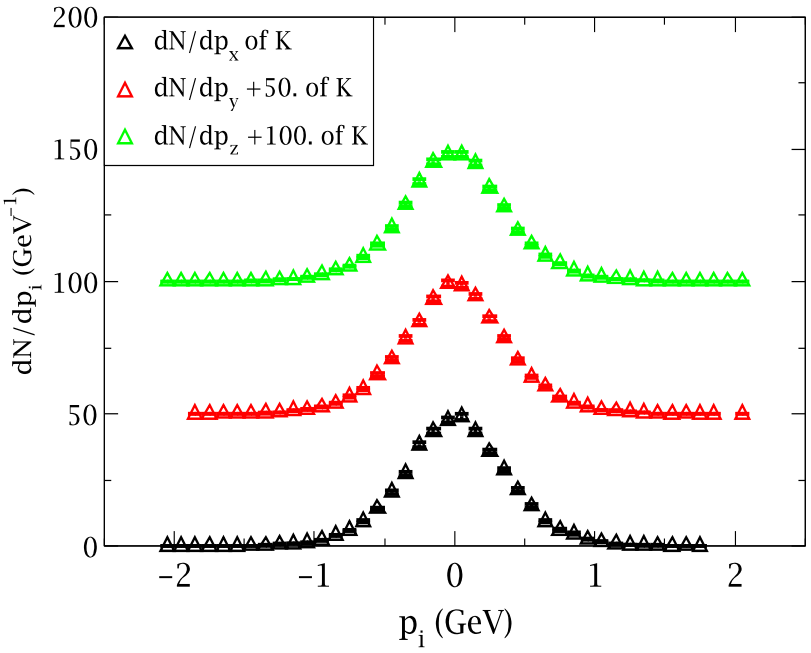

FIGURE 4.3: Momenta distributions in the x,y, and z directions [26]. These all are for kaon spectra at the case of ground state nuclear density and energy density = 0.5 GeV/fm^3.

two reasons for this: one reason is due to the fact that we are using a Monte Carlo simulation, and in such a simulation, it is very difficult to get the temperatures of the different particle species to match perfectly even using high statistics. Another reason is due to distortion of particle spectra from resonance effects. An example of this effect can be glimpsed from Figure 4.4, where the pion spectra at low energy slightly rises above the red line representing a Boltzmann distribution. Note that since we initialize our gases in the case corresponding to Figure 4.2 with nucleons only, any pions that are produced result from resonance decays, and such resonances are responsible for distortion of particle spectra. The temperature of the system

extracted is the chemically weighted temperature of the primary particle species:

$$T_{\text{chem}} = \sum_i \left(\frac{n_i}{\sum_j n_j} \right) T_i, \tag{4.36}$$

where T_i are the temperatures extracted from reduced χ^2 fits to the individual particle species i, and n_i denoting their densities. The primary particle species are nucleons, pions, kaons and hyperons for our study at finite baryon number density, and the species are pions and kaons for our study of mesonic matter. It is necessary to check whether all the primary particle species can be fit to Boltzmann distributions using the aforementioned chemically averaged temperatures. Such an example is illustrated in Figure 4.4 using $T_{\text{chem}} = 169$ MeV. Using this procedure of extracting the system's temperature given the energy and baryon number density as input parameters in UrQMD, we can obtain the system's equation of state(EoS), akin to the calculation performed in [16]. In addition to extracting the system temperature from the energy density input, we extract the pressure of the system:

$$P = \frac{1}{3V} \sum_i^{N_{part}} \frac{\vec{p}_i^2}{E_i}, \tag{4.37}$$

and similarly extract the pressure from the statistical model

$$P(T, \mu_B) = \sum_k g_k \int \frac{d^3p}{(2\pi)^3} \frac{p^2}{3\sqrt{p^2+m^2}} \frac{1}{exp\left[\frac{\sqrt{p^2+m^2}-\mu_B}{T}\right] \pm 1}, \tag{4.38}$$

where the upper sign refers to fermions (hence at finite μ_B) and the lower sign refers to bosons (at $\mu_B = 0$). The resulting EoS for the cases corresponding to $\rho_B = \rho_0$ is shown in Figure 4.5. Since we have disabled detailed balance-violating string excitations which lead to excited states with an exponential mass spectrum, we do not observe a saturation of temperature with increasing energy density as predicted by

Hagedorn and seen in [16], although the specific EoS in the aforementioned reference including detailed-balance preserving string excitations is successfully reproduced.

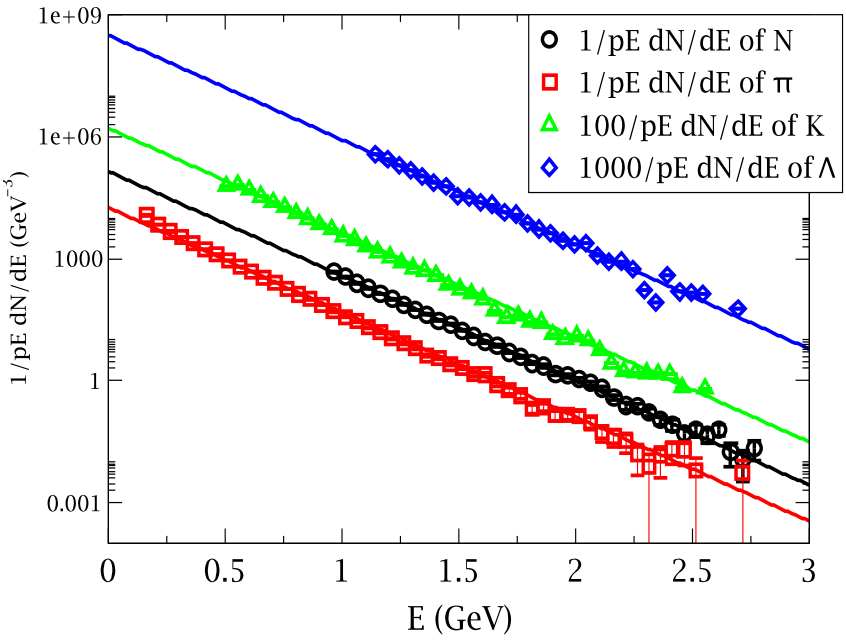

FIGURE 4.4: The observable $\frac{1}{pE}\frac{dN}{dE}$ versus E, which can be well described by a Boltzmann distribution. The above plot corresponds to $\epsilon = 0.5$ GeV/fm^3, $\rho_B = \rho_0$, $T = 169$ MeV. The distributions for the kaons and Λ particles were multiplied by 1000 so that a seperation in spectra can be seen. All the above spectra were fit to the chemically weighted temperature of $T = 169$ MeV [26].

4.5 Entropy Considerations

It should be noted that one must proceed with great care in accurately extracting the entropy of a system simulated by a microscopic transport model. If one is lax about the assumptions made regarding the system, the result may be extremely inaccurate. As a consequence, a discussion of the calculation of entropy via the statistical and thermodynamic definitions is relevant, for the mass-dependence of the entropy upon the constituent particles is a fact that cannot be taken for granted, especially for

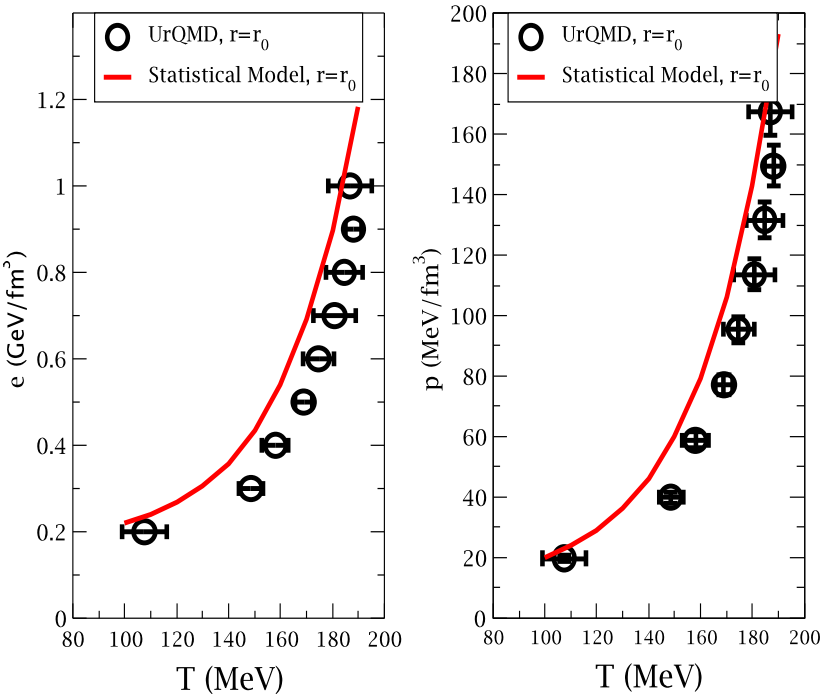

FIGURE 4.5: In the left panel, energy density versus temperature. In the right panel, the pressure as a function of temperature. The solid curve is extracted from the UrQMD-tuned statistical model whereas the black circles are extracted from UrQMD simulations.

hadronic systems where $m/T \sim 1.5 - 20$ [65]. As such, we present three methods for calculating the entropy from UrQMD, and two methods for calculating the entropy from the PCM. The three schemes for calculating entropy in UrQMD involve the Gibbs formula, the kinetic definition of entropy, and the counting of particles with weighted specific entropies.

4.5.1 Entropy Calculation in URQMD

Kinetic Definition of Entropy

The formula for computing the entropy S of a system using the statistical definition of entropy is:

$$S = -\sum_{\ell} \langle \rho_\ell \rangle log \langle \rho_\ell \rangle, \tag{4.39}$$

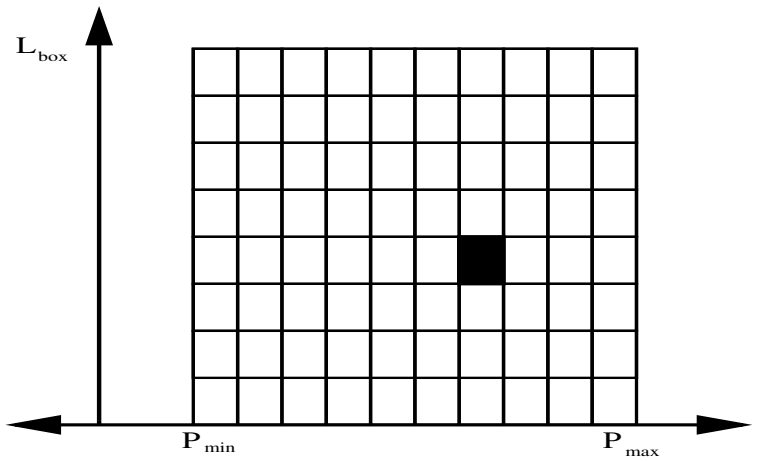

FIGURE 4.6: Schematic of a two-dimensional projection of the 6-dimensional phase space of our system. We denote the number of bins on the momentum axis above as $N_{\rm mom}$ and the number of bins on the real space axis as $N_{\rm real}$. The area of the shaded rectangle is $\hbar$, as required by the uncertainty principle.

where l labels the index of the cells in the phase space of our system, and $\langle \rho_l \rangle$ is the ensemble-averaged density operator of phase space cell l. The authors of [77, 79, 64] define ρ_ℓ such that, for a given event, ρ_l takes the value of unity if the cell is occupied, and zero if it is empty. However, one must choose the number of phase space cells appropriately. According to the uncertainty principle, the volume of a 6-dimensional phase space cell is $\hbar^3$. A sketch of a 2-dimensional projection of this 6-dimensional phase space is given in Figure 5.5. $p_{\rm max}$ and $p_{\rm min}$ refer to the maximum and minimum momentum components a particle could take over the course of the simulation in any of the x, y, or z directions. Let us denote the number of bins on the real space axis of that projection as $N_{\rm real}$, and the number of bins on the momentum axis as $N_{\rm mom}$. Since the particles are confined to a box of size $L_{\rm box}$, the area of one of the two dimensional phase space cell projections should be $(\frac{p_{\rm max}-p_{\rm min}}{N_{\rm mom}})(\frac{L_{box}}{N_{\rm real}}) = \hbar$. We also know the maximum number of particles in any single event should not exceed the number of real space cells, hence implying $N_{\rm part,max} \leq N_{\rm real}^3$. These two relations enable us to determine $N_{\rm mom}$ and $N_{\rm real}$.

However, this motivates another discussion; the number of particles in our sys-

tem at a given Monte Carlo time fluctuates from event to event, yet we are using the framework of the microcanonical ensemble to compute the entropy. In the microcanonical ensemble, the total energy and total particle number remain fixed, whereas in our simulations, while the total energy content in the box is fixed in every event, the total particle number is not. For our computation of entropy to be reasonable, the fluctuations of the number of particles between events must not be too large; typically the largest value of $\frac{N_{\mathrm{part,max}} - N_{\mathrm{part,min}}}{N_{\mathrm{part,avg}}}$ is ~ 5 percent. In addition, the mass-dependence of the particles is not taken into account using the above construction of ρ_ℓ.

Another check we can perform to see whether our entropy results are reasonable is to determine if the entropy results we have computed resemble those of an extensive quantity; equivalently, whether the entropy density is an intensive quantity. The results for entropy density as a function of system size for ground state nuclear density are shown in Figure 5.6, and the curve is practically flat as a function of volume, suggesting that indeed our entropy results resemble those of an extensive quantity.

However, one should note that different particles of equal mass are weighted equally using the above construction of ρ_ℓ. Regardless if a pion or nucleon scatters into a phase space cell ℓ in an event, the cell would count the specific contribution from the pion and the nucleon as being the same, whereas thermodynamics tells us that the specific entropy S/N indeed depends upon the masses of the particles. Hence in order to do a proper calculation of $\langle \rho_\ell \rangle$ with mass dependence taken into account, one might have to make assumptions about the angular distributions of particles in order to be able to extract a tractable calculation.

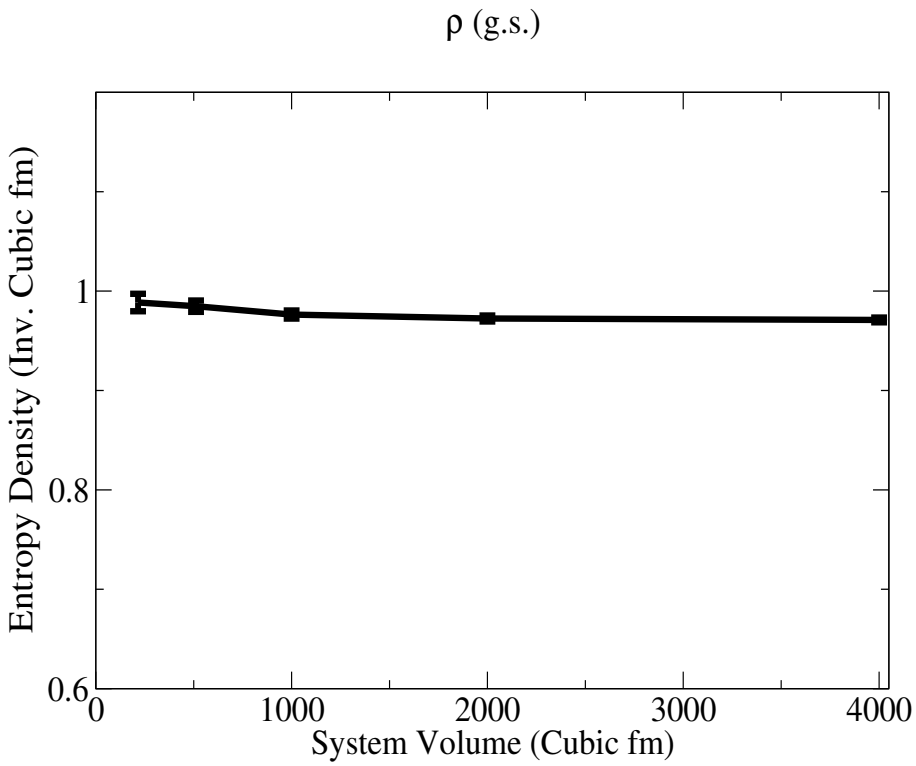

FIGURE 4.7: Entropy density as a function of system size for cases of ground state nuclear density and energy density $\epsilon = 0.2$ GeV/fm^3. Entropy density is found to be independent of system size, which is to be expected.

Gibbs Formula for Entropy

The energy density, pressure, and number densities are calculated from a statistical model for a non-interacting, relativistic gas of massive particles in the grand canonical ensemble [84]. They can be expressed in the following form:

$$\epsilon = \frac{\nu T^4}{2\pi^2} \int_0^\infty \frac{x^2 \sqrt{x^2 + \left(\frac{m}{T}\right)^2} dx}{exp\left[\sqrt{x^2 + \left(\frac{m}{T}\right)^2} - \frac{\mu_B}{T}\right] \pm 1} \tag{4.40}$$

$$P = \frac{\nu T^4}{2\pi^2} \int_0^\infty \frac{x^4 dx}{3\sqrt{x^2 + \left(\frac{m}{T}\right)^2} exp\left[\sqrt{x^2 + \left(\frac{m}{T}\right)^2} - \frac{\mu_B}{T}\right] \pm 1} \tag{4.41}$$

$$n = \frac{\nu T^3}{2\pi^2} \int_0^\infty \frac{x^2 dx}{exp\left[\sqrt{x^2 + \left(\frac{m}{T}\right)^2} - \frac{\mu_B}{T}\right] \pm 1}, \tag{4.42}$$

where ν is the number of degrees of freedom, and +/- refer to fermions/bosons, respectively. It then can be shown that the specific entropy per particle is a function of at most two dimensionless variables, $\frac{m}{T}$ and $\frac{\mu_B}{T}$, where $\mu_B = 0$ for zero net baryon density. We have computed the entropy directly from the Gibbs formula, wh ere the energy density, pressure, and chemical potentials/densities are extracted directly from our UrQMD simulations:

$$s_{\text{Gibbs}} = \left(\frac{\epsilon + P - \mu_B \rho_B}{T}\right) \tag{4.43}$$

We compare this computation with another scheme and show the comparison in Figure 4.8.

Microscopic Counting of Particles

Note that the mass-dependence of the entropy upon the constituent particles is a fact that cannot be taken for granted, especially for hadronic systems where $m/T \sim 1.5 - 20$ [65] With this in mind, we propose computing the weighted average of the specific entropy $\frac{s}{n}$ for the particles in our system, and counting the number of particles:

$$s_{\text{specific}} = \frac{1}{V} \sum_{j=1}^{N_{part}} \left(\frac{s}{n}\right)_j N_j. \tag{4.44}$$

In order to extract the specific entropy, we begin with the Gibbs formula

$$s = \left(\frac{\epsilon + P - \mu_B \rho_B}{T}\right), \tag{4.45}$$

to relate the entropy density s to the energy density, pressure, baryochemical potential, and temperature. The energy density, pressure, and number densities are calculated from a statistical model for a non-interacting, relativistic gas of massive particles in the grand canonical ensemble [84]. They can be expressed in the following form:

$$\epsilon = \frac{\nu T^4}{2\pi^2} \int_0^\infty \frac{x^2 \sqrt{x^2 + \left(\frac{m}{T}\right)^2} dx}{exp\left[\sqrt{x^2 + \left(\frac{m}{T}\right)^2} - \frac{\mu_B}{T}\right] \pm 1} \tag{4.46}$$

$$P = \frac{\nu T^4}{2\pi^2} \int_0^\infty \frac{x^4 dx}{3\sqrt{x^2 + \left(\frac{m}{T}\right)^2} exp\left[\sqrt{x^2 + \left(\frac{m}{T}\right)^2} - \frac{\mu_B}{T}\right] \pm 1} \tag{4.47}$$

$$n = \frac{\nu T^3}{2\pi^2} \int_0^\infty \frac{x^2 dx}{exp\left[\sqrt{x^2 + \left(\frac{m}{T}\right)^2} - \frac{\mu_B}{T}\right] \pm 1}, \tag{4.48}$$

where ν is the number of degrees of freedom, and +/- refer to fermions/bosons, respectively. It then can be shown that the specific entropy per particle is a function of at most two dimensionless variables, $\frac{m}{T}$ and $\frac{\mu_B}{T}$, where $\mu_B = 0$ for zero net baryon density.

Entropy Scaling Law

An interesting check that can be performed is the scaling law

$$s \sim T^{\frac{1}{c_s^2}} \tag{4.49}$$

, where c_s is the speed of sound and T is the temperature. This scaling law can be obtained for our system as follows: starting from the first law of thermodynamics,

$$dU = TdS - pdV + \sum_i \mu_i dN_i. \tag{4.50}$$

If all charges are conserved (in our case strangeness and baryon number are conserved), and our volume is fixed, $d\epsilon = Tds$. For a system in chemical equilibrium, the Gibbs free energy density should be minimized:

$$dg = d\epsilon - Tds - sdT + dp, \tag{4.51}$$

which implies $sdT = dp$ or $sdT = c_s^2 d\epsilon = c_s^2 Tds$, which then yields the scaling relation $s \sim T^{\frac{1}{c_s^2}}$. The speed of sound can be easily obtained from the slope of the EoS where pressure is obtained as a function of energy density: $c_s^2 = \frac{\partial p}{\partial \epsilon}$. A comparison of these two quantities is given in Figure 4.9.

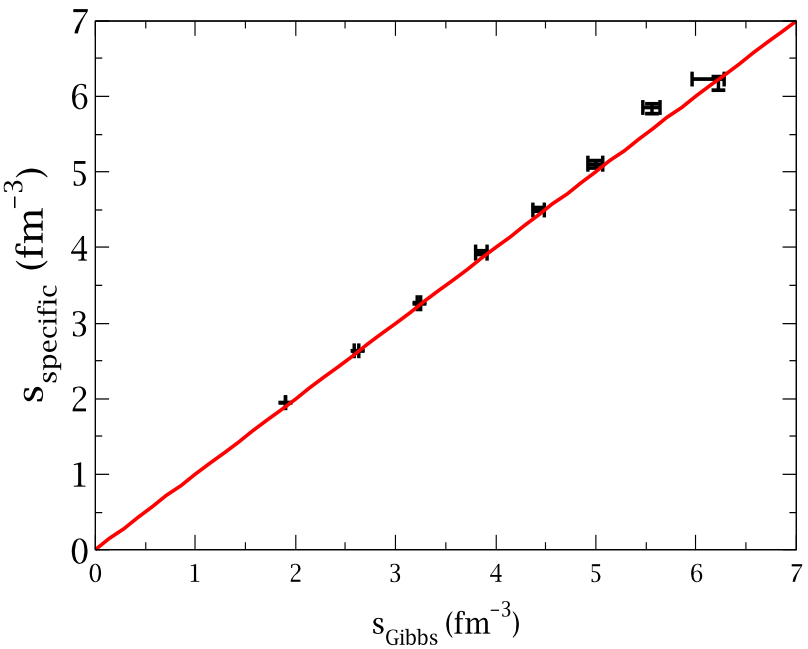

FIGURE 4.8: Entropy density calculated via summation over specific entropies, versus entropy density calculated via the Gibbs formula [26].

4.5.2 Entropy Calculation in the PCM

A similar comparison is made for calculating the entropy in the PCM. However, the calculation of the entropy becomes much simpler, as the quark masses are very small.

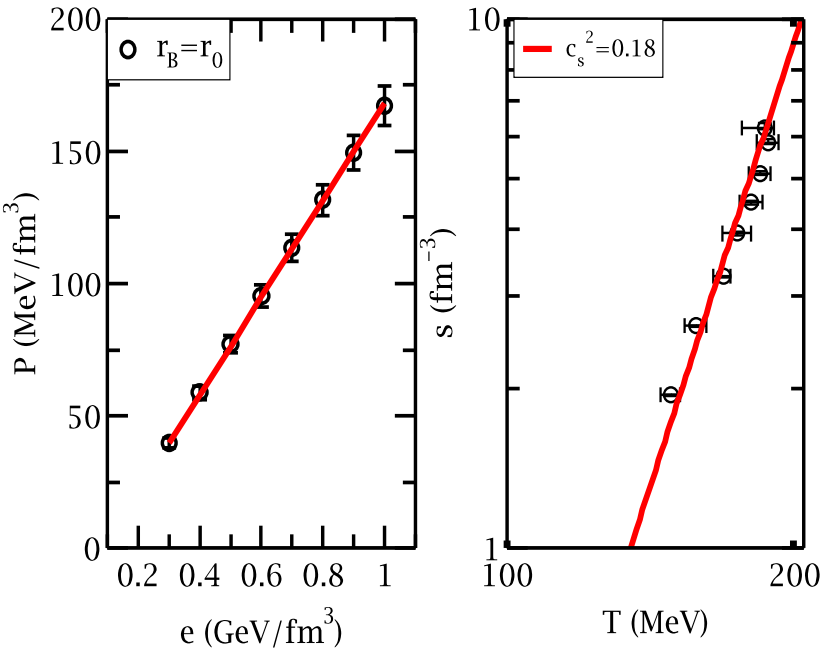

FIGURE 4.9: Left frame: pressure vs energy density. Right frame: entropy density vs temperature. Note the same value of $c_s^2 = 0.18$ was used for both fits [27].

Comparison between the Gibbs formula and the formula for an ideal gas of massless particles yields a very close agreement, as shown in Figure 4.10. The formula for an ideal gas of massless particles is given by the Stefan-Boltzmann formula. We can compare the entropy density directly obtained from our calculation to the Stefan Boltzmann entropy density given by:

$$s = \frac{2\pi^2}{45}\nu(T)T \tag{4.52}$$

where $\nu(T) = N_b + \frac{7}{8}N_f$ and N_b and N_f are the bosonic and fermionic degrees of freedom. The results of the comparison are shown in the left frame of and figure 2 and show good agreement between the Stefan Boltzmann entropy and our system entropy calculated via the Gibbs relation.

Now that the systematics of microscopic transport models employed have been

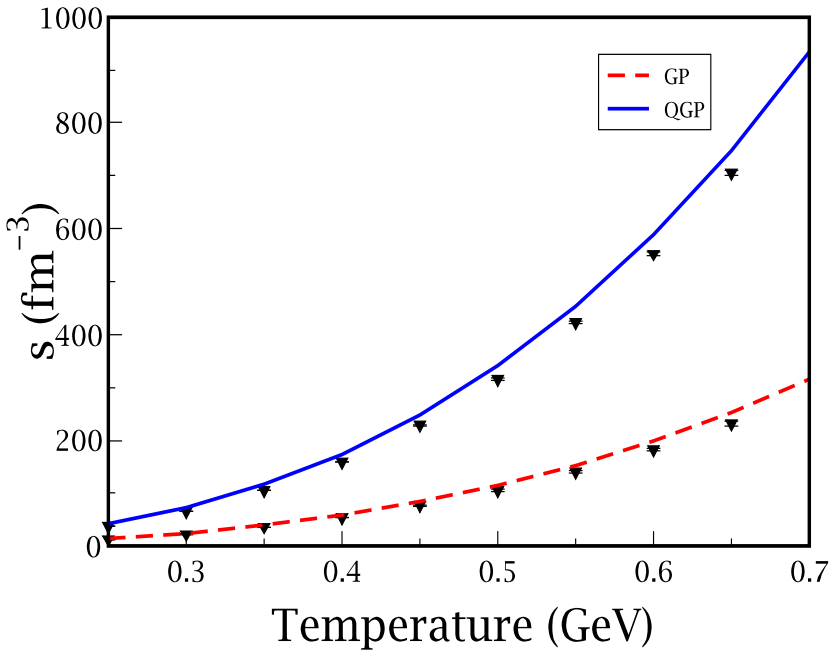

FIGURE 4.10: Entropy versus temperature from the PCM. Both the Gibbs method and Steffen Boltzmann formula were used, and the two methods yield excellent agreement [32].

used, we can proceed to show how transport coefficients are calculated from these two models.

5

Extracting Transport Coefficients from Microsopic Transport Models

This chapter deals with calculation of transport coefficients from two microscopic transport models, namely UrQMD with hadronic degrees of freedom and the PCM with partonic degrees of freedom. While η/s is calculated from both models using the Green-Kubo method, ζ is calculated from UrQMD for certain cases in the relaxation time approximation, and D_B is calculated from UrQMD using the Green-Kubo method. All such calculations are performed for a system in the infinite volume limit. As such, to simulate infinite matter we confine the particles comprising the system to a box with periodic boundary conditions [16]. The numerics associated with the Green-Kubo method are also discussed.

5.1 Transport Coefficients

We obtain the shear viscosity and baryon number diffusion coefficients through using the Kubo-formula, which allow us to relate linear transport coefficients to the time

integral of correlation functions. In the case of shear viscosity, the Kubo formula is

$$\eta = \frac{1}{T}\int d^3r \int_0^\infty dt \langle \pi^{xy}(\vec{0},0)\pi^{xy}(\vec{r},t)\rangle, \tag{5.1}$$

where T is the temperature of the system, t is the post-equilibriation time (the above formula defines $t = 0$ as the time the system equilibriates), and π^{xy} is the shear component of the energy momentum tensor $\pi^{\mu\nu}$ [39]. The corresponding Kubo formula for bulk viscosity is

$$\zeta = \frac{1}{T}\int d^3r \int_0^\infty dt \langle \tilde{P}(\vec{0},0)\tilde{P}(\vec{r},t)\rangle, \tag{5.2}$$

where

$$\tilde{P} \equiv \frac{1}{3}\left(T_{xx} + T_{yy} + T_{zz}\right) - P_{eq} + c_s^2\left(T_{00} - \epsilon_{eq}\right) \tag{5.3}$$

is the pressure current. $\pi^{\mu\nu}$ is obtained by integrating over the three momenta of the system:

$$\pi^{\mu\nu} = \int d^3p \frac{p^\mu p^\nu}{p^0} f(x,p), \tag{5.4}$$

where $f(x,p)$ is the phase space distribution of the system of particles. For a system of point particles uniformly distributed in configuration space,

$$f(x,p) = \frac{1}{V}\sum_{j=1}^{N_{part}} \delta^{(3)}\left(\vec{p} - \vec{p}_j\right), \tag{5.5}$$

where j indexes the particles. The shear component of the stress-tensor then reduces to

$$\pi^{xy} = \frac{1}{V}\sum_{j=1}^{N_{part}} \frac{p^x(j)p^y(j)}{p^0(j)}. \tag{5.6}$$

Similarly, any component of the energy momentum tensor can be calculated in this manner:

$$\Pi^{ik} = \frac{1}{V} \sum_{j=1}^{N_{part}} \frac{p^i(j)p^k(j)}{p^0(j)}. \tag{5.7}$$

Since the point particles are uniformly distributed in real space, we can simplify the Kubo formula for shear viscosity to

$$\eta = \frac{V}{T} \int_0^\infty dt \langle \pi^{xy}(0)\pi^{xy}(t) \rangle, \tag{5.8}$$

where V is the volume of the system. Likewise, the Kubo formula for the self-diffusion coefficient is

$$D = \frac{1}{3} \int_0^\infty dt \langle \vec{v}(0) \cdot \vec{v}(t) \rangle_{\text{equil}}. \tag{5.9}$$

However, since we are particularly interested in baryon number diffusion, the only particles that are averaged over are the baryons:

$$\langle ... \rangle = \frac{1}{N_{\text{events}}} \sum_{k=1}^{N_{\text{events}}} \frac{1}{N_{\text{baryons}}} \sum_{l=1}^{N_{\text{baryons}}} ... \tag{5.10}$$

akin to the averaging process used in [78]. Another transport coefficient of note in relativisitic heavy ion collisions is the thermal conductivity, which in the traditional definition of an ideal fluid is infinite. Since our strategy for simulating equilibriated infinite hadronic matter involves fixing our system with no collective heat current flow, the thermal conductivity coefficient is irrelevant for our system.

5.1.1 Shear Viscosity

Computing the shear viscosity for our system amounts to finding the time integral of the stress-tensor stress-tensor correlations about the equilibrium state. The correlation function of the shear component of the system's energy momentum tensor

is displayed in Figure 5.1 for a case at lower temperatures. If one examines the plot then it empirically decays exponentially as a function of t.

In order to simplify evaluating the integral in equation 5.8, we can propose an exponential ansatz for the correlation function $\langle \pi^{xy}(0)\, \pi^{xy}(t) \rangle$:

$$\langle \pi^{xy}(0)\, \pi^{xy}(t) \rangle \propto exp\left(-\frac{t}{\tau_\pi}\right), \tag{5.11}$$

since such a decay is empirically observed in Figure 5.1.

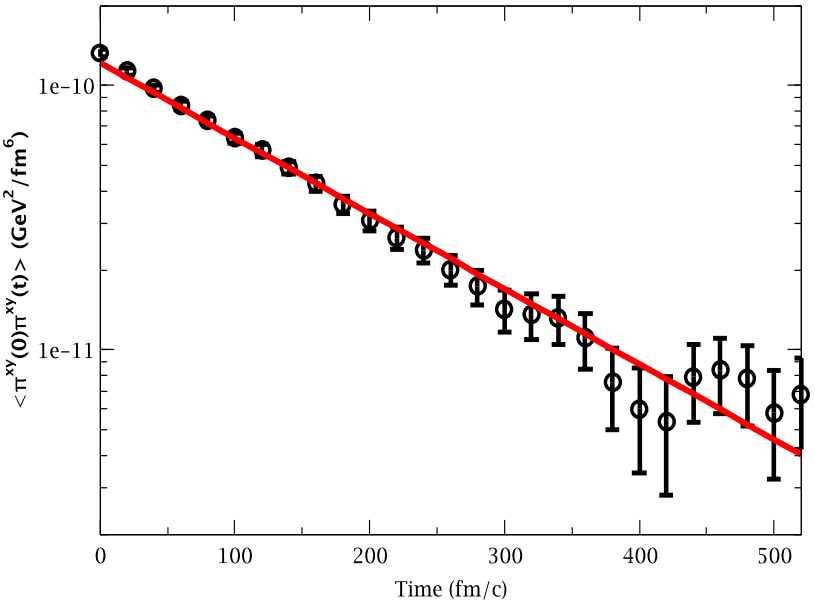

FIGURE 5.1: The shear viscous correlator for $T = 67.9$ MeV as a function of t. Note the empirically observed exponential decay of the correlator as a function of t [27].

Another representative sample of this correlation function for shear viscosity is shown in Figure 5.2 for a higher temperature, and exponential decay is also empirically observed. Using the above exponential ansatz for the stress tensor correlation

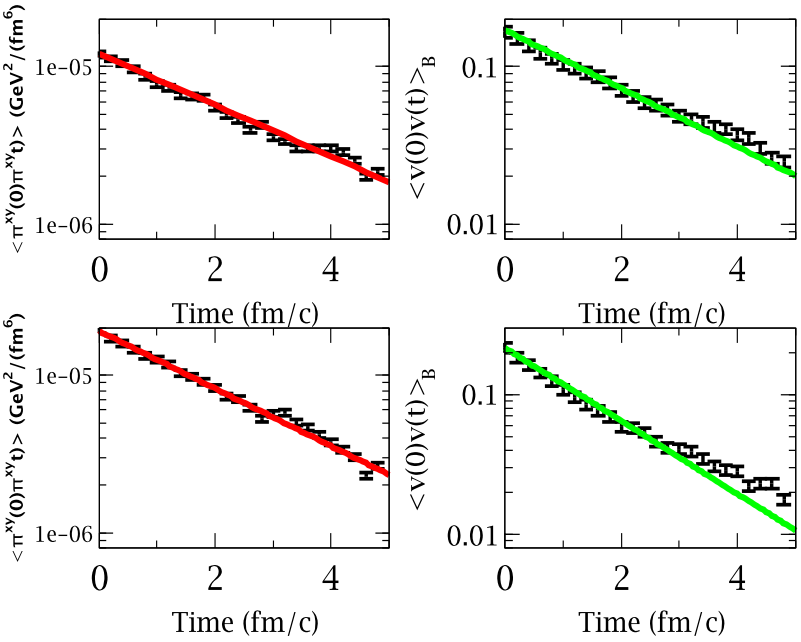

FIGURE 5.2: .Shear viscous and baryon diffusion correlators as a function of t. The black points refer to the calculated points from the simulations, and the solid red line refers to a fit. The top panel is for the case of $\epsilon = 0.3$ GeV and the bottom panel for $\epsilon = 0.8$ GeV. All plots in this panel were obtained for the case of ground state nuclear density.

function, the Kubo formula reduces to

$$\eta = \frac{V}{T}\tau_\pi \langle \pi^{xy}(0)^2 \rangle. \tag{5.12}$$

The parameter τ_π can be interpreted as a relaxation time of the correlation of the viscous tensor. Although relaxation time typically denotes a timescale characterizing the rate of change of the distribution function (see Chapter 3), in this context it characterizes the timescale over which the system loses information on previous correlations between momentum density components in the stress energy tensor. Hence τ_π is akin to a "memory time." τ_π is shown as a function of temperature in Figure 5.3 for the case of full kinetic and chemical equilibrium at $\mu_B = 0$. Note that τ_π

decreases as a function of temperature, and such a behavior is consistent with what would be expected of a collision time due to increased thermal activity at higher temperature.

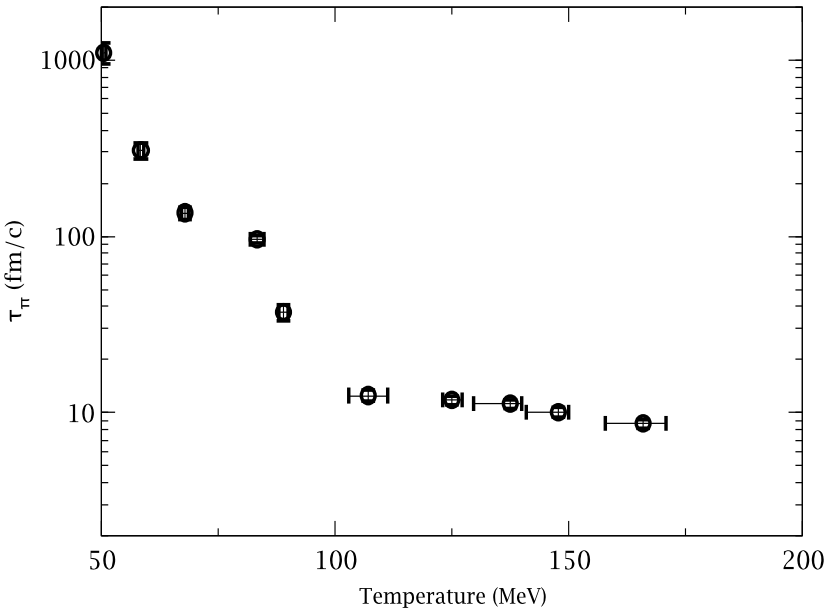

FIGURE 5.3: The viscous correlator relaxation times τ_π in full chemical and kinetic equilibrium as function of temperature for the case. Note the general trend of decreasing τ_π as a function of T.

The results of shear viscosity to entropy density ratio are illustrated in Figure 5.4. Also shown is the computation of $\frac{\eta}{s}$ for a system of chiral pions for the value of $f_\pi = 130$ MeV, and 3 flavor pQCD. Note that our black points increasingly diverge from the chiral pions curve as $T \to 0$. This is because the pions in our system are not chiral but massive. A calculation of the shear viscosity for massive pions results in a larger value than for chiral pions [73], and the corresponding entropy density for massive pions is smaller than the corresponding result for massive pions in this range. Note that including finite baryochemical potential strongly reduces η/s. The

result of viscosity greatly being reduced when baryons are included in the system can be explained classically. Recall that there exists a relation between transport coefficients and the cross section of particles in the medium. For shear viscosity, $\eta \sim \frac{\bar{p}}{\sigma}$, where $\bar{p}$ is the mean momentum per particle in the medium. Resonant meson (anti)baryon cross sections are large, such as ~ 120 mb for $p + \pi$ through the Δ_{1232} resonance [14]. Very large cross sections hence reduce η. Increasing the particle multiplicity enhances the entropy density s, and since $s \sim n$ to zeroth order, η/s is notably reduced at finite baryochemical potential.

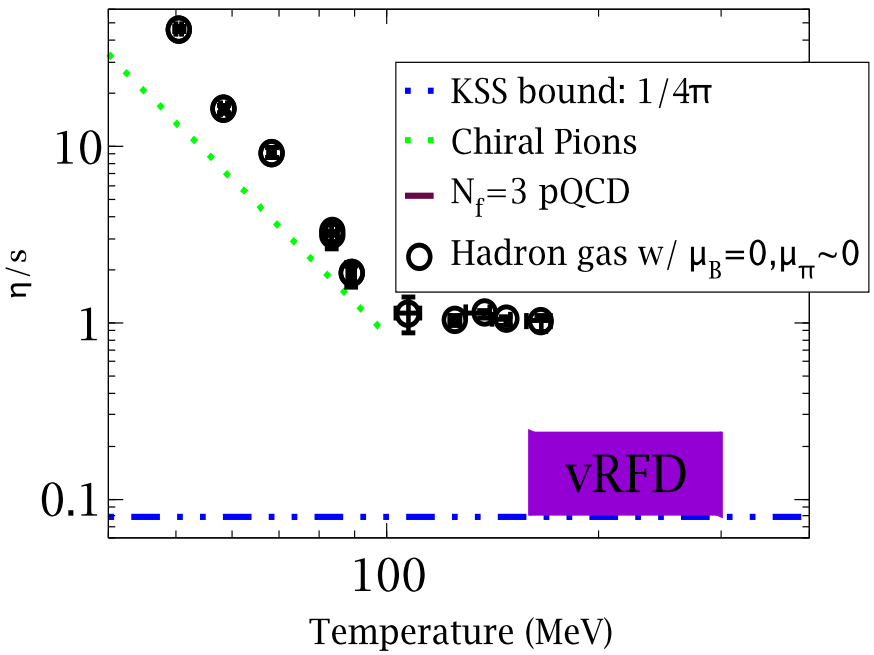

FIGURE 5.4: η/s for UrQMD (black points), chiral pions, and 3 flavor pQCD (AMY calculation) [27].

It should be noted in all such calculations of shear viscosity for hadronic systems, the KSS bound is respected with the exception of [18], where it is violated albeit at an unphysically large temperature greatly exceeding the deconfinement transition temperature calculated from lattice QCD simulations.

5.1.2 Error Analysis

The temperature and shear viscosity coefficient calculations are subject to both systematic and statistical errors. Since the Green-Kubo formula, with the exponential ansatz for the correlation function, depends upon the temperature,

$$\eta = \frac{V}{T}\langle \pi^{xy}(0)^2 \rangle \tau_\pi \tag{5.13}$$

it is important to identify the separate sources of systematic and statistical errors in the extraction of T and η. Recall from Chapter 4 that the temperature is extracted from a plot of the distribution $(1/pEdN/dE)$ after momentum isotropy has been verified. Such a distribution should follow a Boltzmann distribution for a properly thermalized system:

$$\frac{1}{pE}\frac{dN}{dE} \propto exp\left(-\frac{E}{T}\right). \tag{5.14}$$

One can then perform a fit to the distribution to extract the temperature. In particular, for the case of unit fugacity for $130 < T < 170$ MeV, different temperatures T_i are observed for the different particle species when extracted via performing reduced χ^2 fits to $(1/pEdN/dE)$. However, the temperatures T_i extracted via the reduced χ^2 fitting of $(1/pEdN/dE)$ agree better for the cases of NON-unit fugacities in the temperature range $130 < T < 170$ MeV. We observe that controlling the system at temperatures $130 < T < 170$ MeV to ensure unit fugacity for pions and kaons becomes more difficult due to the numerous inelastic collisions experienced by the system in that temperature regime. As a result, the initial yields of the particles were adjusted to compensate for this effect, and the net result is that the system equilibriates with the different individual particle species, (pions, kaons, nucleons) attaining slightly different temperatures. The horizontal error bars for the black points in the region $T > 130MeV$ in Figures 5.3, 5.4 and 5.6 represent the spread

of temperatures T_i for the different species, and this spread is not necessarily symmetric. The temperature for these points was calculated by chemically weighting the temperatures obtained by performing reduced χ^2 fits for the individual temperature species i with their particle densities, as was discussed in Chapter 4 with reference to equation 4.36:

$$T_{chem} = \frac{\sum_i n_i T_i}{\sum_i n_i}. \tag{5.15}$$

The index i runs over that for the kaons, (anti-)nucleons, and pions. The value of T_{chem} then enters into the calculation for η in equation 5.13 for the high temperature black points in Figures 5.3- 5.6. This is a systematic error which was NOT included in the error bar calculation for η. However, statistical errors for calculating the temperature in all cases were propagated.

The viscosity error bar is then obtained by standard error propagation of the Kubo correlator decay time τ_π.

$$\sigma_\eta/\eta = \sqrt{(\sigma_{\tau_\pi}/\tau_\pi)^2 + (\sigma_{T,stat}/T)^2 + (\sigma_{\langle\pi^{xy}(0)^2\rangle}/\langle\pi^{xy}(0)\rangle)^2} \tag{5.16}$$

The error bars in τ_{pi} were obtained by using different values of τ_π in the exponential ansatz

$$\langle\pi^{xy}(0)\pi^{xy}(t)\rangle \propto exp\left(-\frac{t}{\tau_\pi}\right) \tag{5.17}$$

in order to cover the appropriate range of error bars on the points at the tail of the decay of $\langle\pi^{xy}(0)\pi^{xy}(t)\rangle$. The mean of the difference between the maximum and minimum allowable range of τ_π is used to obtain σ_{τ_π}. The error bars in the values of the y-intercept of $\langle\pi^{xy}(0)\pi^{xy}(t)\rangle$ (i.e. $\langle\pi^{xy}(0)^2\rangle$) were obtained by taking the ranges of $\langle\pi^{xy}(0)^2\rangle$ corresponding to the ranges of τ_π used in the fits to the correlator data.

5.1.3 Examining system size effects

In our effort to ensure our Green-Kubo algorithm for calculating transport coefficients is robust, it is helpful to investigate how our extracted transport coefficients depend upon the system size L. In particular, a dimensionless scale characterizing how dilute the system is shall be called the pseudo-Knudsen number, defined by λ_f/L, where λ_f is the mean free path and L is the length of an edge of the box in our system. When a calculation in UrQMD is set up, one must ensure that

- Sufficient particles are included per event in order to be able to calculate an ensemble average for the particles in the box.
- For optimal efficiency of the calculation, one ensures particles encounter sufficient collisions before reaching the walls of the box, since cyclic periodic boundary conditions should not be highly sensitive to this. However, this should be verified, as was shown in Figure 5.5.

As a result, we have quantified the effect of our transport coefficient on λ_f/L for a test case of a pure pion gas at $T = 100$ MeV for a constant elastic pion cross section of $\sigma_{\pi\pi} = 10$ mb. The results are shown in Figure 5.5.

5.1.4 η/s Out of Chemical Equilibrium

We should note that in a heavy ion collision, the temperatures corresponding to kinetic and thermal freezeout are not identical. While the hadronic ratios freezeout at $T_{\text{chem}} \approx 160$ MeV, the momentum distributions freezeout later in the collision, at $T_{\text{kin}} \approx 130$ MeV [37, 46]. As a result of the separation of chemical vs. thermal freezeout timescales in a heavy ion collision, the system evolves out of chemical equilibrium. We mimic this effect by initializing our system with a thermal distribution, but with yields of particles corresponding to a given fugacity at that temperature. The viscosity correlator is then extracted before the system fully relaxes back into

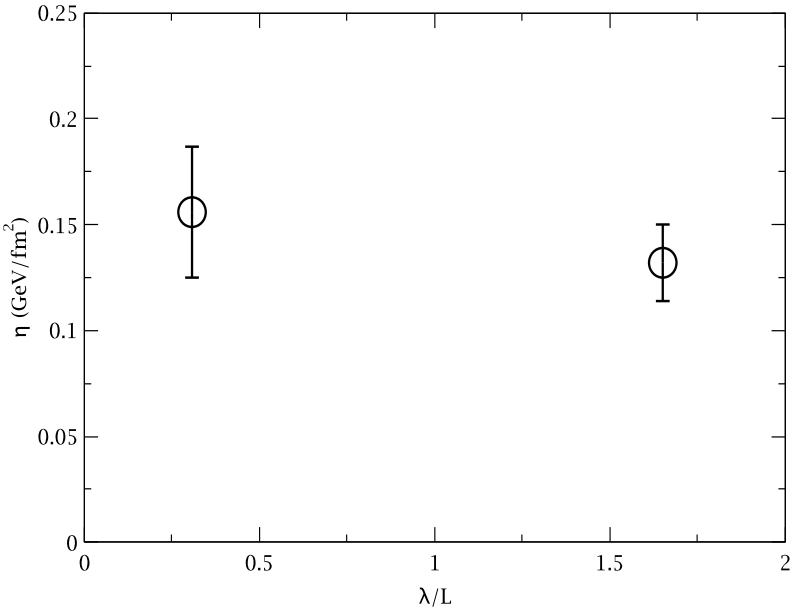

FIGURE 5.5: η as a function of λ_f/L for $\sigma_{\pi\pi} = 10$ mb. This was a test to check for sensitivity to λ_f/L, where L is our system size.

full chemical and thermal equilibrium. It turns out that when η/s is calculated then, there is a real effect from effective non-unit fugacities being introduced by our technique. This systematic trend is illustrated in Figure 5.6. η/s is seen to decrease at non-unit fugacities, and this result can be understood classically. The entropy density is enhanced since $s \sim n$, and at non-unit fugacities the particle multiplicities for species of the fugacities which are now no longer unity increase. A similar effect is seen for η/s calculated for matter at finite baryochemical potential in full chemical and thermal equilibrium. Note that finite baryochemical potential corresponds to introducing a finite net baryon density, and since baryonic cross sections are large, since $\eta \sim \frac{\bar{p}}{\sigma}$, the viscosity coefficient is also decreased. Our trend for finite μ_B is similar to the finding by [42].

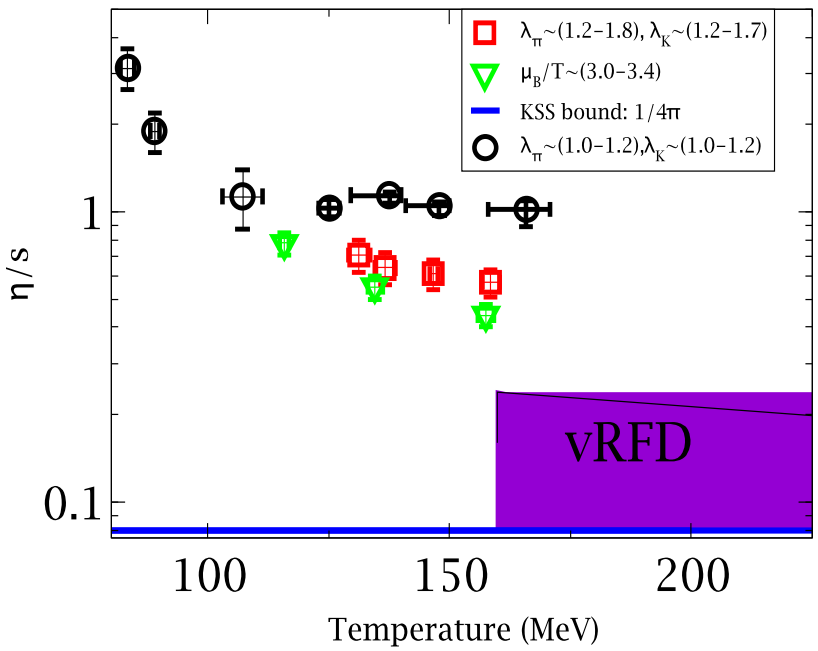

FIGURE 5.6: η/s for zero chemical potential (black points), nonunit fugacicities(red points), and finite baryochemical potential(green points) [27]. Note the trend of decrease i η/s at nonunit fugacities or finite baryochemical potential.

5.1.5 Trajectory of η/s in a Heavy Ion Collision

We have calculated the viscosity over entropy density ratio η/s of a hadron gas as a function of temperature, baryo-chemical potential and fugacities. Using this calculation we can piece together, with what is known about η/s from viscous hydrodynamics calculations, the trajectory of η/s in a heavy ion collision. We have demonstrated that the inclusion of non-unit particle fugacities, which are bound to arise due to the separation of chemical and kinetic freeze-out during the heavy ion collision evolution, will reduce the value of η/s, but not to the value necessary to ensure the successful application of viscous hydrodynamics to the full collision evolution at RHIC. Our calculation of η/s in a hadron gas from a microscopic transport model therefore constrains the origin of the low viscosity matter produced in a rel-

ativistic heavy ion collision, which must occur in the deconfined phase, possibly in the range $1 < T/T_c < 2$. At the formation of the hadronic phase, which is thought to occur in chemical equilibrium, η/s will experience a sharp increase. However, subsequently its value may decrease again due to the system evolving out of chemical equilibrium. Near kinetic freeze-out η/s will rise with decreasing temperature. This lends credence to the notion that the dynamics of the evolution of a collision at RHIC is dominated by the deconfined phase exhibiting very low values of η/s.

5.1.6 Assessing Systematic Uncertainties

In our analysis for η/s there are two important things to note in our analysis. The first is that our calculation neglects multiparticle processes, and the other is the choice of effective baryon-antibaryon annihilation/production to include baryons.

It should be noted that $\eta/s \approx$ 0.9-1.0 in full chemical and kinetic equilibrium, and at RHIC, it is assumed that the hadron gas is in full chemical and kinetic equilibrium at T_c. However, we have used the effective two-body resonance interaction $\rho\phi(1020) \leftrightarrow \mathrm{N\bar{N}}$ to include antibaryon production and annihilation obtain a state close to unit light quark fugacities, as discussed in Chapter 4. In particular, since the $\phi(1020)$ primarily decays into a kaon and anti kaon, the light quark fugacity for systems with the effective 2 body process $\rho\phi(1020) \leftrightarrow N\bar{N}$ is smaller than that for the 2 body process $\rho\omega(1420) \leftrightarrow N\bar{N}$.The effects of multiparticle processes may be important in the region near T_c, and a rise in η/s from the suggested range from viscous hydrodynamics may be delayed by the presence of Hagedorn states [67, 70]. We expect that if we were to include multiparticle processes in a manner that respects detailed balance, our values of η/s would decrease: increased particle production would enhance the entropy density, hence reducing η/s. Another possible effect would be the possible decrease of η due to the enhancement of the thermally averaged cross section, since $\eta \sim \frac{\bar{p}}{\sigma}$. Both these effects would work to decrease η/s.

Another source of systematic uncertainty that could be investigated in more detail is the validity of using a classical Boltzmann equation in our regime of higher temperatures for a hadron gas, $T \sim$ 130-160 MeV. The system is not dilute in this temperature regime, and in particular one should examine the scale of the mean free path to the interparticle spacing. A dilute system implies $\lambda_f >> n^{-1/3}$, and for our system at temperatures above $T \sim 130$ MeV this is not the case.

5.1.7 Baryon Number Diffusion

The investigation of baryon number diffusion by authors of [78] was motivated by investigation of baryon number fluctuations in relativistic heavy ion collisions [80]. Some early models could be used to extract the size of a charge fluctuation from the baryon number diffusion constant [80].

We use also use the Green-Kubo method to extract the baryon number diffusion coefficient. Examining the velocity correlation function with only baryonic averaging in Figure 5.2, we again see the exponential decay of the relevant correlator for the diffusion constant. Assuming the correlation function $\langle \vec{v}\,(0) \cdot \vec{v}\,(t) \rangle_B$ has an exponential ansatz:

$$\langle \vec{v}\,(0) \cdot \vec{v}\,(t) \rangle_B \propto exp\left(-\frac{t}{\tau_D}\right) \tag{5.18}$$

We have extracted the baryon diffusion coefficient D_B, as has been performed by Sasaki and Muroya [78]. Our results are depicted in Figure 5.7. We find that D_B decreases with increasing baryon density at a given temperature. In principle, we should also be able to extend our calculation to the $\mu_B = 0$ regime, since we have implemented baryon-antibaryon annihilation where others before have not. However, in order to get a robust result one must choose a high enough temperature to get sufficient nucleon-antinucleon annihilations. With enough statistics, it is possible to obtain D_B as a function of μ_B vs. T.

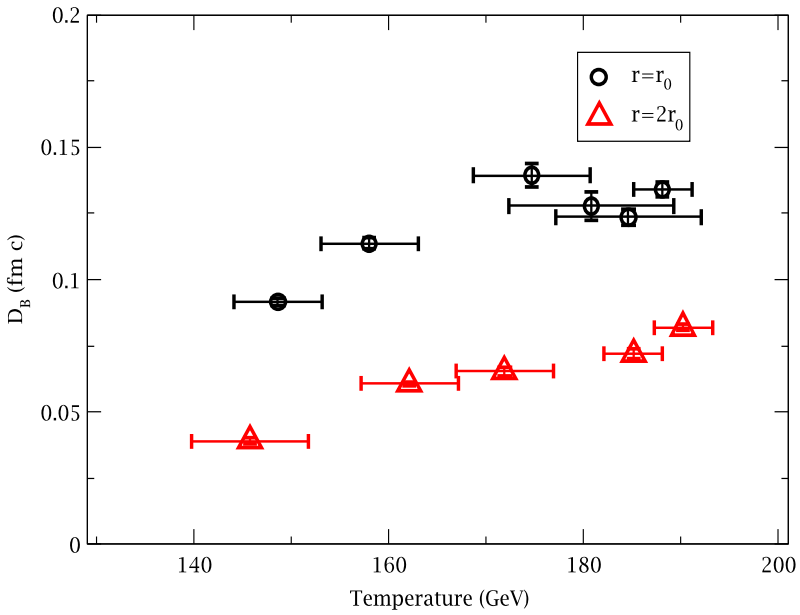

FIGURE 5.7: The baryon number diffusion coefficient as a function of temperature, for ground state and twice ground state nuclear density.

5.2 The Relaxation Time Approximation

Recall from Chapter 3 the formulae for the shear and bulk viscosities using a momentum dependent relaxation time are

$$\eta = \frac{1}{15T}\sum_a \int \frac{d^3p}{(2\pi)^3}\frac{\tau_a p_a^4}{E_a^2} f_a^{eq}(E_a/T), \tag{5.19}$$

$$\zeta = \frac{1}{9T}\sum_a \int \frac{d^3p}{(2\pi)^3}\frac{\tau_a\left(E_a\right)}{E_a^2}\left[\left(1-3c_s^2\right)E_a^2 - m_a^2\right]^2 f_a^{eq}(E_a/T), \tag{5.20}$$

where c_s^2 is the speed of sound squared.[33] Note that the relaxation time described has been generalized to a momentum-dependent relaxation time as opposed to in Chapter 3, where $\tau_a\left(E_a\right)$ was taken out of the integrals in equations 5.19 and 5.20.

The relaxation time in equations 5.19 and 5.20 is the timescale associated with the rate of change of the distribution function. However, it can be shown that in a certain dilute limit, the relaxation time approximately becomes the mean collision time, as was shown in [73]. Recall from Chapter 3 that the Boltzmann equation rewritten in the relaxation time approximation reads

$$\left(\frac{\partial}{\partial t}+\frac{\vec{p}}{E}\cdot\nabla_r\right)f\approx\tilde{f}Z_1^{+,0}-fZ_1^{-,0}\equiv-\frac{-\delta f}{\tau_1^r(k_1)} \tag{5.21}$$

where

$$[\tau_1^r(k_1)]^{-1}=\sum_2[\tau_{12}^r(k_1)]^{-1} \tag{5.22}$$

and, if only elastic scattering is assumed,

$$[\tau_1^r(k_1)]^{-1}=\frac{g_2}{1+\delta_{12}}\frac{csh(\epsilon_1/2)}{E_1}\int d\Gamma_2 d\Gamma_3 d\Gamma_4\,(2\pi)^4\,\delta^4(k_1+k_2-k_3-k_4)\mid T_{12}\mid^2, \tag{5.23}$$

where $d\Gamma_i\equiv d\omega_i/\left[2csh(\epsilon_i/2)\right]$, and $cshx_1=coshx_i/sinhx_i$ for Fermi/Bose statistics, respectively [73].

$$\epsilon_i\equiv(E_i-\mu_i)/T, \tag{5.24}$$

where μ_i is the chemical potential of the species i and T is the common temperature of the system. One can take thermal averages to extract the mean relaxation rate, defined through

$$\bar{\gamma}_1(T,\mu)=\frac{\int d^3k_1 f_1^0\gamma_1(k_1)}{\int d^3k_1 f_1^0}, \tag{5.25}$$

where

$$\gamma_1(k_1)\equiv 1/\tau_1^r(k_1) \tag{5.26}$$

We can perform a similar process for the collision time

$$\tau_1^c(k_1)\equiv 1/Z_1^{-,0} \tag{5.27}$$

to give the mean collision rate

$$\bar{\nu}_1(T,\mu) = \frac{\int d^3k_1 f_1^0 \nu_1(k_1)}{\int d^3k_1 f_1^0}, \tag{5.28}$$

, where

$$\nu_1(k_1) \equiv 1/\tau_1^c(k_1). \tag{5.29}$$

The authors of [73] approximate that, in the dilute limit,

$$\tau_1^c(k_1) \approx \tau_1^r(k_1). \tag{5.30}$$

Hence, in the dilute limit, we can extract collision times from a microscopic transport model and insert the expression into the integrals in equations 5.19 and 5.20 to extract the viscosities and compare such expressions to the viscosities extracted via the Kubo formula for temperatures in the dilute limit.

5.3 Comparing Transport Coefficients Extracted from the Relaxation Time Approximation Versus the Green-Kubo Method

As such we perform a comparison for the case of $T = 100$ MeV for a gas on only elastic pion collisions with a fixed cross section of $\sigma_{\pi\pi} = 50$ mb. A large cross section was chosen so that sufficient collisions can be generated within a particle's path in the box in order to improve efficiency of the calculation. The reason this temperature was chosen is that it is a practical temperature where the relaxation time in equation 5.20 and 5.19 becomes approximately equal to the mean collision time τ_1^c. The collision time is extracted from UrQMD by calculating a momentum dependent collision rate per unit bin, fitting the form to a Lorentzian function, then integrating over the momenta to get an inverse collision time. This then can be inserted into equations 5.19 and 5.20 to extract the mean collision time.

5.3.1 Bulk Viscosity

We extract the bulk viscosity for a particular case using the Green-Kubo method in order to compare to the relaxation time approximation. The plot of the momentum dependent collision rate is shown in Figure 5.8. ζ/η for the relaxation time approximation assuming a constant relaxation time yields $\sim 10^{-6}$, whereas via the Green-Kubo method yields $\sim 1/3$. The reason for this discrepancy is not resolved. The relaxation time for the correlators for the bulk viscosity coefficient versus shear viscosity coefficient are shown in Figure 5.9. This tells us that we should use a momentum-dependent relaxation time. The correlation function for the bulk viscosity coefficient decreases slowly as a function of time. Precisely calculating fluctuations of the pressure current from equilibrium values is more difficult for the bulk viscosity coefficient, since for shear viscosity, $\langle \pi^{xy} \rangle_{equil} = 0$. Furthermore, it has been shown by the authors of [24] that the finite lifetime of collisions in the system can either enhance or suppress the pressure in the system, which can mean that the precise equilibrium pressure in the system can change over the timescale of the decay of the correlation function.

In particular, the authors of [24] showed that, given a uniform many-body system, with density n and temperature T, all intensive thermodynamic quantitates can be obtained from the free energy per unit volume f. Then the free energy f, to second order in the density, can be written as

$$f(n,T) = f_0(n,T) + \Delta P(n,T), \tag{5.31}$$

where f_0 is free energy for a noninteracting system and ΔP is the correction to pressure[17, 49]

$$P = P_0 + \Delta P = n\,T - T\,n^2 \left(\frac{4\pi}{mT}\right)^{3/2} \frac{1}{2} \int dE\, \mathrm{e}^{-E/T}\, \frac{1}{\pi} \sum_{\ell} (2\ell+1) \frac{d\delta_\ell}{dE}. \tag{5.32}$$

The effects of statistics were ignored in the above calculation. Furthermore, the authors of [24] show the correction to pressure may be further expressed as

$$\begin{aligned}\Delta P &= \frac{1}{2}\int \frac{d\mathbf{p}_1}{(2\pi)^3}\frac{d\mathbf{p}_2}{(2\pi)^3} f(p_1)\, f(p_2)\, \mathrm{Re}\,\langle(\mathbf{p}_1-\mathbf{p}_2)/2|\,\mathcal{T}\,|(\mathbf{p}_1-\mathbf{p}_2)/2\rangle \\ &\quad -T\,\frac{1}{2}\int \frac{d\mathbf{p}_1}{(2\pi)^3}\frac{d\mathbf{p}_2}{(2\pi)^3} f(p_1)\, f(p_2) \int d\Omega\, \frac{d\sigma}{d\Omega}\, v\, \Delta\tau_s(\Omega). \qquad (5.33)\end{aligned}$$

Here $f = \mathrm{e}^{(\mu-E)/T}$ is phase-space occupancy. The first term on the r.h.s. of (5.33) accounts for the forward time delay or mean field.The second term accounts for delay in scattering and, depending on the sign of $\Delta\tau_s$, allows further for an interpretation in terms of the reduction in the number of degrees of freedom or in terms of excluded volume. As such the lifetime of a time delay τ_s induced through the collision in UrQMD may make precise subtraction of the equilibrium pressure for the pressure current in the Kubo formula for bulk viscosity difficult.

5.4 Calculation of η and η/s from the PCM

The same technology used in UrQMD can also be used for the PCM to calculate η/s in the Parton Cascade Model. The calculations were performed for systems of pure gluonic matter and for a system of mixed quarks and gluons. The first one, denoted by GP, is for a gluon plasma with a regular Deybe screening mass and temperature-dependent coupling. The second mode, denoted by QGP, uses the same temperature-dependent parametrizations for m_D and the coupling constant, but is for a quark-gluon plasma with three light quark flavors. One should consider the QGP mode to be the most realistic mode of calculation presented here.

Sample correlation functions for shear viscosity correlators are illustrated in Figure 5.10. Figure 5.11 displays the results of our calculation for the shear viscosity for a system of gluons as well as a system of gluons and three light quark flavors.

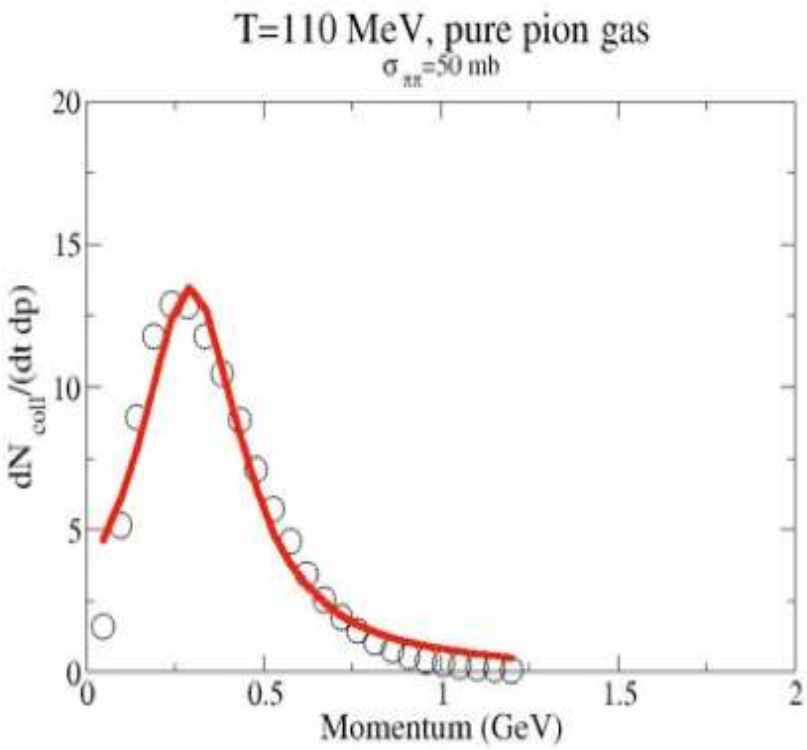

FIGURE 5.8: Collision rate per unit bin in momentum from UrQMD for $\sigma_{\pi\pi} = 50mb$ in a pure pion gas with only elastic collisions. The collision rate was then fit with a Lorentzian to obtain ζ in the relaxation time approximation.

The shear viscosity rises strongly as a function of increasing temperature. It is interesting to note that the QGP shows a higher shear-viscosity than the GP for a given temperature, which is probably due to the smaller interaction cross-sections among the quarks of the system, since recall that $\eta \sim \frac{\bar{p}}{\sigma}$.

Having calculated both, the shear-viscosity as well as the entropy-density of our system, we can now turn to the ratio η/s, made famous by the KSS bound: figure 5.11 shows η/s as a function of temperature for the GP (full circles) and QGP (full triangles) case, compared to an analytic AMY calculation of a three-flavor QGP [7] (solid line). The QGP calculation of η/s shows a monotonous rise as a function of temperature, similar to that of the AMY calculation. The Gluon Plasma exhibits an upturn in η/s for temperatures below 500 MeV – we attribute this unexpected

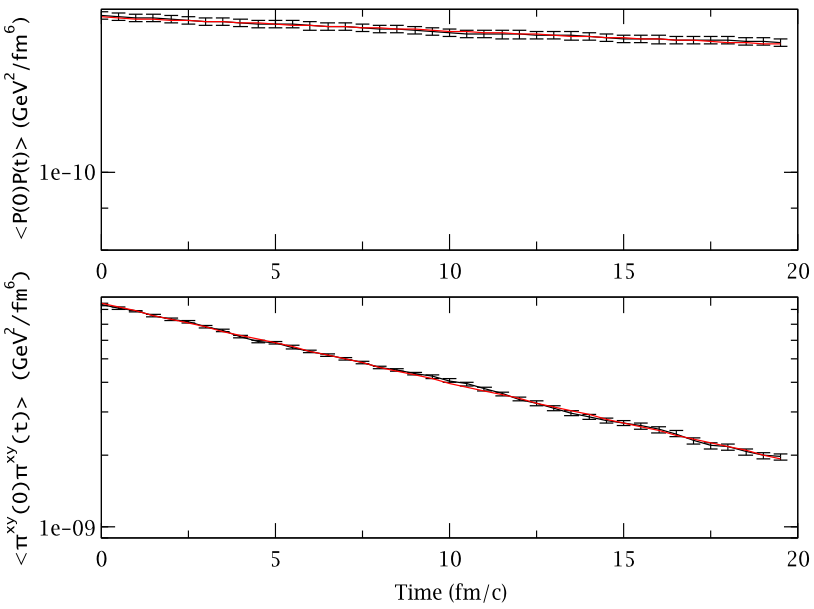

FIGURE 5.9: Top panel: bulk viscosity correlator. Bottom panel: shear viscosity correlator. The correlators are computed for $T = 100$ MeV for a pure pion gas with only elastic collisions $\sigma_{\pi\pi} = 50$ mb.

rise towards lower temperatures to a breakdown in the perturbative approximations present in our calculations.

Comparing η/s of a GP and a QGP at the same temperature may seem misleading due to the significantly larger parton density present in a QGP. Hence in figure 5.12we compare η/s for the two scenarios at equivalent energy-density and find for energy-densities above 35 GeV/fm^3 excellent agreement between the two systems. This is relevant because the flavor composition of the deconfined QCD matter created in ultra-relativistic heavy-ion collisions may change strongly as a function of time – from a gluon-dominated system being created by the decay of a Color-Glass-Condensate to a QGP in full thermal and chemical equilibrium as the system progresses in its hydrodynamic expansion. Our result indicates that η/s, a quantity which controls

the hydrodynamic evolution of the system, should be fairly robust with respect to its flavor composition when taken as a function of energy-density instead of temperature.

In figure 5.13 we study the effects of our different Debye-mass parametrizations and the temperature-dependence on η/s. For this purpose we calculate η/s for a gas of gluons with a Boltzmann Debye-mass at fixed coupling of $\alpha_s = 0.3$ (i.e. the same system as e.g. in [88, 28, 29, 89]) and compare this calculation to one with our default parametrization (taken with $N_c = 3$ and $N_f = 0$). We find the effect of the different m_D parametrizations to be small, on the 10% to 15% level, with the Boltzmann Debye-mass giving consistently smaller values of η/s. If we now replace the fixed coupling with a temperature dependent coupling constant, the value of η/s increases roughly by a factor of 2.

So far we have restricted our investigation in the partonic sector to a purely perturbative partonic system with the respective temperature-dependent screening masses and coupling strengths. However, it has been strongly suggested that the medium created in ultra-relativistic heavy-ion collisions is non-perturbative in nature – at the very least within the temperature range from T_c to approximately $(3-4)T_c$, which is covered by our PCM viscosity calculations. One method to explore the behavior of η/s at stronger coupling is to treat the coupling constant α_s in our calculations as a free parameter and then study η/s at fixed temperature as a function of the coupling. Figure 5.14 shows η/s as a function of coupling strength for the gluon plasma and the quark-gluon-plasma. In the strong coupling limit, in particular for the gluon plasma, values of $\eta/s \ll 1$ can be obtained, yielding results compatible with a fluid-dynamical analysis of RHIC data as discussed in Chapter 2 [51]. Similar results have been obtained by [59], who directly increased the gluon-gluon scattering cross-section, which seems equivalent to an increase in the coupling constant. However, caution should be taken. Note that treating the coupling constant as a free parameter introduces inconsistencies in the medium. In particular, the particle density and

screening mass are still controlled by the temperature, whereas the coupling is not. Also, for large couplings $\alpha_s \simeq 1$ the perturbative assumptions underlying the PCM are not valid anymore.

The final question we wish to address is the effect the angular distribution of the scattering partons , i.e. the exact form of the differential matrix-element, has on eta/s: figure 5.13 shows a comparison between our default gluon plasma calculation compared with results at fixed coupling and regular matrix elements as well as with matrix elements using an isotropic angular distribution. The result of the last particular question are as follows: the main effect is a decrease of η/s by a factor of 3, which results from the choice of a fixed coupling constant vs. a temperature dependent one. Changing from forward-backward peaked to isotropic scattering provides an additional 10% - 20% effect, but not a dramatic reduction in η/s. This finding is of particular interest in the context of work done by [88], employing a PCM including simple radiative corrections (i.e. $2 \rightarrow 3$ and $3 \rightarrow 2$ processes) and effectively using a near-isotropic angular distribution for the third particle in the outgoing channel. Our results utilizing solely $2 \rightarrow 2$ scattering processes indicate that it is most likely a combination of multiple effects:

- A fixed coupling constant.
- The isotropic angular distribution of the multiparticle process inclusion.
- Possibly also a contribution of the multi-particle scattering which is responsible for the low viscosity findings for this calculation.

5.5 ζ and ζ/s in the Parton Cascade Model

Recall from equation 3.10 in Chapter 3 and formula 5.20 that the bulk viscosity should vanish for a conformal system, since for a conformal system particles are

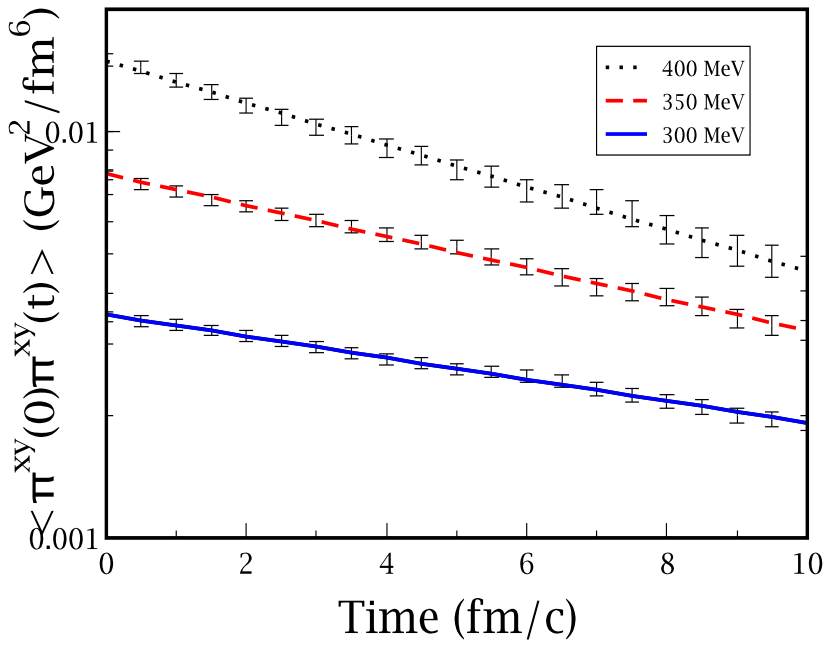

FIGURE 5.10: Shear viscous correlator for pure gluonic matter at different temperatures. Also shown in [32]. The exponential decay is empirically seen in the PCM, as was seen in UrQMD.

massless and $c_s^2 = 1/3$. Also, the entropy calculations from Chapter 4 in the PCM, in conjunction with the entropy scaling law $s \sim T^{1/c_s^2}$ that using $c_s^2 = 1/3$ is a very accurate characterization of the system modeled by the PCM. An ideal gas of massless particles has zero bulk viscosity, and hence the bulk viscosity for the QGP described by the PCM is expected to be also extremely small, if not vanishing.

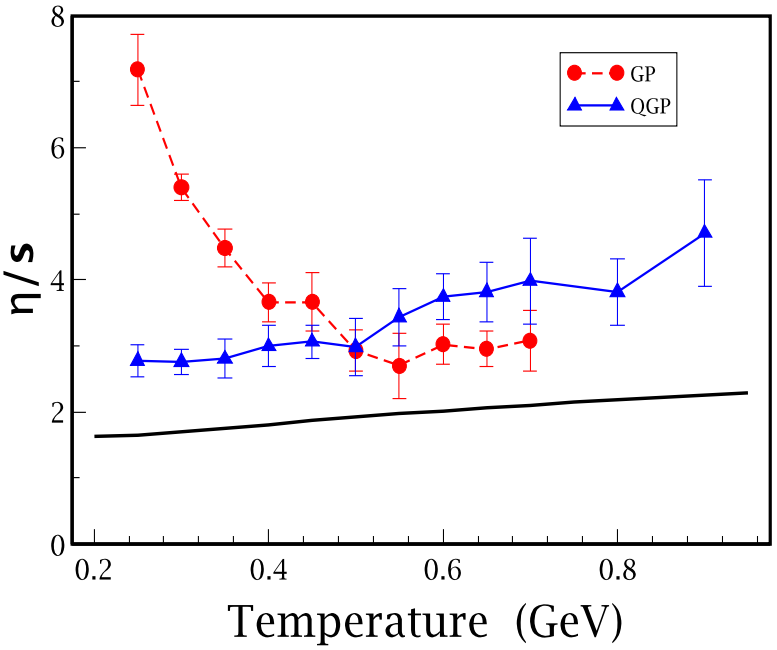

FIGURE 5.11: η/s vs T for the PCM, compared with finite T pQCD calculation. Shown in [32]. Note the much larger values of η/s in the PCM versus from UrQMD.

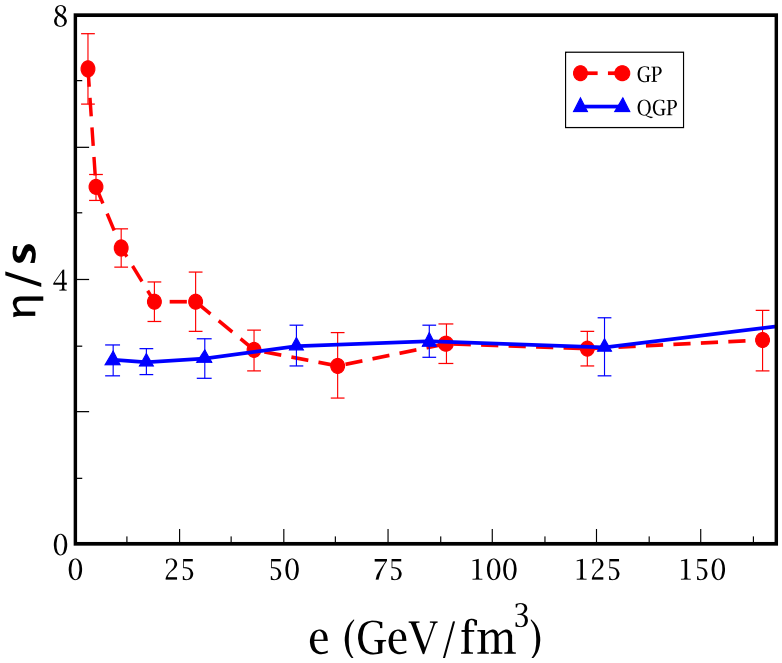

FIGURE 5.12: η/s vs ϵ for the PCM [32]. Note the chemical composition for higher temperatures does not make as much a different in this parameterization of η/s vs ϵ.

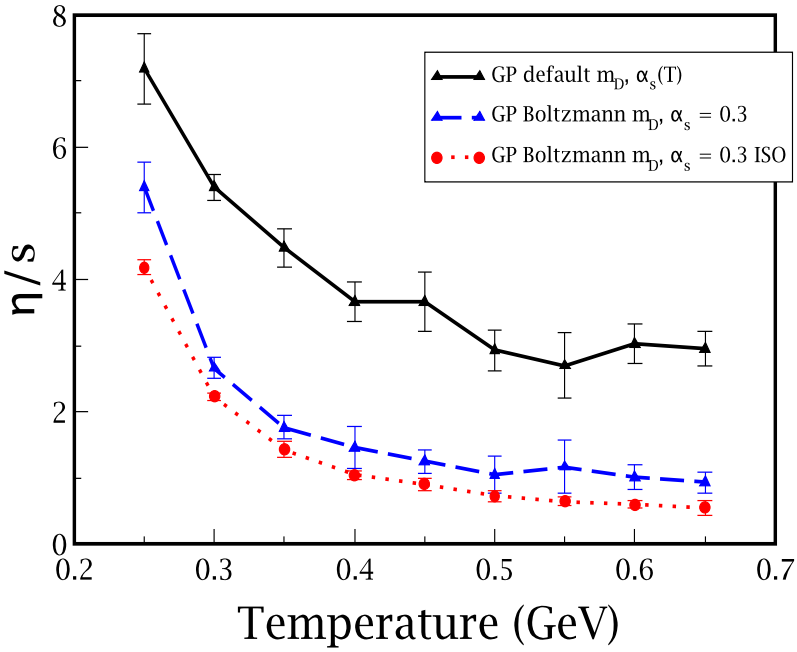

FIGURE 5.13: η/s for different Debye mass parameterizations, and for fixed coupling. Not much difference is seen for different Debye mass parameterizations, although a big effect is seen when running versus fixed coupling is used [32].

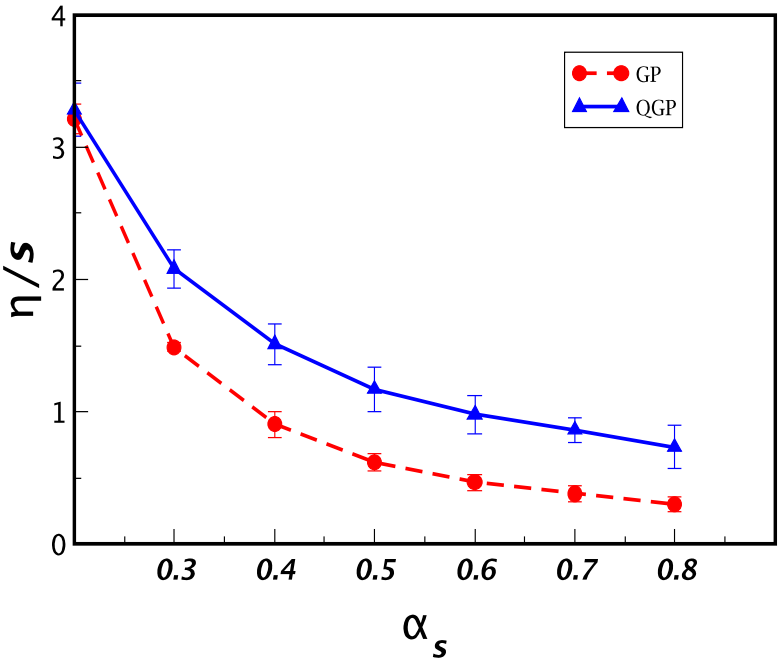

FIGURE 5.14: η/s vs α_s for the PCM. Note the decreasing η/s as a function of increasing α_s, although perturbation theory calculations become more unreliable with greater α_s. [32].

6

The Langevin Equation with Memory Effects

In addition to the behavior of shear and bulk viscosity (and the corresponding viscosity/entropy density ratios) of the deconfined and hadronic matter at RHIC, another transport property that has generated significant interest is that of heavy quark diffusion. It is thought that heavy quarks are produced through hard processes in the quark gluon plasma. For example,

$$gg \rightarrow c\bar{c}\, or\, b\bar{b}. \tag{6.1}$$

It is expected that since b or c quarks are so massive, most of the energy loss experienced by a heavy quark probe in a medium is lost not due to radiation, but due to collisions. Due to Boltzmann suppression, one would expect that the QGP is composed of mostly light quarks and gluons, with rare heavy quarks being present. There has been a surprisingly high v_2 coefficient measured for D-mesons, which contain a c quark [1]. One would expect from kinetic theory that v_2 of mesons containing charmed quarks is much lower than that for lighter mesons. This means that the mechanism by which heavy quarks lose energy in the QGP needs to be much better understood,It is expected that since b or c quarks are so massive, most of the energy

loss experienced by a heavy quark probe in a medium is lost not due to radiation, but due to collisions. It has been proposed to use the Langevin approach to study the diffusion of heavy quarks in a medium of mostly light quarks [61, 4, 5]. Such an algorithm is appropriate if one wants to study the diffusion of a probe particle in a thermal medium. The bath particles need not necessarily be the same mass as that of the probe particle.

The Langevin equation is a discretized equation describing the update of the positions and momenta of a probe particle in the medium as it interacts with the thermal background. In order to write the Langevin equation for a medium, one begins by writing Newton's law for the probe particle, with the thermal noise representing a random force acting on the particle, and the drag a probe particle experiences as it diffuses through the medium (represented by drag coefficient α) is related to fluctuations of the noise ζ. This is a famous result known as the fluctuation-dissipation theorem

$$\alpha = \frac{1}{T}\int_0^t \langle \vec{\zeta}(0)\cdot\vec{\zeta}(s)\rangle_0 ds. \tag{6.2}$$

If we define the strength of the white noise in the medium through

$$\langle \zeta^i(t)\zeta^j(t-n\Delta t)\rangle = \frac{\kappa}{\Delta t}\delta^{ij}\delta^{n0}\delta(t) \tag{6.3}$$

then the drag coefficient (as defined in 6.2) becomes

$$\alpha = \frac{\kappa}{T\Delta t}. \tag{6.4}$$

Langevin Equation for White Noise in Thermal Medium

The standard Langevin Equation (without memory effects) for a particle with mass M in a thermal medium is given by

$$\frac{d\vec{p}(t)}{dt} = -\int_{-\infty}^{t} dt^{'}\,\alpha(t-t^{'})\vec{v}(t^{'}) + \vec{\zeta}(t), \tag{6.5}$$

where $\alpha(t-t^{'})$ is the drag kernel, and $\vec{\zeta(t)}$ is the white noise in the medium. Note that the dimensions of the drag kernal are different than those of the drag coefficient as defined in 6.2. The "white noise" is a random force which represents the random collisions the probe particle in the medium undergoes in a heat bath at equilibrium temperature T. The goal is now to investigate memory effects in the very early time dynamics of a QGP.

Fluctuation-Dissipation Theorem

To derive the relationship between the drag and thermal noise, we begin with writing the equation of motion for a probe particle in the absence of external forces (other than the random noises from the thermal medium). This derivation is in the spirit of the treatment of the fluctuation-dissipation theorem in [75].

$$\frac{d\vec{p}(t)}{dt} = \vec{\zeta}(t), \tag{6.6}$$

Integrating the above equation over a time interval τ which is large compared to the mean period of the fluctuations ζ, then taking an ensemble average, we obtain

$$\langle \vec{p}(t+\tau) - \vec{p}(t) \rangle = \int_{t}^{t+\tau} dt^{'} \langle \vec{\zeta}(t^{'}) \rangle, \tag{6.7}$$

Naively, by definition of white noise $\langle \vec{\zeta}(t) \rangle = 0$, but the goal here is to obtain a slowly varying velocity intending to restore the particle to equilibrium. One therefore needs to determine how $\langle \vec{\zeta} \rangle$ changes as the velocity of the particle changes. Suppose that at time t the particle has velocity $\vec{v}(t)$ in a thermal medium with temperature T. The system as this time has a configuration described by $\langle \vec{\zeta} \rangle = 0$, with probability

of being in a state r of W_r^0. Now, in order to investigate how $\langle\zeta\rangle$ is affected by the motion of the particle, consider the situation at a slightly later time $t^{'} = t + \tau^{'}$ when the particle has velocity $\vec{v}(t + \tau^{'})$. Then the mean random force $\langle\vec{\zeta}(t^{'})\rangle$ depends on the value at earlier time t. One can also think about the formulation of the problem in this manner. If the system is ergodic, then performing an ensemble average by making multiple copies of the system at some snapshot time t is equivalent to making multiple copies of the same system at different times $t^{'}$. However, $\zeta(t^{'})$ will be slightly different than $\zeta(t)$. If after a time $\tau^{'} > \tau^{*}$, where τ^{*} is the timescale on the order of mean collision times, the velocity of the particle changes from $\vec{v}(t)$ to $\vec{v}(t + \tau^{'})$ and that the energy of the system changes from $E(t)$ to $E(t + \tau^{'})$ with the number of microstates accessible to the system changing from $\Omega(E)$ to $\Omega(E + \Delta E)$ respectively. Then the probability of the system or being in state r at time $t + \tau^{'}$ can be found from

$$\frac{W_r(t + \tau^{'})}{W_r^0} = \frac{\Omega(E + \Delta E)}{\Omega(E)} = e^{\Delta E/T}. \tag{6.8}$$

We are assuming that the velocity change and change of the mean random force are small enough such that

$$W_r(t + \tau^{'}) = W_r^0 e^{(\Delta E/T)} \approx W_r^0 \left(1 + \frac{\Delta E}{T}\right) \tag{6.9}$$

implying that the mean value of the force at slightly later time $t + \tau^{'}$ is given by

$$\langle\zeta\rangle = \sum_r W_r(t + \tau^{'})\zeta_r = \sum_r W_r^0 \left(1 + \frac{\Delta E}{T}\right)\zeta_r = \langle(1 + \Delta E/T)\rangle_0 \tag{6.10}$$

where the last value is to be calculated with probability distribution W_r^0. Since by definition $\vec{\zeta_0} = 0$,

$$\langle\vec{\zeta}\rangle = \frac{1}{T}\langle\vec{\zeta}\Delta E\rangle_0. \tag{6.11}$$

Note that the energy increase from a time t to time $t+\tau$ is given by the negative of the work done on the particle. Hence,

$$\Delta E = -\int_t^{t+\tau} \vec{v}(t^{'}) \cdot \vec{\zeta}(t^{'}) dt^{'} \approx -\vec{v}(t) \cdot \int_t^{t+\tau} \vec{\zeta}(t^{'}) dt^{'} \tag{6.12}$$

this leads to

$$\langle \vec{\zeta}(t+\tau) \rangle = -\frac{1}{T} \langle \vec{\zeta}(t+\tau) \vec{v}(t) \cdot \int_t^{t+\tau} \vec{\zeta}(t^{'}) dt^{'} \rangle_0 = -\frac{\vec{v}}{T} \cdot \int_t^{t+\tau} dt^{'} \langle \vec{\zeta}(t^{'}+\tau) \cdot \vec{\zeta}(t^{'}) \rangle_0 \tag{6.13}$$

where $\vec{v}$ is the mean speed. Introducing the timeshift variable $s \equiv t^{'} - (t+\tau)$, the Langevin equation can be rewritten in the form

$$\langle \vec{p}(t+\Delta t) - \vec{p}(t) \rangle = \vec{F}_{ext} \Delta t - \alpha \vec{v}(t) \tag{6.14}$$

where

$$\alpha = \frac{1}{T} \int_0^t \langle \vec{\zeta}(0) \cdot \vec{\zeta}(s) \rangle_0 ds \tag{6.15}$$

is an effective frictional drag coefficient experienced by the probe particle. Note that in the absense of any external forces, the particle's mean velocity will go to zero in the long time limit.

We have generalized the drag coefficient in equation 6.15 to incorporate possible memory effects. Note that the above derivation of the relationship between the drag coefficient and thermal noise indicate assumed "white noise" meaning that the noise is completely random and the noise a particle experiences at one position in the medium is completely independent of the earlier noise the particle experiences in the medium.

Langevin Equation with Memory Effects Incorporated

As has been stated in earlier chapters, hydrodynamics assumes a rapid early thermalization for the quark gluon plasma. However, the exact physical mechanism for the

thermalization is not known, although ideas have been proposed that the system can thermalize through plasma turbulence. If one is to investigate heavy quark diffusion through a bulk QGP where turbulent electric and color magnetic fields are present, then the heavy quark probe would have to traverse through domains of coherent color fields, and the noise experienced by such a probe particle would not be completely random. As such we shall proceed with an investigation of how the Langevin equation would be modified if memory effects were included in the medium.

A model for very early time effects can be constructed by considering turbulent color electric/magnetic fields. As such we choose to modify the Langevin equation (1) to incorporate memory effects. In particular, we choose to represent the memory effects in the electric and magnetic fields:

$$\frac{d\vec{p}(t)}{dt} = -\int_{-\infty}^{t} dt^{'}\alpha(t-t^{'})\vec{v}(t^{'}) + \vec{\zeta}(t) + gQ^{a}[\vec{E}^{a}(t) + \vec{v}(t)\times\vec{B}^{a}(t)], \tag{6.16}$$

where $\vec{E}^{a}(t)$ and $\vec{B}^{a}(t)$ are the color electric/magnetic fields respectively, Q^{a} are the color charges, and $a = 1, ..., N_c^2 - 1$, working with an $SU(N_c)$ gauge. The relationship between the drag coefficient and the noise gets modified due to the presence of external forces with color electric and magnetic fields. The change in energy a particle experiences as its velocity changes slowly is the negative of the work done by the particle. Since this is the net force acting on the particle dotted into its velocity, the magnetic field does no work, and there exists an additional term related to the correlation of the color electric fields. Hence, the memory kernel from equation 6.5 now gets modified to

$$T\alpha(t-t^{'})\delta^{ij} = \langle\zeta^{i}(t)\zeta^{j}(t^{'})\rangle + g^{2}\langle Q^{a}E(t)^{ai}Q^{b}E^{bj}(t^{'})\rangle. \tag{6.17}$$

It is necessary to establish a hierarchy of timescales in the theory to ensure the

validity of a Langevin approach. There is the discrete Langevin timestep Δt, the characteristic "memory time" of the noise $\tau_{\rm mem}$, and the characteristic timescale for the macroscopic properties of the system to change $T(t)/\dot{T}$, defined by

$$\dot{T} \equiv dT/dt = \left(\frac{\partial}{\partial t} + \vec{v}\cdot\nabla\right) T, \tag{6.18}$$

Hence the following inequalities need to be satisfied:

$$\Delta t \ll \tau_{\rm mem} \ll T(t)/\dot{T}. \tag{6.19}$$

this implies that the medium must be quasistatic.

Updating Color/Electric Magnetic Fields

We incorporate the memory effect by updating the color electric/magnetic fields according to the following prescription (for simplicity we drop the color subscript and restore it later):

$$\vec{E}(t+\Delta t) = w_{\rm E}\eta(t+\Delta t) + (1-w_{\rm E})\vec{E}(t)e^{\beta_E \Delta t}) \tag{6.20}$$

$$\vec{B}(t+\Delta t) = w_{\rm B}\tilde{\eta}(t+\Delta t) + (1-w_{\rm B})\vec{B}(t)e^{\beta_B \Delta t} \tag{6.21}$$

We refer to $w_{\rm E/B}$ as the memory coefficients for the electric and magnetic fields, respectively. $\eta/\tilde{\eta}$ refer to color noise for the electric/magnetic fields, respectively. $\beta_{\rm E/B}$ refer to the growth rates of the color electric/magnetic fields, respectively. Note that in the event of the memory coefficients being zero, the fields exhibit perfectly deterministic growth, or perfect memory in the case of zero growth rate. In the event of memory coefficients being unity, the fields are completely random.

One can understand two sources affecting the growth of the magnetic field. One is the effect of interacting with the medium, and the other is an imposed deterministic

condition for the growth of such color fields. The desire is to model the type of exponentially increasing magnetic field growth which would happen for example in a Weibel instability in the appropriate limit. When the memory coefficient is zero, we have

$$\vec{B}(t+\Delta t) = e^{\beta \Delta t}\vec{B}(t) \tag{6.22}$$

and a similar expression for $\vec{E}(t)$. It is necessary to find a relationship between the electric field strength and the color noise strength so that we can proceed with finding the relationship etween the noise and drag coefficient. However, we should note that the system in general is NOT ergodic. We proceed by iterating equation 6.20

$$\vec{E}(t) = w_{\mathrm{E}}\eta(t) + (1 - w_{\mathrm{E}}w_{\mathrm{E}}\eta(t-\Delta t)e^{\beta_{\mathrm{E}}\Delta t} + ... + (1-w_{\mathrm{E}})^n\vec{E}(t-n\Delta t)e^{n\beta_{\mathrm{E}}\Delta t} \tag{6.23}$$

Squaring the above relation and taking the expectation value, noting that the expectation values of cross terms with white noise vanish by definition, we obtain

$$\langle E^2(t)\rangle = w_{\mathrm{E}}^2\left[\frac{1-(1-w_{\mathrm{E}})^2e^{2n\beta_{\mathrm{E}}\Delta t}}{1-(1-w_{\mathrm{E}})^2e^{2\beta_{\mathrm{E}}\Delta t}}\right]\langle\eta^2(t)\rangle + (1-w_{\mathrm{E}})^{2n}e^{2n\beta_{\mathrm{E}}\Delta t}\langle E^2(t-n\Delta t)\rangle \tag{6.24}$$

Also, calculating the electric field correlation at different times yields

$$\langle\vec{E}(t)\cdot\vec{E}(t-n\Delta t)\rangle = (1-w_{\mathrm{E}})^n\langle E^2(t-n\Delta t)\rangle e^{n\beta_{\mathrm{E}}\Delta t} \tag{6.25}$$

This yields the following autocorrelation function for the electric fields at different times:

$$\frac{\langle\vec{E}(t)\cdot\vec{E}(t-n\Delta t)\rangle}{\sqrt{E^2(t)}\sqrt{E^2(t-n\Delta t)}} = \sqrt{1-w_{\mathrm{E}}^2\left[\frac{1-(1-w_{\mathrm{E}})^{2n}e^{2n\beta_{\mathrm{E}}\Delta t}}{1-(1-w_{\mathrm{E}})^{2n}e^{2\beta_{\mathrm{E}}\Delta t}}\right]\frac{\langle\eta^2(t)\rangle}{\langle E^2(t)\rangle}}. \tag{6.26}$$

Note that in the limit of $w_{\rm E} = 0$, the autocorrelation function tends to unity, and in the limit of $w_{\rm E} = 1$ the autocorrelation function tends to zero, as expected. We parameterize the strength of the electric and thermal white noise, respectively, as follows

$$\langle \eta^i(t)\eta^j(t-n\Delta t)\rangle \equiv \frac{\kappa_{\rm E}}{\Delta t}\delta_{ij}\delta_{n0} \tag{6.27}$$

$$\langle \zeta^i(t)\zeta^j(t-n\Delta t)\rangle \equiv \frac{\kappa}{\Delta t}\delta_{ij}\delta_{n0} \tag{6.28}$$

Reintroducing the color indices into our electric field correlation, we find that

$$\langle E^{ia}(t)E^{jb}(t-n\Delta t)\rangle = (1-w_{\rm E})^{-n}e^{-n\beta_{\rm E}\Delta t}\left\{w_{\rm E}^2\left[\frac{1-(1-w_{\rm E})^{2n}e^{2n\beta_{\rm E}\Delta t}}{1-(1-w_{\rm E})^2e^{2\beta_{\rm E}\Delta t}}\right]\times\right. \tag{6.29}$$

$$\left.\frac{\kappa_{\rm E}}{\Delta t} + (1-w_{\rm E})^{2n}e^{2n\beta_{\rm E}\Delta t}\langle E^2(t-n\Delta t)\rangle\right\}\delta^{ij}\delta^{ab} \tag{6.30}$$

Because of the discretized nature and the time-dependent relationship between the drag force and thermal force/electric field strength, it is useful to recast the Langevin equation with memory effects in the so-called Ito-discretization

$$\vec{p}(t+\Delta t) = \vec{p}(t) - \left[\Delta t\sum_{n=0}^{\infty}(1-\frac{\delta_{n0}}{2})\alpha_n\vec{v}(t-n\Delta t) + \vec{\zeta}(t) + gQ^a\left(\vec{E}^a(t) + \vec{v}(t)\times\vec{B}^a(t)\right)\right]\Delta t \tag{6.31}$$

where $\alpha_n = \alpha(t = n\Delta t)$. Recall that in equation 6.5, the memory kernel was defined through

$$T\alpha(t-t')\delta^{ij}\delta^{ab} = \langle\zeta^i(t)\zeta^j(t)\rangle + g^2\langle Q^aE^{ai}(t)Q^bE^{bj}(t')\rangle \tag{6.32}$$

It is then necessary to cast the second term on the right hand side above to yield a useful form. Note that the evolution of color charges in a non-Abelian color gauge

field is given by

$$\frac{dQ^a}{dt} = g f^{abc} Q^a A^c_\mu v^\mu \tag{6.33}$$

implying that

$$Q^a(t^{'}) = Pexp\left(\int_{r(t)}^{r(t^{'})} f_{abc} A^b_\mu dx^\mu\right) Q^c(t) \equiv U_{ac}(r(t^{'}, r(t)) Q^c(t). \tag{6.34}$$

Hence this enables us to rewrite the electric color force correlation term as

$$g^2\langle Q^a(t) E^{ai}(t) Q^b(t) E^{bj}(t^{'})\rangle = g^2\langle Q^a(t) Q^b(t)\rangle\langle E^{ai}(t) E^{bj}(t^{'})\rangle \tag{6.35}$$

If the random color fields are independent, then

$$\langle Q^a Q^b\rangle = \frac{C_2}{N_c^2 - 1}\delta^{ab}, \tag{6.36}$$

where C_2 is the Casimir operator number, N_c is the number of colors in the gauge group. Putting all this together, the discretized drag coefficient becomes

$$\begin{aligned} \alpha_n &= \frac{1}{T}\left(\frac{\kappa}{\Delta t} + \frac{g^2 C_2}{N_c^2 - 1}(1 - w_{\mathrm{E}})^{-n} e^{-n\beta_{\mathrm{E}}\Delta t}\times\right. \\ &\left.\left[w_{\mathrm{E}}^2\left(\frac{1 - (1 - w_{\mathrm{E}})^{2n} e^{2n\beta_{\mathrm{E}}\Delta t}}{1 - (1 - w_{\mathrm{E}})^2 e^{2n\beta_{\mathrm{E}}\Delta t}}\right)\frac{\kappa_{\mathrm{E}}}{\Delta t} + (1 - w_{\mathrm{E}})^{2n} e^{2n\beta_E\Delta t}\langle E^2(t - n\Delta t)\rangle\right]\right) \end{aligned} \tag{6.37}$$

Note that in the absence of electric/magnetic files, the expression reduces to

$$\alpha_n = \frac{\kappa}{T\Delta t}, \tag{6.38}$$

consistent with our construction of white noise in equation 6.4. Analytically we have derived a framework for studying thermalization of a representative quark particle in a thermal medium to study the equilibriation of the QGP with memory effects. The next step is to proceed with the numerical implementation of the algorithm we have derived.

7

Summary

This dissertation presented research on how to extract transport coefficients of hot and dense quantum chromodynamic (QCD) matter, whether it be hadronic or partonic, from microscopic transport models. As a result we have gained insight into what is currently known about the viscosity to entropy density ratio of the hot QCD matter created at the Relativistic Heavy-Ion Collider (RHIC) at Brookhaven National Laboratory. The deconfined, partonic phase of QCD matter is called the quark gluon plasma (QGP) and is formed when hadronic matter at high temperatures of $T \sim 160 - 180$ MeV undergoes a transition from hadronic bound states to deconfined quasi-free quarks and gluons. Due to the transient nature of the QGP being realized in an actual heavy ion collision, it becomes crucial to separately investigate transport properties of the hadronic aftermath of the decayed QGP in order to understand the time-evolution of transport coefficients in the different phases of a relativistic heavy ion collision. Ideal and viscous relativistic hydrodynamics calculations, in conjunction with what is known about the elliptic flow (v_2) data from RHIC, suggest that a thermally equilibriated QGP was created with very small values of the shear viscosity to entropy density ratio η/s, followed by a hadronic phase with a larger value

of η/s which then evolves out of chemical equilibrium. The work presented in this thesis thoroughly investigates the behavior of η/s in the hadronic phase both in and out of chemical equilibrium, with additional results presented on other transport coefficients such as the baryon number diffusion coefficient, and preliminary results on the bulk viscosity to entropy density ratio ζ/s. Such results, taken in conjunction with what is known about the RHIC data from other measurements, shed light on the trajectory of η/s in a heavy ion collision, and provide a framework for similar investigations into the future about trajectories of ζ/s and diffusion coefficients in a relativistic heavy ion collision.

After reviewing what has been known about the shear and bulk viscosity to entropy density ratios in Chapter 2, I have reviewed three standard techniques for calculating transport coefficients in Chapter 3. We apply two such approaches, the Green-Kubo formalism and the relaxation time approximation, when appropriate to extract ζ/s and η/s from microscopic transport models for hadronic and partonic media, the Ultrarelativistic Quantum Molecular Dynamics (UrQMD) model and Parton Cascamde Model (PCM), respectively. In Chapter 4, I describe the details of UrQMD and the PCM, and show how we are able to simulate thermally equilibriated hadronic and partonic gases in the infinite volume limit. In Chapter 5, I present my calculations for η/s for a hadronic medium in and out of chemical equilibrium, and describe the relevant consequences for the behavior of η/s in the hadronic and partonic phases at RHIC. I also present preliminary calculations for ζ/s and compare the results to a relaxation time approximation calculation from UrQMD. Results are also presented for calculations of η/s for a hot equilibriated perturbative QGP at RHIC.

The results of my calculations of transport coefficients in Chapter 5 suggest that the QGP observed at RHIC cannot be described solely using traditional techniques from perturbation theory in QCD (pQCD). The deconfied matter at RHIC either

has to be modeled using strong interaction physics beyond the scope of pQCD, or might be a manifestation of turbulent color electric and magnetic fields equilibriating a weakly coupled QGP with a small anomalous viscosity.

In chapter 6, I provide an algorithm which describes how one can investigate diffusion of heavy quarks in a thermal medium of mainly light quarks and gluons. The algorithm also includes a method of dealing with memory effects, which may result from coherent domains of color magnetic and electric fields being formed as a result of plasma turbulence. The proper relationship for the diffusion coefficient is recovered when the limit of no memory effects existing in the QGP is taken.

The goal of this thesis was to advance the knowledge of transport coefficients of hot QCD matter, which are especially not well known in certain limits where traditional techniques of QCD are not applicable. In particular, the evolution of the system of RHIC through a hadronic phase after the transient QGP state only more strongly emphasizes the need to understand the behavior of transport coefficients in the separate phases of a heavy ion collision, and appreciate the fact that transport coefficients are dynamic quantities which are strongly time-dependent.

Interesting open questions remain that require further investigation. For example, while the behavior of η/s in a heavy ion collision was strongly improved upon, especially in quantifying the viscous hadronic effects, the behavior of ζ/s in a heavy ion collision still needs to be further investigated, and analyzing the effects of bulk viscosity on elliptic flow are in progress by other groups that perform relativistic viscous hydrodynamics calculations. Also, the numerical implementation of a Langevin algorithm to investigate heavy quark diffusion in a thermal QGP with memory effects needs to be executed. Further investigations of these particular questions will help the community at large make further progress towards a more comprehensive picture of the behavior of transport coefficients in hot QCD matter.

Bibliography

[1] B. I. Abelev et al. Transverse momentum and centrality dependence of high-p_T non-photonic electron suppression in Au+Au collisions at $\sqrt{s_{NN}} = 200$ GeV. *Phys. Rev. Lett.*, 98:192301, 2007.

[2] John Adams et al. Experimental and theoretical challenges in the search for the quark gluon plasma: The star collaboration's critical assessment of the evidence from rhic collisions. *Nucl. Phys.*, A757:102–183, 2005.

[3] K. Adcox et al. Formation of dense partonic matter in relativistic nucleus nucleus collisions at rhic: Experimental evaluation by the phenix collaboration. *Nucl. Phys.*, A757:184–283, 2005.

[4] Yukinao Akamatsu, Tetsuo Hatsuda, and Tetsufumi Hirano. Electron-muon correlation as a new probe to strongly interacting quark-gluon plasma. *Phys. Rev.*, C80:031901, 2009.

[5] Yukinao Akamatsu, Tetsuo Hatsuda, and Tetsufumi Hirano. Heavy Quark Diffusion with Relativistic Langevin Dynamics in the Quark-Gluon Fluid. *Phys. Rev.*, C79:054907, 2009.

[6] Peter Arnold, Guy D. Moore, and Laurence G. Yaffe. Transport coefficients in high temperature gauge theories. i: Leading-log results. *JHEP*, 11:001, 2000.

[7] Peter Arnold, Guy D Moore, and Laurence G. Yaffe. Transport coefficients in high temperature gauge theories. II: Beyond leading log. *JHEP*, 05:051, 2003.

[8] I. Arsene et al. Quark gluon plasma and color glass condensate at rhic? the perspective from the brahms experiment. *Nucl. Phys.*, A757:1–27, 2005.

[9] M. Asakawa, S. A. Bass, and B. Muller. Anomalous viscosity of an expanding quark-gluon plasma. *Phys. Rev. Lett.*, 96:252301, 2006.

[10] M. Asakawa, S. A. Bass, and Berndt Muller. Anomalous viscosity of an expanding quark-gluon plasma. *J. Phys.*, G34:S839–842, 2007.

[11] Masayuki Asakawa, Steffen A. Bass, and Berndt Muller. Anomalous transport processes in anisotropically expanding quark-gluon plasmas. 2006.

[12] B. B. Back et al. The phobos perspective on discoveries at rhic. *Nucl. Phys.*, A757:28–101, 2005.

[13] S. A. Bass and A. Dumitru. Dynamics of hot bulk qcd matter: From the quark-gluon plasma to hadronic freeze-out. *Phys. Rev.*, C61:064909, 2000.

[14] S. A. Bass et al. Microscopic models for ultrarelativistic heavy ion collisions. *Prog. Part. Nucl. Phys.*, 41:225–370, 1998.

[15] J.D. Bekenstein. A universal upper bound on the entropy to energy ratio for bounded systems. *Phys. Rev. D*, 23:287, 1981.

[16] M. Belkacem et al. Equation of state, spectra and composition of hot and dense infinite hadronic matter in a microscopic transport model. *Phys. Rev.*, C58:1727–1733, 1998.

[17] E. Beth and G. Uhlenbeck. The quantum theory of the non-ideal gas. II. Behaviour at low temperatures. *Physica*, 4:915–924, 1937.

[18] Jiunn-Wei Chen and Eiji Nakano. Shear viscosity to entropy density ratio of qcd below the deconfinement temperature. *Phys. Lett.*, B647:371–375, 2007.

[19] M. Cheng et al. Equation of State for physical quark masses. *Phys. Rev.*, D81:054504, 2010.

[20] B. L. Combridge, J. Kripfganz, and J. Ranft. Hadron Production at Large Transverse Momentum and QCD. *Phys. Lett.*, B70:234, 1977.

[21] Laszlo P. Csernai, Joseph. I. Kapusta, and Larry D. McLerran. On the strongly-interacting low-viscosity matter created in relativistic nuclear collisions. *Phys. Rev. Lett.*, 97:152303, 2006.

[22] Roger Cutler and Dennis W. Sivers. Quantum Chromodynamic Gluon Contributions to Large p(T) Reactions. *Phys. Rev.*, D17:196, 1978.

[23] P. Danielewicz and M. Gyulassy. Dissipative phenomena in quark gluon plasmas. *Phys. Rev.*, D31:53–62, 1985.

[24] Pawel Danielewicz and Scott Pratt. Delays associated with processes in nuclear reaction simulations. *Phys. Rev.*, C53:249–266, 1996.

[25] Nasser Demir and Steffen A. Bass. η/s of a Relativistic Hadron Gas at RHIC: Approaching the AdS/CFT bound? *Nucl. Phys.*, A830:733c–736c, 2009.

[26] Nasser Demir and Steffen A. Bass. Extracting hadronic viscosity from microscopic transport models. *Eur. Phys. J.*, C62:63–68, 2009.

[27] Nasser Demir and Steffen A. Bass. Shear-Viscosity to Entropy-Density Ratio of a Relativistic Hadron Gas. *Phys. Rev. Lett.*, 102:172302, 2009.

[28] Andrej El, Azwinndini Muronga, Zhe Xu, and Carsten Greiner. Shear viscosity and out of equilibrium dissipative hydrodynamics. *Phys. Rev.*, C79:044914, 2009.

[29] Oliver Fochler, Zhe Xu, and Carsten Greiner. Towards a unified understanding of jet-quenching and elliptic flow within perturbative QCD parton transport. *Phys. Rev. Lett.*, 102:202301, 2009.

[30] R. J. Fries, S. A. Bass, and B. Muller. Correlated emission of hadrons from recombination of correlated partons. *Phys. Rev. Lett.*, 94:122301, 2005.

[31] R. J. Fries, B. Muller, C. Nonaka, and S. A. Bass. Hadron production in heavy ion collisions: Fragmentation and recombination from a dense parton phase. *Phys. Rev.*, C68:044902, 2003.

[32] John Fuini, Nasser S. Demir, Dinesh K. Srivastava, and Steffen A. Bass. Shear Viscosity in a Perturbative Quark-Gluon-Plasma. 2010.

[33] Sean Gavin and Mohamed Abdel-Aziz. Measuring Shear Viscosity Using Transverse Momentum Correlations in Relativistic Nuclear Collisions. *Phys. Rev. Lett.*, 97:162302, 2006.

[34] Klaus Geiger. Vni 3.1: Mc-simulation program to study high-energy particle collisions in qcd by space-time evolution of parton-cascades and parton-hadron conversion. *Comput. Phys. Commun.*, 104:70–160, 1997.

[35] Klaus Geiger and Berndt Muller. Dynamics of parton cascades in highly relativistic nuclear collisions. *Nucl. Phys.*, B369:600–654, 1992.

[36] Ulrich W. Heinz, Huichao Song, and Asis K. Chaudhuri. Dissipative hydrodynamics for viscous relativistic fluids. *Phys. Rev.*, C73:034904, 2006.

[37] Tetsufumi Hirano and Keiichi Tsuda. Collective flow and two pion correlations from a relativistic hydrodynamic model with early chemical freeze out. *Phys. Rev.*, C66:054905, 2002.

[38] Tetsufumi Hirano and Keiichi Tsuda. Collective flow and hbt radii from a full 3d hydrodynamic model with early chemical freeze out. *Nucl. Phys.*, A715:821–824, 2003.

[39] Akio Hosoya, Masa-aki Sakagami, and Masaru Takao. Nonequilibrium thermodynamics in field theory: Transport coefficients. *Ann. Phys.*, 154:229, 1984.

[40] W. Israel. Nonstationary irreversible thermodynamics: A Causal relativistic theory. *Ann. Phys.*, 100:310–331, 1976.

[41] W. Israel and J. M. Stewart. Transient relativistic thermodynamics and kinetic theory. *Ann. Phys.*, 118:341–372, 1979.

[42] Kazunori Itakura, Osamu Morimatsu, and Hiroshi Otomo. Shear viscosity of a hadronic gas mixture. *Phys. Rev.*, D77:014014, 2008.

[43] Dmitri Kharzeev, Eugene Levin, and Marzia Nardi. QCD saturation and deuteron nucleus collisions. *Nucl. Phys.*, A730:448–459, 2004.

[44] J. Kinast, S. L. Hemmer, M. E. Gehm, A. Turlapov, and J. E. Thomas. Evidence for Superfluidity in a Resonantly Interacting Fermi Gas. *Phys. Rev. Lett.*, 92:150402, 2004.

[45] Igor R. Klebanov. World-volume approach to absorption by non-dilatonic branes. *Nucl. Phys.*, B496:231–242, 1997.

[46] Peter F. Kolb and Ralf Rapp. Transverse flow and hadro-chemistry in au + au collisions at s(nn)**(1/2) = 200-gev. *Phys. Rev.*, C67:044903, 2003.

[47] P. Kovtun, D. T. Son, and A. O. Starinets. Viscosity in strongly interacting quantum field theories from black hole physics. *Phys. Rev. Lett.*, 94:111601, 2005.

[48] Roy A. Lacey et al. Has the QCD critical point been signaled by observations at RHIC? *Phys. Rev. Lett.*, 98:092301, 2007.

[49] L.D. Landau and E.M. Lifshitz. *Statistical Physics*. Pergamon Press, 1958.

[50] Richard L. Liboff. *Kinetic theory : Classical, Quantum, and Relativistic Descriptions*. Springer-Verlag, third edition, 2003.

[51] Matthew Luzum and Paul Romatschke. Conformal Relativistic Viscous Hydrodynamics: Applications to RHIC results at $\sqrt{s_{NN}} = 200$ GeV. *Phys. Rev.*, C78:034915, 2008.

[52] Juan Martin Maldacena. The large N limit of superconformal field theories and supergravity. *Adv. Theor. Math. Phys.*, 2:231–252, 1998.

[53] Larry D. McLerran and Benjamin Svetitsky. Quark Liberation at High Temperature: A Monte Carlo Study of SU(2) Gauge Theory. *Phys. Rev.*, D24:450, 1981.

[54] Larry D. McLerran and Raju Venugopalan. Computing quark and gluon distribution functions for very large nuclei. *Phys. Rev.*, D49:2233–2241, 1994.

[55] Larry D. McLerran and Raju Venugopalan. Gluon distribution functions for very large nuclei at small transverse momentum. *Phys. Rev.*, D49:3352–3355, 1994.

[56] Harvey B. Meyer. A calculation of the shear viscosity in su(3) gluodynamics. *Phys. Rev.*, D76:101701, 2007.

[57] Harvey B. Meyer. A calculation of the bulk viscosity in SU(3) gluodynamics. *Phys. Rev. Lett.*, 100:162001, 2008.

[58] Denes Molnar and Miklos Gyulassy. Saturation of elliptic flow at RHIC: Results from the covariant elastic parton cascade model MPC. *Nucl. Phys.*, A697:495–520, 2002.

[59] Denes Molnar and Pasi Huovinen. Dissipation and elliptic flow at rhic. *Phys. Rev. Lett.*, 94:012302, 2005.

[60] E. Molnar, H. Niemi, and D. H. Rischke. Numerical tests of causal relativistic dissipative fluid dynamics. *Eur. Phys. J.*, C65:615–635, 2010.

[61] Guy D. Moore and Derek Teaney. How much do heavy quarks thermalize in a heavy ion collision? *Phys. Rev.*, C71:064904, 2005.

[62] M.Riordan and W.A. Zajc. The First Few Microseconds. *Scientific American*, 294:24–31, 2006.

[63] Azwinndini Muronga. Shear viscosity coefficient from microscopic models. *Phys. Rev.*, C69:044901, 2004.

[64] Shin Muroya and Nobuo Sasaki. A calculation of the viscosity over entropy ratio of a hadronic gas. *Prog. Theor. Phys.*, 113:457–462, 2005.

[65] C. Nonaka, B. Muller, S. A. Bass, and M. Asakawa. Possible resolutions of the d-paradox. *Phys. Rev.*, C71:051901, 2005.

[66] Chiho Nonaka and Steffen A. Bass. Space-time evolution of bulk qcd matter. *Phys. Rev.*, C75:014902, 2007.

[67] Jacquelyn Noronha-Hostler, Jorge Noronha, and Carsten Greiner. Transport Coefficients of Hadronic Matter near T_c. 2008.

[68] Office of Nuclear Physics and Office of Advanced Scientific Computing Research. Scientific Grand Challenges: Forefront Questions in Nuclear Science and the Role of Computing at the Extreme Scale. Technical Report PNNL-18739, prepared for US Dept. of Energy under contract DE-AC05-76RLO1830, 2009.

[69] K. M. O'Hara, S. L. Hemmer, M. E. Gehm, S. R. Granade, and J. E. Thomas. Observation of a Strongly Interacting Degenerate Fermi Gas of Atoms. *Science*, 298:2179–2182, 2002.

[70] Subrata Pal. Shear viscosity to entropy density ratio in nuclear multifragmentation. *Phys. Rev.*, C81:051601, 2010.

[71] Particle-Data-Group. *Phys. Rev.*, D54, 1996.

[72] B. et. al. Povh. *Particles and Nuclei: An Introduction to the Physical Concepts*. Springer-Verlag, 4th edition, 2004.

[73] Madappa Prakash, Manju Prakash, R. Venugopalan, and G. Welke. Nonequilibrium properties of hadronic mixtures. *Phys. Rept.*, 227:321–366, 1993.

[74] Jorgen Randrup and Stanislaw Mrowczynski. Chromodynamic weibel instabilities in relativistic nuclear collisions. *Phys. Rev.*, C68:034909, 2003.

[75] F. Reif. *Fundamentals of statistical and thermal physics*. McGraw-Hill Kogakusha,, international student ed. edition, 1965.

[76] Paul Romatschke and Michael Strickland. Collective modes of an anisotropic quark gluon plasma. *Phys. Rev.*, D68:036004, 2003.

[77] N. Sasaki, O. Miyamura, S. Muroya, and C. Nonaka. A calculation of baryon diffusion constant in hot and dense hadronic matter based on an event generator URASiMA. *Phys. Rev.*, C62:011901, 2000.

[78] N. Sasaki, O. Miyamura, S. Muroya, and C. Nonaka. Baryon diffusion constant in hot and dense hadronic matter based on an event generator urasima. 2000.

[79] N. Sasaki, O. Miyamura, S. Muroya, and C. Nonaka. Charge diffusion constant in hot and dense hadronic matter: A hadro-molecular-dynamic calculation. *Europhys. Lett.*, 54:38–44, 2001.

[80] Edward V. Shuryak and Misha A. Stephanov. When can long range charge fluctuations serve as a QGP signal? *Phys. Rev.*, C63:064903, 2001.

[81] Huichao Song and Ulrich W. Heinz. Viscous hydrodynamics with bulk viscosity – uncertainties from relaxation time and initial conditions. *Nucl. Phys.*, A830:467c–470c, 2009.

[82] Huichao Song and Ulrich W Heinz. Interplay of shear and bulk viscosity in generating flow in heavy-ion collisions. *Phys. Rev.*, C81:024905, 2010.

[83] G. Torrieri, S. Jeon, J. Letessier, and J. Rafelski. Sharev2: Fluctuations and a comprehensive treatment of decay feed-down. *Comput. Phys. Commun.*, 175:635–649, 2006.

[84] Giorgio Torrieri et al. Share: Statistical hadronization with resonances. *Comput. Phys. Commun.*, 167:229–251, 2005.

[85] A. Turlapov, J. Kinast, B. Clancy, L. Luo, J. Joseph, and J.E. Thomas. Is a gas of strongly interacting atomic fermions a nearly perfect fluid? *J. Low Temp. Phys.*, 150:567–576, November 2008.

[86] Jan Uphoff, Oliver Fochler, Zhe Xu, and Carsten Greiner. Production and elliptic flow of heavy quarks at RHIC and LHC within a partonic transport model. *J. Phys. Conf. Ser.*, 230:012004, 2010.

[87] Steven Weinberg. Entropy generation and the survival of protogalaxies in an expanding universe. *Astrophys. J.*, 168:175, 1971.

[88] Zhe Xu and Carsten Greiner. Thermalization of gluons in ultrarelativistic heavy ion collisions by including three-body interactions in a parton cascade. *Phys. Rev.*, C71:064901, 2005.

[89] Zhe Xu and Carsten Greiner. Elliptic flow of gluon matter in ultrarelativistic heavy- ion collisions. *Phys. Rev.*, C79:014904, 2009.

[90] D.N. Zubarev. *Nonequilibrium Statistical Thermodynamics*, pages 246–359. Plenum, second edition, 1974.

Biography

Nasser Soliman Demir was born in Kuwait on December 25, 1982. He graduated from the Massachusetts Institute of Technology with a S.B. in Physics in June 2004, with a minor in Mathematics. He then decided to pursue doctoral studies at Duke University, where he was awarded a Charles H. Townes Fellowship from August 2004-August 2006. He worked as a Teaching Assistant from 2004-2006, and worked as a Research Assistant from September 2006-August 2010. He earned his M.A. in Physics from Duke University in May 2007, and shall obtain his Ph.D in Physics from Duke University in December 2010. He shall be employed as an Instructor in the Physics Department at Duke University.

Publications

- P. Corio, A. Jorio, N. Demir, and M.S. Dresselhaus, "Spectro-electrochemical studies of single wall carbon nanotubes films", *Chem. Phys. Lett.* **392** (2004), pp.396-402

- E.B. Barros, N.S. Demir, A.G. Souza-Filho, J. Medes-Filho, A. Jorio, G. Dresselhaus, and M.S. Dresselhaus, "Raman Spectroscopy of Graphitic Foams", *Phys.Rev.B* **71**, 165422 (2005)

- N. Demir and S.A. Bass, "Extracting hadronic viscosity from microscopic transport models", *Eur. .Phys. .J.***C62**:63-68,2009

- N. Demir and S.A. Bass, "Shear-Viscosity to Entropy Density Ratio of a Relativistic Hadron Gas", arXiv:0812.2422 [nucl-th], *Phys. Rev. Lett.* **102**, 172302 (2009).

- N. Demir and S.A. Bass, "eta/s of a Relativistic Hadron Gas at RHIC: Approaching the AdS/CFT bound?",**Nucl. Phys. A830733C – 736C**, (2009).

- J. Fuini, III, N.S. Demir, D.K. Srivastava, S.A. Bass, "Shear Viscosity in a Perturbative Quark-Gluon-Plasma", arXiv:1008.2306 [nucl-th], submitted to J.Phys.G. (2010).